

University of Kentucky

UKnowledge

University of Kentucky Master's Theses

Graduate School

2004

TOLERANCE ALLOCATION FOR KINEMATIC SYSTEMS

Mathieu Barraja University of Kentucky, mbarr0@engr.uky.edu

Right click to open a feedback form in a new tab to let us know how this document benefits you.

Recommended Citation

Barraja, Mathieu, "TOLERANCE ALLOCATION FOR KINEMATIC SYSTEMS" (2004). *University of Kentucky Master's Theses.* 315.

https://uknowledge.uky.edu/gradschool_theses/315

This Thesis is brought to you for free and open access by the Graduate School at UKnowledge. It has been accepted for inclusion in University of Kentucky Master's Theses by an authorized administrator of UKnowledge. For more information, please contact UKnowledge@lsv.uky.edu.

ABSTRACT OF THESIS

TOLERANCE ALLOCATION FOR KINEMATIC SYSTEMS

A method for allocating tolerances to exactly constrained assemblies is developed. The procedure is established as an optimization subject to constraints. The objective is to minimize the manufacturing cost of the assembly while respecting an acceptable level of performance. This method is particularly interesting for exactly constrained components that should be mass-produced.

This thesis presents the different concepts used to develop the method. It describes exact constraint theory, manufacturing variations, optimization concepts, and the related mathematical tools. Then it explains how to relate these different topics in order to perform a tolerance allocation.

The developed method is applied on two relevant exactly constrained examples: multi-fiber connectors, and kinematic coupling. Every time a mathematical model of the system and its corresponding manufacturing variations is established. Then an optimization procedure uses this model to minimize the manufacturing cost of the system while respecting its functional requirements. The results of the tolerance allocation are verified with Monte Carlo simulation.

KEYWORDS: Tolerance Allocation, Manufacturing Variation, Kinematic Design Theory, Optimization

Mathieu Barraja

September 9, 2002

TOLERANCE ALLOCATION FOR KINEMATIC SYSTEMS

By

Mathieu Barraja

Prof. R. Ryan Vallance, PhD
Director of Thesis

Dr. George Huang, PhD

Director of Graduate Studies

RULES FOR THE USE OF THESES

Unpublished theses submitted for the Master's degree and deposited in the University of Kentucky Library are a rule open for inspection, but are to be used only with due regard to the rights of the authors. Bibliographical references may be noted, but quotations or summaries of parts may be published only with the permission of the author, and with the usual scholarly acknowledgements.

Extensive copying or publication of the theses in whole or in part also requires the consent of the Dean of the Graduate School of the University of Kentucky.

THESIS

Mathieu Barraja

The Graduate School
University of Kentucky
2002

TOLERANCE ALLOCATION FOR KINEMATIC SYSTEMS

THESIS

A thesis submitted in partial fulfillment of the requirements for the degree of MSME in the College of Engineering at the University of Kentucky

By

Mathieu Barraja

Lexington, Kentucky

Director: Dr. R.R. Vallance, Assistant Professor of Mechanical Engineering Department

Lexington, Kentucky

2002

ACKNOWLEDGEMENTS

First of all I would like to thank Mr. Georges Verchery and Mr. Shahram Aivazzadeh for giving me the opportunity to enter a Master's degree program at the University of Kentucky. I hope they consider this very first UK thesis written by an *isatian* as the result of their hard work for establishing an academic partnership between UK and ISAT Nevers. For the same reason, I would like to thank Dr. G.T. Lineberry who accepted my application for the University of Kentucky. And I can't forget Miss Christine Gonzalez, who could overcome all the administrative difficulties that were swarming in my application file.

Next, I would like to express my deepest gratitude to my advisor, Dr. R. Ryan Vallance. I fully realize that my experience in UK would not have been so enriching if I hadn't met him. I cannot imagine an advisor more dedicated to his students and more thoughtful to their researches. I admire him for his outstanding engineering knowledge, but also for his great human qualities.

I am also really thankful towards people in TCS for having given me the opportunity to work on an exciting project. I would like to thank John Lehman, Burke Hunsaker, and especially Dr. Sepehr Kiani. They've always supported my research, and I hope the result of my work can be equal to the gratitude I would like to show them. I have learnt a lot from them.

Finally, I would like to thank Dr. Stephens and Dr. Mengüç as my examining committees. I wish the results of my project might find some application in their researches; knowing that they would find such an interest in my works would be a personal reward.

TABLE OF CONTENTS

ACKNOWLEDO	GEMENTS	iii
LIST OF TABLE	ES	vii
LIST OF FIGUR	RES	viii
LIST OF FILES.		X
CHAPTER 1:	INTRODUCTION AND THESIS OVERVIEW	1
	UND TO THE THESIS	
1.2. PRIOR WO	RK AND LITERATURE REVIEW	2
	actly Constrained Systems	
	mensional Variations	
	ast Cost Tolerance Allocation	
	thematics and Statistics	
	'ERVIEW	
	pothesis	
1.3.2. Co.	ntent Overview	
CHAPTER 2:	CONCEPTS USED IN THE METHOD	6
2.1. Exactly (CONSTRAINED SYSTEMS	6
2.1.1. The	eory	6
	pes of Connection	
	ample of Kinematic Spindle	
	TURING VARIATIONS	
	esentation	
2.2.1.1.	Introduction	
2.2.1.2.	Sources of Variations	
	thematical Representation	
2.2.2.1.	Dimensions as Random Variables	
2.2.2.2.	Mathematical Model of the Geometric Specifications	
	thods to Analyze the Variations	
2.2.3.1.	Monte Carlo Simulation	
2.2.3.2.	Analytical Model	
2.2.3.3.	Multivariate Error Analysis	
2.2.3.4. 2.3. LEAST COS	Comparison of the Methods ST TOLERANCE ALLOCATION	
	roduction	
	lerance Allocation by Optimization	
	st / Tolerance Relations	
	SUMMARY	
CHAPTER 3:	APPLICATION TO OPTICAL FIBER CONNECTORS	
	TION	
	esentation	
3.1.1.1.	Fiber Optics	
3.1.1.2.	Transmission Losses	
3.1.1.3.	Optical Fiber Connectors	
	ckground and Prior Work	
	lerance Allocation	
	TICAL MODEL	

	3.2.2.	Parametric Model of the Components in the Connector	
	3.2.2.1		
	3.2.2.2	\mathcal{E}	
	3.2.2.3		
	3.2.2.4		
	3.2.2.5 3.2.3.		
	3.2.3.1	Mathematic Description of the Geometric Model	
	3.2.3.1	J J	
	3.2.3.2		
3.3.		ANCE ALLOCATION	
3.3.	3.3.1.	Overview	
	<i>3.3.2.</i>	Variation Analysis by the Law of Error Propagation	
	3.3.3.	Cost / Tolerance Functions	
	3.3.4.	Results of the Tolerance Allocation Algorithm	
	3.3.5.	Comparison with Monte Carlo Simulation	
3.4.		FACTURING PROCESS	
	3.4.1.	Introduction	
	3.4.2.	Description of the Process	65
	<i>3.4.3</i> .	Metallography Study	66
	<i>3.4.4</i> .	Stylus Profilometry of Grooves	68
	3.4.5.	Conclusions	71
CH	APTER 4	: APPLICATION TO KINEMATIC COUPLINGS	72
4.1.	INTROI	DUCTION	72
т.1.	4.1.1.	Presentation	
	4.1.2.	Background and Prior Work	
	4.1.3.	Tolerance Allocation	
4.2.	Матн	EMATICAL MODEL	
	4.2.1.	Parametric Representation of Contacting Surfaces	
	4.2.2.	Resting Position and Orientation	
	4.2.3.	Multivariate Error Analysis of Variation in Resting Location	83
	4.2.4.	Variation at Operating Points	
4.3.	Toler	ANCE ALLOCATION	
	4.3.1.	Manufacturing Cost and Tolerances	
	4.3.2.	Tolerance Allocation by Optimization	
	4.3.3.	Verification by Monte Carlo Simulation	
4.4.	CONCL	USION	95
CH	APTER 5	: CONCLUSIONS AND FUTURE WORK	96
5.1.	Concl	USIONS	96
5.2.		E Work	
API	PENDIX A	1:	98
PRO	OBABILI	TY DENSITY FUNCTION OF SUM OF SQUARES	98
API	PENDIX I	3:	101
MA	TLAB CO	DDES FOR KINEMATIC COUPLINGS	101
P 1		TION: OBJECTIVE FUNCTION	101
		TION: CONSTRAINT FUNCTIONS	
		TION: LONSTRAINT FUNCTIONS	
		ARLO SIMULATION	
		TION: KCT_BALLGEOM	
		TION KCT CENTROID	109

B7. Sub-function: kct_errors	111
B8. Sub-Function: kct_groovegeom	115
B9. Sub-Function: kct_perturb	118
B10. Sub-Function: kct_rest	
B11. Sub-Function: kct_seat	125
APPENDIX C:	128
DETERMINING THE HTM FROM A METROLOGY DATUM FRAME TO A CENTROII	
DETERMINING THE HTM FROM A METROLOGY DATUM FRAME TO A CENTROII	128

List of Tables

Table 2-1: 3D Symbols of Connections for Kinematic Diagrams (after ISO 3952-1)	8
Table 2-2: Comparison of Methods for Analyzing System Variability	23
Table 3-1: Variables Used in the 2D Parametric Model of the Connector	46
Table 3-2: Computed Tolerances for Exemplary Connector	62
Table 3-3: Statistics of 2D Geometric Parameters Describing Vee-Groove Variation	71
Table 4-1: Coefficients for Cost / Tolerance Relations	89
Table 4-2: Constraints Used for Exemplary Tolerance Allocation	93
Table 4-3: Computed Tolerances	93
Table 4-4: Comparison Optimization / Simulation	95

List of Figures

Fig 2-1: Kinematic Analysis of the Concept of a Spindle	10
Fig 2-2: Kinematic Analysis of the First Possible Architecture for the Spindle	11
Fig 2-3: Kinematic Analysis of the Second Possible Architecture for the Spindle	11
Fig 2-4: Kinematic Diagrams of Equivalent Contacts	12
Fig 2-5: Mapping of the Contacts in the Final Design of the Exactly Constrained Spin	
	12
Fig 2-6: Kinematic Diagram of the Final Design of the Exactly Constrained Spindle.	
Fig 2-7: Exactly Constrained Spindle Corresponding to the Presented Kinematic Ana	
	14
Fig 2-8: Flatness Specifications Transformed into Dimensional Tolerances	18
Fig 2-9: Flowchart of Least Cost Tolerance Allocation for Kinematic System	
Fig 3-1: Structure of an Optical Fiber	
Fig 3-2: Misalignments Generating Connection Losses Between Mating Fibers	
Fig 3-3: Optical Fiber Connector with Kinematically Designed Ferrules	
Fig 3-4: Flowchart of the Tolerance Allocation for Optical Fiber Connector	
Fig 3-5: Kinematic Analysis of the Exactly Constrained Connector	
Fig 3-6: 3D Kinematic Diagram of the Exactly Constrained Connector	
Fig 3-7: Male Ferrule in the <i>xy</i> -Plane	
Fig 3-8: 2D Model of a Perfect Fiber and a Real Fiber	
Fig 3-9: 2D Model of a Perfect Array of Fibers	
Fig 3-10: 2D Model of an Array of Fibers with Manufacturing Variations	
Fig 3-11: 2D Model of Mating Arrays of Fibers with Manufacturing Variations	
Fig 3-12: Different Possible Errors in a Cylindrical Feature	
Fig 3-13: 2D Parametric Representation of a Ferrule	
Fig 3-14: Location of a Random Cylinder in a Random Vee-Groove	
Fig 3-15: Shape of a Random Ferrule in 2D	
Fig 3-16: Experimental Determination of a Relation	
Fig 3-17: Outputs of Monte Carlo Simulation	
Fig 3-18: Computed Losses for Optimized Exemplary Connector	
Fig 3-19: Flowchart of Monte Carlo Simulation for Multi-Fiber Connectors	
Fig 3-20: Monte Carlo Simulation for Exemplary Connector with Optimized Toleran	
Fig 3-21: SEM Image of Micro Vee-grooves Following Wired EDM Operation	
Fig 3-22: Metallography Study of a Vee-Groove Produced with Wire EDM	
Fig 3-23: Metallographic Study of Coated Vee-Groove	
Fig 3-24: Point Cloud from Profilometry Traces	
Fig 3-25: 3D Profilometry Data Projected onto a 2D Plane for Comparison to Ideal	
Model	69
Fig 3-26: Manufacturing Errors in a Vee-Groove	
Fig 4-1: Three-Groove Kinematic Coupling	
Fig 4-2: Flowchart of the Tolerance Allocation for Kinematic Couplings	
Fig 4-3: Parametric Representation of Spherical and Flat Contacting Surfaces	
Fig 4-4: Solution for Resting Position and Orientation.	

Fig 4-5: Vector Loop Between Ball and Flat Surface	83
Fig 4-6: Coupled Kinematic Coupling with Operating Point	
Fig 4-7: Cost / Tolerance Relations for Dimensions	
Fig 4-8: Dimension Schemes for the Ball Pallet, in its Datum Frame	92
Fig 4-9: Dimension Schemes for the Groove Body, in its Datum Frame	92
Fig 4-10: Flowchart of Monte Carlo Simulation for Kinematic Couplings	

List of Files

Mbarraja.pdf	 1,497 KB

Chapter 1: Introduction and Thesis Overview

1.1. Background to the Thesis

Kinematic design is widely used in precision engineering. In effect, kinematic systems, also known as exactly constrained systems, present good repeatability if stiffness and load capacity are not critical parameters [1]. Moreover, the behavior of kinematic systems can be described in a mathematical model, since the location of the exact constraints are analytically defined by one unique solution [2]. It is then possible to develop an analytical tool that can help the designer of a kinematic system to make an optimized design [3].

On the other hand, kinematic design provides economical solutions for making repeatable assemblies. In effect, the design of kinematic systems is often relatively simple, and they can be easily manufactured. These good characteristics make the kinematic systems interesting for mass production, where they can be used in manufacturing, fixturing, and material handling. For instance, Vallance and Slocum [4] described the use of kinematic couplings for positioning pallets in flexible assembly systems.

However, a poor tolerance allocation may affect the precision of a kinematic system, despite its good repeatability. This is a major problem if the kinematic systems are intended for interchangeable assemblies, for instance a fixturing feature that is used on several workstations of a production line. Hence an efficient tolerance allocation is of primary interest for exactly constrained systems.

Teradyne Connection Systems (TCS), a manufacturer of daughtercard and backplane connectors, is developing a multifiber optical connector by following the kinematic design principles. This connector will be manufactured in mass production, so TCS wants to allocate the tolerances on this product so that its manufacturing cost is minimized while its required accuracy is preserved. Furthermore, the Precision Systems Laboratory of the University of Kentucky is conducting an extensive study on kinematic couplings; a tolerance allocation on these exactly constrained features could contribute to this wide analysis.

These two requirements have led to the development of a general approach for allocating tolerances on kinematic systems. This thesis is the result of this work. It describes the method in detail, with the different engineering principles used. Then the tolerance allocation is applied to the multifiber optical connector and the kinematic coupling for illustrating the developed method.

1.2. Prior Work and Literature Review

This section introduces the main principles of mechanics and mathematics with the corresponding relevant literature reviews that will serve as the background to the work done in this thesis. The materials covered are the exactly constrained systems, the dimensional variations of a manufactured part, and tolerance allocation using least cost optimization.

1.2.1. Exactly Constrained Systems

The principle of kinematic design states that point contact should be established at the minimum number of points required to constrain a body in the desired position and orientation [1]. In this case, the degrees of freedom of the rigid system are exactly constrained, so a mathematical model of the system can exactly predict its location. Prior studies used this property to develop analytical methods for designing kinematic systems.

One of the best examples is given by Schmiechen and Slocum [3], who published a design method using linear algebra to represent the geometry of a kinematic assembly. They could derive a simple expression for determining the error motions within the assembly in function of the applied forces. They could also quantify the stability of the kinematic system. This publication demonstrates that an analytical model of a kinematic system is a powerful tool for improving its design. A similar approach can be used to develop a variation study of the exactly constrained system.

Blanding [5] made an extensive study of the theoretical aspect of kinematic design. On a more practical point of view, the standard ISO 3952-1 [6] presents a convenient way to represent symbolically the kinematic links of a mechanical system,

and it is a powerful tool for the designer to determine whether a system is exactly constrained or not.

1.2.2. Dimensional Variations

Manufacturing perfect dimensions is impossible. In effect, it is well known that any manufacturing process is subject to variations, and the produced parts can't have exactly the same dimensions. Furthermore, the dimensions may change with time or environmental conditions, which can for instance generate wear or thermal expansion. This is the reason why a designer has to affect tolerances to the nominal dimensions, in order to specify the acceptable limits of the variations. The functionality of a part should be accepted if its dimensions stay within their assigned tolerances.

Tolerances can be either dimensional or geometric. If they are dimensional, they define the acceptable range of values that a length or an angle can get. If they are geometric, they put conditions on the shape of the part, such as flatness, roundness or angularity. Standards [7,8] cover this subject in detail and provide to the designer useful recommendations for assigning efficiently the tolerances.

Manufactured dimensions are hence subject to variations. It is then possible to express them as randomly distributed variables to analyze them through a mathematical model. Actually, the Statistical Process Control (SPC) method, widely used in industry for quality insurance, is based on this concept [9].

A thorough analysis of the geometry of a kinematic system should take into consideration these dimensional variations. The mathematical model of the system will set up the nominal value and the tolerances of the dimensions in terms of expected value and standard deviation of the corresponding random variables. The variation analysis of the kinematic coupling will then be based upon concepts from statistics.

1.2.3. Least Cost Tolerance Allocation

Chase [10] presented several relevant techniques for allocating tolerances on mechanical systems. The most efficient one is arguably the tolerance allocation using least cost optimization.

Studies have experimentally determined relations between cost and tolerance for different manufacturing processes since the 1940s [11]. Linear regressions of the measured data provide empirical functions describing these relations. By combining these functions to the mathematical model of the analyzed kinematic system, it is possible to determine the manufacturing cost of the system for a given accuracy.

Such a mathematical model can be implemented in a tolerance allocation routine. By using an optimization technique, the designer can assign the tolerances such that the manufacturing cost of the system is minimized while its functional requirements are respected. The tolerance allocation is then formulated as a minimization subject to constraints.

Some mathematical software packages include an optimization toolbox [12]. It is a convenient tool for solving optimization problems with multiple parameters, which can be faced in any discipline. The user has to implement the problem in an algorithm, by defining the objective and the constraints in a mathematical form.

If it is decided to optimize the design of a kinematic system by least cost tolerance allocation, the objective function is the manufacturing cost of the parts, which has to be minimized. The constraints are the mathematical expressions of the functional requirements of the product, which are generally directly related to the accuracy of the system.

1.2.4. Mathematics and Statistics

This thesis presents overall an analytical work, so it relies heavily on several topics from mathematics and statistics. Mathematical models of the exactly constrained systems are based on analytic geometry [13]. One of the methods for analyzing the variations of the system calls for homogeneous transformation matrices [1,14], then a

multivariate error analysis [15] is performed. A completely analytical model of the systems, which combines continuous random variables in non-linear relations, is another alternative for evaluating the location and orientation variations of a system; hence a reliable reference in engineering statistics is required [16]. In several cases, the methods resort to regression analyses [16] for fitting the experimental data. Finally, random simulations using the Monte Carlo method [17] are extensively used for estimating the statistics of the output parameters.

1.3. Thesis Overview

This thesis describes a method for allocating tolerances on kinematic systems. The objective is to find virtually the best combination of tolerances to set on an exactly constrained assembly in order to reduce its manufacturing cost related to its geometric and dimensional variations, while its functional requirement is respected.

1.3.1. Hypothesis

Prior work reviews show that a thorough analysis of kinematic systems can predict with accuracy their mechanical behavior [3,18]. On the other hand, there exist many methods for assigning tolerances to mechanical assemblies [19], with different levels of efficiency. Hence the hypothesis stipulates that it is possible to define a tolerance allocation method made especially for kinematic systems. Since this method would be based on exact analytical models, it should be better than the current tolerance allocations available for mechanical assemblies in general.

1.3.2. Content Overview

Chapter 2 describes the different concepts used in the method. It covers kinematic design theory, the manufacturing variations, and the principles of least cost tolerance allocation, with the corresponding mathematical tools. The developed method is applied to kinematically designed optical fiber connectors in Chapter 3. Then Chapter 4 presents the tolerance allocation procedure applied to kinematic couplings. Finally, Chapter 5 discusses future work and thesis conclusions.

Chapter 2: Concepts Used in the Method

2.1. Exactly Constrained Systems

2.1.1. Theory

Any motion of a free rigid body in a 3D space can be described as a combination of three pure translations and three rotations. Each of these six motion parameters is called a *degree of freedom*. They can be quantitatively described if a reference frame is attached to the space. In two dimensions, position and orientation of a free object are only defined by two translations and one rotation.

A body is constrained if at least one of its degrees of freedom is suppressed. A mechanical connection between two bodies suppresses one or more of their degrees of freedom. In a mechanical assembly, the degrees of freedom to be suppressed are defined by the functional requirements of the system. Robustness of the design of a mechanism is improved if only the degrees of freedom that need to be removed are constrained; if a motion can stay free, it is better not to constrain it.

Kinematic design theory [5] stipulates that a body is exactly constrained when every degree of freedom that has to be suppressed is blocked by one single constraint. If two or more constraints are suppressing the same degree of freedom, the system is overconstrained. In this case, position and orientation of the body is established by several conflicting references. Due to manufacturing variations and other sources of errors, these references cannot match perfectly. Consequently, an over-constrained body may not fit correctly in its assembly. If the dimensions are too loose, there will be an excessive clearance in the assembly that may affect the functionality of the mechanism; if they are too tight, the over-constrained body may satisfy the redundant constraints by enduring an elastic or plastic deformation that generates internal stress within the body. In both cases, repeatability of the assembly is affected.

Kinematic design offers some important advantages for precision engineering. Since every suppressed degree of freedom is restricted by one single constraint, there only exists one solution for determining the position and orientation of the constrained body. This property provides a good repeatability to the exactly constrained mechanism,

if the external conditions stay relatively constant. Kinematically designed assemblies can be manufactured at low cost, since their design is relatively simple and they don't need relatively tight tolerances to reach a good repeatability, compared to over-constrained mechanisms. Moreover, location of the exactly constrained body can be predicted by establishing a mathematical model of the assembly; there exists a straightforward correspondence between exact constraint and exact mathematical solution. The presented tolerance allocation method relies upon this characteristic.

However, kinematic design may not be a suitable solution for applications where mechanical loads are important. In effect, exact constraint design tends to minimize the area of the contacting surfaces, and then it increases tremendously the contact stress. Another design philosophy may be used to prevent these problems: *elastic averaging* intentionally over-constrains the bodies in order to carry larger loads [1]. Contact between parts is spread on broad surfaces, so contact pressure is reduced and stiffness of the system is increased. Manufacturing errors are averaged out, which may improve accuracy of the assembly, but tolerances have to be tight to obtain a good level of repeatability, which significantly increases the manufacturing cost of the system.

Exact constraint theory is therefore an adequate design tool for precision engineering when mechanical loads are not a critical parameter. Kinematic design provides a good repeatability at a relatively low cost.

The ideal scheme of exact constraints would be to suppress every degree of freedom by a punctual contact. However, practical considerations, like manufacturability of the parts or stiffness of the assembly, may prevent this theoretical scheme. Exact constraint theory is then completed by the definition of *connections*, which are the different possible combinations of constraints suppressing a set of degrees of freedom.

2.1.2. Types of Connection

When two bodies are mechanically connected, some of their degrees of freedom are constrained. The nature of their connection is defined by determining which motions are suppressed. An ISO standard [6] extensively describes the different types of connections, as presented in Table 2-1.

Table 2-1: 3D Symbols of Connections for Kinematic Diagrams (after ISO 3952-1)

Type of Connection	Symbol	Relative Motions Possible	Examples
Fixed		0 Rotation 0 Translation	Bolted assemblies; Welded parts
Pin		1 Rotation (x) 0 Translation	Spindle in its housing; Rotating wheel on fixed axis
Sliding		0 Rotation 1 Translation (x)	Translation stage
Helical		1 Rotation (x) 1 Translation (x) (correlated)	Screw in tapped hole
Cylindrical		1 Rotation (x) 1 Translation (x)	Cylinder in vee-groove
Joint	$\stackrel{z}{\swarrow}_{x}$ $\stackrel{y}{\diamondsuit}$	2 Rotations (<i>x</i> , <i>z</i>) 0 Translation	Universal joint
Spherical	$\stackrel{z}{\triangleright}_{x} \Phi$	3 Rotations 0 Translation	Sphere in cone
Planar	z y x	1 Rotation (z) 2 Translations (x,y)	Flat surface on flat surface
Ring		3 Rotations 1 Translation (<i>x</i>)	Sphere in vee-groove
Linear	z v x	2 Rotations (<i>x</i> , <i>z</i>) 2 Translations (<i>x</i> , <i>y</i>)	Cylinder on flat surface
Punctual		3 Rotations 2 Translations	Sphere on flat surface; Cylinder on perpendicular cylinder

Every elementary connection may be symbolically represented by a kinematic diagram. There exists a design procedure based upon these diagrams. By drawing the entire kinematic diagram of the mechanism, the designer can efficiently prevent redundant constraint and establish an exactly constrained system. This procedure starts by mapping the constraints between the different components. It consists in enumerating every part of the assembly, then identifying which degrees of freedom are suppressed by the connections in every pair of interacting parts. Creating a reference coordinate system is generally useful for determining the connections and preventing the redundant constraints. Afterwards the designer can draw the kinematic diagram of the assembly by representing the different connections with the corresponding symbol. It is also important to notice that a combination of elementary connections can constrain another degree of freedom that was not suppressed by the present elementary connections. For clarity, a figure separated from the overall kinematic diagram of the whole assembly can explain what the combination stands for; this is similar to a detailed view in an engineering drawing.

Kinematic diagrams may appear at different levels of the design. First of all, they can be used for modeling the *core concept* of the mechanism. At this point, the kinematic diagram should be the simplest one and does not necessarily represent all the components of the assembly. Basically, this first kinematic diagram should answer the question: "What is this mechanism for?" There should be only one kinematic diagram possible for representing the core concept of the system.

After defining the core concept of the mechanism, the following question is "How does it work?" New kinematic diagrams can then be established for representing the *architecture* of the system. Compared to the previous ones, these diagrams are more detailed and describe the connections between the interacting parts of the assembly. At this level, the designer can establish different diagrams, each of them illustrating a different type of possible architecture. Once a set of potential solutions is established, further engineering analyses will help to select the best architecture with respect to the functionality of the mechanism. Contrarily to the diagram corresponding to the core concept, which should be simple and fixed forever, the diagram representing an

architecture should be constantly improved by testing new possible combinations of connections and detailing every elementary link in the assembly.

The progressive revisions of the mechanism will finally lead to its *definitive version*. The corresponding kinematic diagram should accurately represent the system as it will be built, with all the most elementary parts and connections. It is the result of integrating all the physical and practical considerations in the chosen architecture; hence it should answer the question: "How is it made?" There should be only one possible kinematic diagram corresponding to the final version of the mechanism. A mathematical model of the system should be established by representing parametrically this last kinematic analysis.

2.1.3. Example of Kinematic Spindle

As an illustrative example, a kinematic analysis is performed on a kinematically designed spindle [18]. Exact constraint principles applied to this kind of device improve its accuracy and repeatability, compared to other existing spindle designs.

The concept of this mechanism is to allow only one rotation of the spindle in its housing. Let this degree of freedom be identified as the rotation about the z-axis. The assembly then constrains the three possible translations and the two other rotations. There is basically a pin contact between the spindle and its housing. The mapping and the kinematic diagram of the core concept of this assembly is presented in Fig 2-1:



Fig 2-1: Kinematic Analysis of the Concept of a Spindle

It is relatively difficult to make a direct pin contact between two parts. The assembly can be divided into a combination of elementary connections that constrain the same degrees of freedom. The designer has to pay attention not to constrain twice the

same degree of freedom; otherwise the system would be over-constrained. Two possible architectures equivalent to a pin contact are illustrated in Fig 2-2 and Fig 2-3.

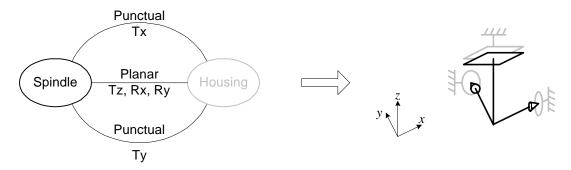


Fig 2-2: Kinematic Analysis of the First Possible Architecture for the Spindle

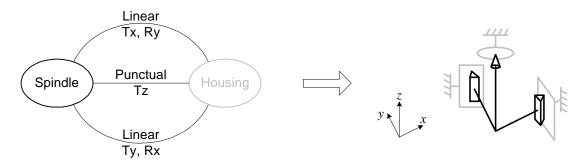


Fig 2-3: Kinematic Analysis of the Second Possible Architecture for the Spindle

An extensive study of the spindle showed that the second architecture was a better design in regard to its current applications [18]. The next step is to complete the design of the mechanism by incorporating practical considerations, like material choice or manufacturability. A direct punctual contact between the spindle and the housing has to be avoided to prevent excessive wear of the contact point. Inserting a steel ball between the two components is a better solution. This ball will punctually touch a flat surface of the housing, and it will be in spherical contact with a conic shape made in the spindle.

On the other hand, adding ceramic at the linear contacts would lower friction and consequently improve the quality of the mechanism. Each linear contact is then replaced by an equivalent combination of two parallel punctual contacts, made by positioning cylindrical ceramic rods perpendicularly to the axis of the cylindrical spindle. For simplifying the manufacturability of the mechanism, the ceramic rods are fixed by epoxy

to the housing. The equivalence of the contacts is illustrated in Fig 2-4. The mapping of the connections in the final design of the mechanism is established in Fig 2-5, while the corresponding kinematic diagram is modeled in Fig 2-6. Finally, an exactly constrained spindle following these kinematic principles is shown in Fig 2-7.



Fig 2-4: Kinematic Diagrams of Equivalent Contacts

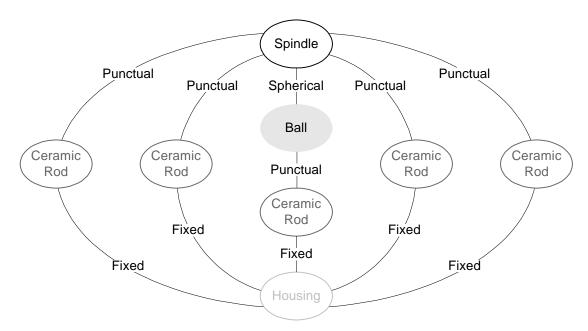


Fig 2-5: Mapping of the Contacts in the Final Design of the Exactly Constrained Spindle

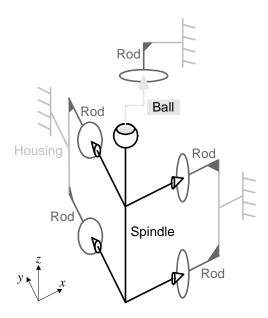


Fig 2-6: Kinematic Diagram of the Final Design of the Exactly Constrained Spindle

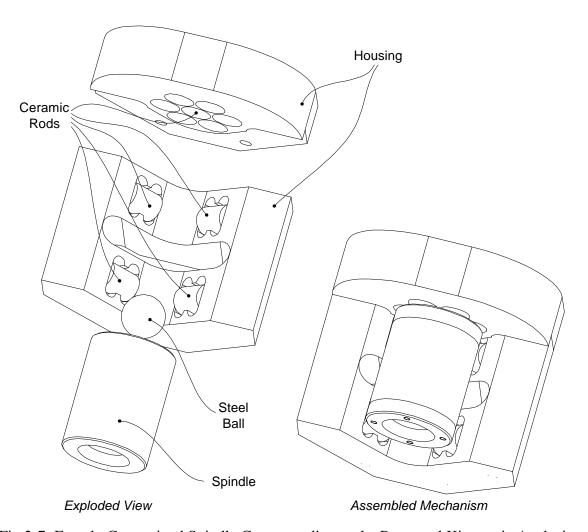


Fig 2-7: Exactly Constrained Spindle Corresponding to the Presented Kinematic Analysis

2.2. Manufacturing Variations

2.2.1. Presentation

2.2.1.1. Introduction

Manufactured dimensions cannot perfectly equal their nominal values, and manufactured shapes cannot present a perfect geometry. In effect, produced parts are subject to variations, coming from different sources, that will affect their accuracy. These dimensional and geometric errors should be taken into consideration when designing a system, so that the assembly can be mounted and the mechanism can fulfill its functional requirements despite these unavoidable variations. The designer has then to

define *tolerances* on the dimensions and the geometric specifications in order to define the range of values in which the variations stay acceptable. Some methods to analyze the combination of these variations will be introduced in this section. There also exist some well-known methods to control the manufacturing variations for a quality policy [20,21,22].

2.2.1.2. Sources of Variations

A first category of sources of errors comes from the manufacturing operation itself. Even if the manufacturing process is well controlled, there are always sources of variations that affect the accuracy of the parts. An improper mounting of the product on the machine will generate a misalignment with regard to its theoretical reference frame that will bring about errors in the part. Furthermore, manufacturing machines may have components with a noteworthy weight moving at relatively high speed; this is the case for most of the machines used in material removal processes. Inertia of these moving components will produce vibrations that will spread through the entire machine. There exist some isolation systems to prevent these vibrations, but a residual amount of noise that will reach the product and the operating parts of the machine will still remain. These vibrations will affect the accuracy of the operation and create manufacturing variations in the product.

A second type of sources of errors is related to time. One of the most notable sources of error varying with time is tool wear, which affects accuracy of a machining process throughout tool life. Moreover, adjustment of the machines modifies the set-up of the manufacturing processes; hence accuracy of a production may vary periodically, every time a set-up is adjusted.

Finally, environmental conditions are a third source of errors. For instance, change of temperature can affect relative positioning of the manufactured product and the operating parts of the machine because of thermal expansion. Purity of the working atmosphere can also have consequences for the accuracy of the manufacturing process. And variations in the structure of the row material in which the part is made may affect the quality of the final product.

These are the main sources of manufacturing variations, but there exist a lot of other ones that have a minor effect. Furthermore, there exist some random sources of errors that cannot be predicted.

2.2.2. Mathematical Representation

The tolerance allocation procedure needs a mathematical model of the variations in order to combine them and predict analytically their effects on the functional requirements of the mechanism. Statistics are used to model the manufacturing dimensions and their errors.

2.2.2.1. Dimensions as Random Variables

Most of the current methods for combining manufacturing variations implicitly define the produced dimensions as random variables following probability distributions [19]. The worst-case analysis, which is relatively simple to use, assumes that the dimensions follow a uniform distribution in a range bounded by the assigned tolerances. But more efficient yet complex methods state that the dimensions follow a normal distribution; the central limit theorem [16] justifies the suitability of such an assumption. The statistical process control (SPC) method, widely used in industry, relies upon this assumption [20]. The variables are assumed to be independent.

In statistics, a normally distributed variable is defined by its expected value that locates it and its standard deviation that characterizes its dispersion. On the other hand, a designer specifies a dimension by its nominal value and its tolerances. There are several ways to attribute a tolerance, but the simplest one may be to specify the nominal value plus or minus a deviation. Assuming that the manufacturing process is correctly controlled, the expected value equals the nominal dimension while the tolerancing deviation equals three times the standard deviation. In effect, this range of six standard deviations centered on the expected value covers 99.73% of the cases, and it is commonly accepted that it corresponds to the range limited by the tolerances on a technical drawing. These basic relations create a link between theoretical statistics and practical engineering specifications.

2.2.2.2. Mathematical Model of the Geometric Specifications

Dimensional tolerancing, which deals with lengths and angles, is generally not enough for specifying the acceptable variations of an assembly. It is also important to assign proper tolerances to the geometric features, with the design tools defined in the standards [7,8], because they are critical to part functionality. Variations in shape, orientation, and location will affect the variation of the complete assembly, so an efficient tolerance analysis has to take them into consideration. However, geometric tolerances as specified on a technical drawing cannot be included in a straightforward way in a tolerance analysis process. Geometric tolerances should therefore be broken into elementary dimensional specifications that can be quantified and combined in a variation analysis. Including geometric feature variations in a tolerance analysis is a current problem for computer-aided tolerancing programs [23]. However, a relatively simple method can be used manually, with a comprehensive analysis of the geometric specifications [24].

The geometrical feature variations are individually considered to be turned into dimensional tolerances. The modified representation of the geometric variation depends upon the type of kinematic connection between the assembled parts, identified with the method of the kinematic diagrams presented in Section 2.1. This means that different combinations of dimensional tolerances may represent the same type of geometric specification, depending on its required performance. The tolerances are set on the functional translations and rotations of the considered connection; the geometric specifications are then transformed into lengths and angles that can be easily inserted in the tolerance analysis.

For example, consider the same flatness specification used in two different cases, as illustrated in Fig 2-8. A flatness tolerance specifies a zone defined by two virtual parallel planes within which the surface must lie. In the first case, the flat surface is in contact with a ball; it is then a punctual contact that only suppresses a translation. The flatness specification may be transformed into a dimensional tolerance assigned to the suppressed translation. In the second case, a flat surface with the same flatness specification is in contact with a round pin; this time there is a linear connection that

constrains one translation and one rotation in the 3D space. The flatness specification may be turned into two dimensional tolerances, one for the acceptable stroke on the suppressed translation and the other one for the acceptable variation in the suppressed angle.

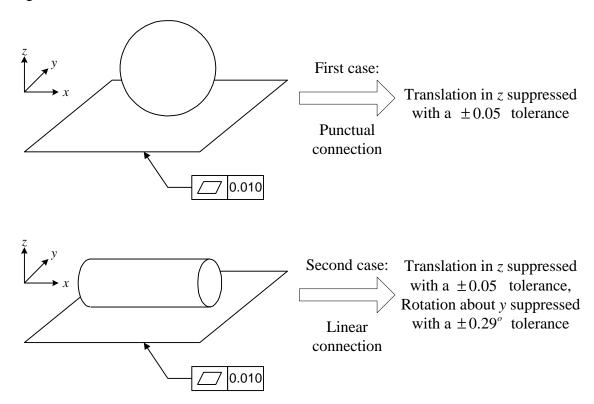


Fig 2-8: Flatness Specifications Transformed into Dimensional Tolerances

Geometric specifications may refer to virtual datum features. The advantage of the parametric model of the assembly is that this datum reference frame can be mathematically represented as if it were a real part of the assembly. However, if the geometric specification is subject to a thorough metrology control, it is better to model it so that it can be physically measured despite its virtual nature. For instance in Sections 3.2.2.4 and 4.3.2, the aperture angle of a vee-groove will be divided into two half-angles in order to have a physical way to measure the inclination angle of the vee-groove.

Finally, the designer should have in mind the manufacturing process with which the geometric feature is made in order to estimate the possible variations affecting its specification.

2.2.3. Methods to Analyze the Variations

There exist a variety of methods for combining the variations in a tolerance allocation procedure. Their suitability depends on the complexity of the mathematical model representing the assembly. An efficient method that analyzes the system variability should be repeatable to provide reliable results, computationally fast because tolerance allocation will use an iterative process, and as simple as possible for avoiding the mistakes when establishing it. This section presents the three different methods that are used in the examples detailed in the two next chapters.

2.2.3.1. Monte Carlo Simulation

One of the simplest methods for combining the manufacturing variations is arguably Monte Carlo simulation [17]. It consists in generating a lot of numeric experiments in which the outputs variables are calculated from a set of randomly distributed input variables. The programmer has to define the random distribution of the input variables, with their expected values and their standard deviations. The number of experiments generated should be big enough to determine with reliability the statistic parameters of the output variables.

Performing Monte Carlo simulation for a tolerance analysis is pretty straightforward. Once the mathematical model of the assembly is established, the assignable dimensions are generated as normally distributed variables, with a mean equal to their nominal dimension and the standard deviation equal to one third of their tolerancing deviation. Many assemblies are numerically generated with the mathematical model, and the resulting output values, which are the parameters affecting the performance of the system, are collected every time. The populations of output values are finally treated statistically in order to determine their distributions and their corresponding statistical parameters.

This method is relatively simple, once the mathematical model of the assembly is established: the input variables are generated simply, and they are combined in a direct way that is very close to reality. It is then quite easy to follow the elementary operations performed within the program and debug the eventual mistakes. However, computing time may be an issue on common computers. In effect, it is necessary to generate a great

number of experiments to get reliable results, and the required iterative loop may be very time consuming. This method is then used in the examples presented in Chapters 3 and 4 as a tolerance analysis to verify the results of more complex methods, but not for a tolerance allocation, for which processing time is a critical parameter.

2.2.3.2. Analytical Model

An alternative method for analyzing the assembly tolerances is to apply directly the law of error propagation [25] to the mathematical model of the system. The parametric model should be simple enough to return every performance parameter z_j with one single direct combination f_j of the n different input variables w_i , as shown in Eq (2-1). Assume that the input variables are independent.

$$z_{j} = f(w_{1}, w_{2}, w_{3}, \dots, w_{n})$$
(2-1)

The input variables w_i follow known probability distributions, with determined means \mathbf{m} and standard deviations \mathbf{s}_i . The expected value \mathbf{m}_{z_j} of the performance parameter z_j is simply calculated from Eq (2-2), while its standard deviation \mathbf{s}_{z_j} is obtained by using Eq (2-3).

$$\mathbf{m}_{z_i} = f_j(\mathbf{m}_1, \mathbf{m}_2, \mathbf{m}_3, \dots, \mathbf{m}_n)$$
 (2-2)

$$\mathbf{S}_{z_{j}}^{2} = \sum_{i=1}^{n} \left(\frac{\partial f_{j}}{\partial w_{i}} \right)^{2} \mathbf{S}_{i}^{2}$$
 (2-3)

The variation of the performance parameter is then expressed with one single equation. This analytical model of the resulting errors is appropriate for a tolerance allocation procedure, since calculations are relatively fast once the algorithm is established. However, the last equation requires the calculation of all the partial derivatives of function f_j , which may rapidly turn into huge mathematical entities difficult to manipulate, in accordance with the complexity of the function. This will affect the transparency of the algorithm.

The major problem of this method appears when the output variables are not perfectly independent. The current method does not calculate the correlation coefficients

between the different output variables, and it may be a penalty if they should be combined. A solution would be to determine an experimental approximation of the effect of these unknown correlation coefficients. This study may be done by regression analysis of results returned by Monte Carlo simulations of the performance of the assembly.

This method is used in Chapter 3 for determining the system variability of the 2D model of optical fiber connectors. An approximation of the effect of an unknown correlation coefficient existing between two output variables is illustrated in this example.

2.2.3.3. Multivariate Error Analysis

A third method for combining variations within a mechanical assembly is based on multivariate error analysis [15]. This method, derived from Taylor series expansion, is suitable for tolerance allocation because it can handle the calculation of a relatively large number of output variables resulting from the combinations of a large number of input variables [26]. It is for instance appropriate for allocating tolerances on the kinematic coupling presented in Chapter 4, for which 6 output variables result from 43 input parameters.

The analysis starts again from Eq (2-1). The corresponding Taylor series expansion presented in Eq (2-4) expresses the output parameter z_j as a function of the expected values, \mathbf{m} , and the errors, $\mathbf{D}w_i$, of the input variables.

$$z_{j} \approx f_{j}(\mathbf{m}_{1}, \mathbf{m}_{2}, ..., \mathbf{m}_{n}) + \Delta w_{1} \frac{\partial f_{j}}{\partial w_{1}} + \Delta w_{2} \frac{\partial f_{j}}{\partial w_{2}} + ... + \Delta w_{n} \frac{\partial f_{j}}{\partial w_{n}} + Higher \ Order \ Terms \ \ (2-4)$$

The basic definition of the error, \mathbf{d}_{z_j} , in the output parameter z_j is presented in Eq (2-5); then it is rearranged by inserting the Taylor series expansion, as shown is Eq (2-6).

$$\mathbf{d}_{z_j} = z_j - f_j(\mathbf{m}_1, \mathbf{m}_2, \mathbf{m}_3, \dots, \mathbf{m}_n)$$
(2-5)

$$\boldsymbol{d}_{z_{j}} = \Delta w_{1} \frac{\partial f_{j}}{\partial w_{1}} + \Delta w_{2} \frac{\partial f_{j}}{\partial w_{2}} + \ldots + \Delta w_{n} \frac{\partial f_{j}}{\partial w_{n}} + Higher \ Order \ Terms \tag{2-6}$$

Assuming that the higher order terms are negligible, this last equation returns a linear combination of the dimensional errors in the input variables. Consider that there

are m output variables; the complete set of linear transformations can be arranged in matrix form, as illustrated in Eq (2-7). The $m \times n$ matrix of partial derivatives is commonly referred as to the Jacobian matrix, [J].

$$\begin{bmatrix} \mathbf{d}_{z_1} \\ \mathbf{d}_{z_2} \\ \vdots \\ \mathbf{d}_{z_m} \end{bmatrix} = \begin{bmatrix} \frac{\partial z_1}{\partial w_1} & \frac{\partial z_1}{\partial w_2} & \dots & \frac{\partial z_1}{\partial w_n} \\ \frac{\partial z_2}{\partial w_1} & \frac{\partial z_2}{\partial w_2} & \dots & \frac{\partial z_2}{\partial w_n} \\ \vdots & \vdots & \ddots & \vdots \\ \frac{\partial z_m}{\partial w_1} & \frac{\partial z_m}{\partial w_2} & \dots & \frac{\partial z_m}{\partial w_n} \end{bmatrix} \begin{bmatrix} \Delta w_1 \\ \Delta w_2 \\ \vdots \\ \Delta w_n \end{bmatrix}$$

$$(2-7)$$

An advantage of the multivariate error analysis method is that exact expressions of the output variables are not necessarily required. In effect, the elements of the Jacobian matrix can be estimated numerically. This is done by perturbing individual input parameters from their expected value, virtually generating the consequent assembly, and then calculating the errors in the output parameters.

The input variables are actually the assignable dimensions, so it is simple to establish their covariance matrix, $[C_w]$, if their tolerances are known. A simple expression presented in Eq (2-8) relates the covariance matrix of the input parameters to the covariance matrix of the output variables, $[C_z]$.

$$[C_z] = [J][C_w][J]^T$$
 (2-8)

By extracting the errors from the diagonal of the resulting matrix $[C_z]$, the multivariate error analysis returns the variations in the output parameters as a function of the tolerances assigned to the input variables. This analysis can then be implemented in a tolerance allocation procedure.

2.2.3.4. Comparison of the Methods

As a synthesis, Table 2-2 presents a qualitative comparison of the three described methods. They are evaluated in accordance to their suitability in a tolerance allocation procedure. However, they may be used for other analyses.

Table 2-2: Comparison of Methods for Analyzing System Variability

	Monte Carlo Simulation	Analytical Model	Multivariate Error Analysis
Simplicity of establishing the algorithm, once the mathematical model is known	Good	Regular	Regular
Transparency of the algorithm, when bringing modifications or corrections	Good	Bad	Regular
Repeatability of the results	Good	Very good*	Very good
Computing speed	Very bad	Very good	Regular
Ability to allocate tolerances On simple assemblies	Regular	Very good	Good
Ability to allocate tolerances on complex assemblies	Bad	Regular	Good

* Subject to independence of output variables

In conclusion, Monte Carlo simulation is relatively easy to establish, but is not really suitable for tolerance allocation; it can be used to verify the results of the other methods by performing a tolerance analysis, though. The analytical model is very efficient if the assembly is not too complex; it presents great advantages, but also suffers notable drawbacks. Finally, multivariate error analysis provides a good compromise of computing characteristics that makes it very interesting for allocating tolerances in general.

2.3. Least Cost Tolerance Allocation

2.3.1. Introduction

First of all, it is important to note the difference between tolerance analysis and tolerance allocation. Tolerance analysis calculates the performance of a system for a given set of fixed tolerances, while tolerance allocation selects the tolerances to assign so that the system can satisfy its functional requirements. The objective of the presented work is to minimize the manufacturing cost of an exactly constrained system. This cost is affected by the values of the tolerances assigned to the different dimensions of the system. The current problem is then a *least cost tolerance allocation*.

On one hand, making tight tolerances increases the manufacturing cost of the system. On the other hand, if the tolerances are too large, the accuracy of the entire system may be so affected that it may not be able to fulfill its functional requirements anymore. A compromise between cost minimization and functionality of the product then has to be established. This can be done by finding the best set of tolerances that allows the system to keep respecting its functionality for the least cost possible. Hence the problem is expressed as a *minimization subject to constraints*. An optimization algorithm has to be established, in which the tolerances can be modified so that the manufacturing cost can be lowered while the performance of the system stays at an acceptable level.

Least cost tolerance allocation may be identified as a fundamental problem in industry: finding a balanced compromise between precision and mass production. In effect, precision is represented by the functional requirements of the system, while manufacturing cost is a major concern in mass production. The proposed way to solve this problem is an optimization procedure. However, optimization techniques may be used in many other disciplines or even other engineering analyses [27].

2.3.2. Tolerance Allocation by Optimization

The real difficulty when dealing with an optimization problem is its formulation for computational purposes. Once the different elements of the problem are identified and expressed in a mathematical form, it is relatively easy to write the corresponding algorithm, and some software packages can solve it with a specific optimization toolbox. This section presents the elements to identify in order to solve the current problem, which is a minimization subject to constraints.

The first entities to identify are the *design variables*. They are the quantifiable parameters that can be changed by the algorithm while looking for the optimized solution. These elements should be linearly independent in order to avoid conflicting solutions. In effect, if several specifications can define one single design variable, they may be contradictory when the optimization program is run, so it would be impossible to return a properly optimized value for the design variable concerned. In the current

problem, the design variables are the tolerances in the exactly constrained assembly. Assuming they are expressed as deviations from the nominal dimensions, their values should be positive. Moreover, for satisfying the independence requirement, one single value should represent a group of tolerances made by the same elementary manufacturing sequence. In effect, it is impossible to make different levels of tolerance during the same manufacturing process; so all the tolerances made by one sequence are strongly correlated.

The second feature to identify is the *objective* of the optimization. It is a function, depending on the design variables, that has to be optimized. For least cost tolerance allocation, the objective function is the manufacturing cost that has to be minimized. It should be expressed in terms of the values of the assignable tolerances; it is then necessary to establish mathematically some cost / tolerance functions. This topic will be discussed in the next section.

Finally, the system may be subject to *constraints*. They can be defined either as equalities or as inequalities, influenced by the design variables. Constraint functions are then bounded by limits, which are the functional requirements of the system. There may be multiple constraints, one for each requirement of the system. For the tolerance allocation problem, the constraints are expressed as inequalities. They are the deviations resulting from the combinations of the assignable tolerances, which are the design variables. These combinations are made with one of the different techniques presented in Section 2.2.3 that establish a mathematical model of the system. These final deviations characterize the performance of the system, so they shouldn't be greater than a defined limit, otherwise the system won't be able to fulfill its functional requirements.

2.3.3. Cost / Tolerance Relations

The objective function of the tolerance allocation procedure requires an expression of the manufacturing cost of the assembly as a function of the tolerances. It is then necessary to establish cost / tolerance relations. There exists a notable amount of publications dealing with this subject for metal removal processes. Chase [10] provides

an efficient synthesis of these studies, with empirical functions describing the relationships between tolerance and cost.

For material removal processes, the tolerances can be tightened or loosened by modifying the manufacturing parameters, such as feed, cutting speed, or depth of cut. Quality of tooling, of fixtures, and of cutting tools also affects the tolerances and the manufacturing cost. In addition, the workpiece may also be changed by selecting a more machinable alloy. All these parameters create a relation between tolerances and manufacturing cost. It is nearly impossible to predict analytically these relations; hence empirical models have to be established from experimental data.

The manufacturing cost of a dimension depends upon several parameters:

- The selected *manufacturing process*. The existing material removal processes don't produce the same tolerancing deviation for the same operating cost. Some of them are suitable for roughing operations, while other ones are adapted for finishing sequences. Moreover, some processes are only efficient for a given range of dimensions. A manufacturing cost should then be defined for every material removal process.
- The dimension's nominal value, also known as the *range*. It is more expensive to hold a given tolerance for a big dimension than for a smaller one. Cost / tolerance relations then depend upon the range of the manufactured dimensions.
- The assigned *tolerance*. Tightening tolerances increases cost. This is the design variable that can be modified to adjust the cost, once the nominal dimension is defined and the manufacturing process is selected.

Different sets of experiments were run while varying these three parameters, and the resulting cost was estimated. This cost was expressed in a relative way to eliminate the effects of inflation. The resulting experimental data were treated by a curve fit procedure to establish empirical relations. According to Chase's researches, the reciprocal power equation presented in Eq (2-9) looks to be an appropriate function to represent the variable part of cost / tolerance relations.

$$Cost = A \times \frac{Range^{a}}{Tolerance^{b}}$$
 (2-9)

where A, a and b are positive constants depending on the selected manufacturing process.

Once the design of the assembly is fixed and the manufacturing process is selected, it is possible to transform this equation into a direct relation between cost and tolerance. One function will then be specific to one assignable dimension.

Relations for material removal processes have already been established. However, cost / tolerance functions for other manufacturing processes have not yet been analyzed in a broad scope. Further investigation should be conducted in this field for establishing a complete analysis of the possible cost / tolerance relations.

2.4. Chapter Summary

Exact constraint theory, analysis of manufacturing variations, and concepts of optimization are used to establish a method for allocating tolerances to kinematic systems. The procedure can be divided into four major steps:

- Describe the geometry and dimensional variations in a mathematical form. This is done by establishing a parametric model of the assembly in order to characterize the performance of the system as a function of its manufacturing variations, as described in Section 2.2.2. This method is especially suitable for exactly constrained systems, as explained in Section 2.1.
- Combine dimensional variations within the assembly to estimate resulting variation in the system. Monte Carlo simulation, analytical modeling, and multivariate error analysis are some of the mathematical tools that can be used for performing this combination; they are presented in Section 2.2.3.
- Relate resulting variations to the performance requirements of the system. This is specific to the functionality of every system, so there is no general method that can be presented. However, the functional requirements of a mechanical assembly are related to the assembly variation, previously calculated.

• Relate dimensional tolerances to manufacturing cost. Since the problem is a least cost tolerance allocation, the objective is to minimize the cost of the system by adequately assigning its tolerances. Cost / tolerance relations are then needed; they are presented in Section 2.3.3.

These four steps are included in an optimization algorithm illustrated in Fig 2-1. This program varies the tolerances of the assembly in order to find the minimum manufacturing cost while respecting the functional requirements of the system. There exist different methods for combining the manufacturing variations. One should be selected advisedly, in accordance with the complexity of the system.

An optimization procedure is performed on one fixed design, for which the nominal dimensions and the manufacturing processes have been previously selected. Different design or manufacturing concepts can be compared by simply modifying the input data of the optimization, then comparing the resulting costs provided by the different tolerance allocations.

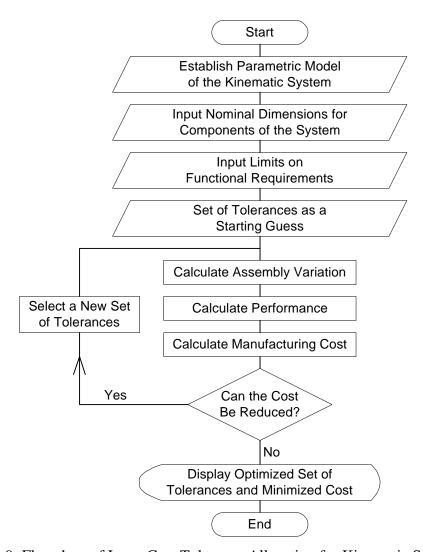


Fig 2-9: Flowchart of Least Cost Tolerance Allocation for Kinematic System

Chapter 3: Application to Optical Fiber Connectors

3.1. Introduction

3.1.1. Presentation

3.1.1.1. Fiber Optics

Until the 1980s, copper cables carried most electronic communication. Then optical fibers were introduced, where light signals replace the electrical ones. An optical fiber is a transparent rod, usually made of glass or clear plastic, through which light may propagate. Its structure consists of a *core*, where light travels, coated with a *cladding*, as illustrated in Fig 3-1. A jacket can eventually protect the fiber.

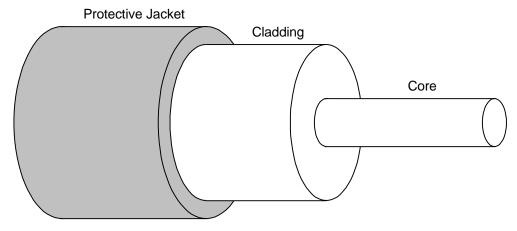


Fig 3-1: Structure of an Optical Fiber

The core and the cladding have different optical characteristics. The core refractive index is slightly greater than the cladding one; hence light stays inside the core and reflects against the core/cladding interface. For typical communication fibers, the cladding diameter is $\sim 125~\mu m$. The core diameter can vary a lot, depending on the nature of the fiber. For multimode fibers, in which light propagates in many modes, the core diameter is commonly $\sim 50~\mu m$. For single-mode fibers, the core diameter can vary from 5 to 12 μm .

Fiber optic communication presents numerous advantages compared to other communication methods [28]:

- Transmission loss is relatively low; thus long-distance transmission is possible without using a costly amplification system,
- Fiber is lighter than copper cable,
- An optical fiber can carry more information than an equivalent copper cable can,
- There is a complete electrical isolation between the sender and the receiver,
- There is no interference in the transmission of light from electrical disturbances or electrical noise,
- Optical fiber is more reliable, since it is not subject to corrosion and can better withstand environmental conditions,
- Communication is more secure since it is impossible to intercept the light signal from outside,
- The manufacturing cost of a fiber optic communication system is lower than the cost of an equivalent cable communication system.

3.1.1.2. Transmission Losses

As shown in Eq (3-1), transmission coefficient (T) is defined as the ratio of the output signal power (P_{out}) over the input signal power (P_{in}), where both powers are expressed in the same units while the transmission coefficient is a non-dimensional number.

$$T = \frac{P_{out}}{P_{in}} \tag{3-1}$$

It is often convenient to express signal loss in decibels, with the relation given in Eq (3-2). Since the transmission coefficient T is a number between 0 and 1, loss in decibels is always a negative number. However, it is common to talk only of its absolute value because loss implies the negative sign.

$$Loss_{dB} = 10 \times \log_{10} \left(\frac{P_{out}}{P_{in}} \right)$$
 (3-2)

Transmission loss is relatively low in fiber optic communication. In effect, a common copper cable reduces the signal power to ~ 1% of its input value after one kilometer, which represents a 20 dB loss, while a non-interrupted single-mode fiber can typically carry up to 96% of the signal on the same distance, which corresponds to a 0.16 dB loss. Signal loss increases with fiber length, so for comparison purposes, most of the calculations refer to a standard length of one kilometer.

There exist three main sources of light loss in a fiber [28]:

- *Material loss*. Absorption occurs when light interacts with the molecular structure of the material. Impurities inside the fiber may increase this signal loss.
- *Light scattering*. Molecules, impurities and structural imperfections of the material scatter light, which stops propagating and is lost.
- *Bend loss*. In practical applications, an optical fiber never follows a straight line but instead is curved. If the radius of curvature is too small, light can't reflect correctly on the core/cladding interface and is dissipated.

These losses are wavelength dependent. For most applications, the greater the wavelength, the lower the loss, but some applications need a specific wavelength. These losses occur inside the fiber. On the other hand, connection losses generally have more important consequences. For instance, a lateral misalignment of 1 micron between two connected single-mode fibers generates a 0.21 dB signal loss.

As illustrated in Fig 3-2, there exist three types of connection losses [28] that are directly related to the positional manufacturing errors within the connectors:

- Lateral misalignment is due to the offset of the centerlines of the mating fibers,
- End-separation misalignment comes from the gap between the ends of the connected fibers,
- And finally, *angular misalignment* occurs when there exists an angle between the two axes of the fibers.

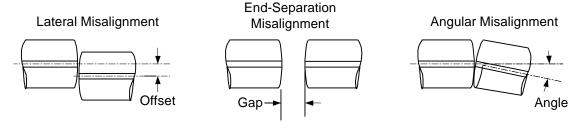


Fig 3-2: Misalignments Generating Connection Losses Between Mating Fibers

Every one of these misalignments generates a loss that can be calculated thanks to analytical formulae found in literature [29]. The lateral misalignment is of most concern for connection loss since angular misalignment is negligible and end-separation is usually resolved by mechanical contact between the fibers or index-matching compounds. Optical fiber connectors should then limit in priority this kind of misalignment in order to improve efficiently their performance.

Polishing the end surfaces of the fibers is also important for limiting connection loss. In the current study, it is assumed that the quality of the polishing operation is ood enough to ignore the resulting connection loss compared the one generated by the lateral misalignment.

3.1.1.3. Optical Fiber Connectors

Most of the mass-produced connections for optical fibers are made by mechanical connectors, which are separable and relatively economical. However, these devices have to be manufactured accurately to align correctly the fiber cores.

A common type of array connector is an assembly of two mechanically transferable (MT) ferrules aligned by pins. An MT ferrule holds the fibers in position by locating features such as cylindrical channels or vee-grooves. An aligning pin is housed in a cylindrical hole of a theoretically equal diameter, but manufacturing variations for the pin and the MT ferrule make this purely theoretical equality impossible. If the diameter of the hole is greater than the diameter of the pin, there is a clearance between them and the assembly is under-constrained. If the hole has a smaller diameter than the pin, the system is over-constrained and there is an elastic or plastic deformation of the

components that affects their accuracy. In both cases, precision of the alignment is notably affected.

A solution to avoid these effects is to design the ferrules so that the components are exactly constrained when assembled together. The concept of the connector is illustrated in Fig 3-3. A kinematic analysis of this assembly is presented in Section 3.2.1.

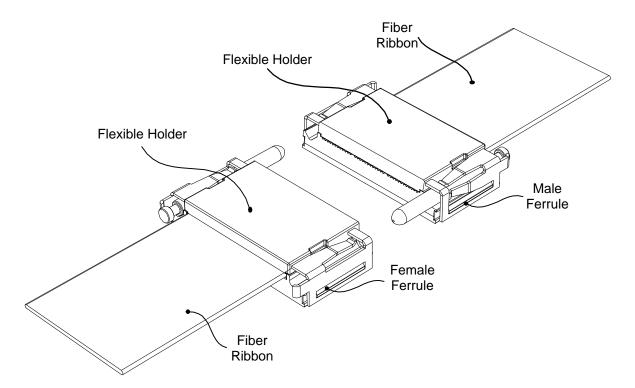


Fig 3-3: Optical Fiber Connector with Kinematically Designed Ferrules

These connectors are used in a *passive alignment* configuration: the fibers are directly put into the ferrules to be aligned; no improvement system is applied to correct their positioning; therefore the lateral misalignment between two mating fiber cores depends directly on the dimensional and geometric variations of the components.

3.1.2. Background and Prior Work

Transmission loss is a major issue when connecting optical fibers. When fiber optics communication was introduced, most of the current manufacturing processes couldn't attain the precision required for making mechanical connectors that could

provide a reasonable coupling efficiency by simply aligning two fibers. Some sophisticated techniques were then developed. For instance, lenses could expand the light beam at the end of the cores [30], micro actuators could improve the fiber alignment [31], or the core diameters could be artificially increased by thermal expansion [32]. However, these techniques substantially increase the manufacturing cost of the connectors.

Recent developments in manufacturing have made possible the production of mechanical connectors capable of positioning the fibers with suitable accuracy [33]. The resulting passive alignment is now so efficient that it is possible to avoid the correcting systems previously mentioned. This solution is a way to reduce the number of parts within the connector, and consequently its manufacturing cost.

Production of optical fiber connectors can involve various manufacturing processes, like injection molding [34], LIGA technique [35] or etching [36], and different materials [37,38]. Manufacturing variations are a critical issue in connector design [39]. In effect, manufacturing errors generate misalignments that increase transmission loss [29]. Prior research performed tolerance analyses on MT ferrules using Monte Carlo simulation [40] or analytical techniques [41].

This chapter describes a tolerance allocation technique for kinematically designed connectors which is more efficient than the existing methods used for MT ferrules. The developed procedure is based upon an exact mathematical model of the connector, which improves the reliability of the method. The technique has been experimented with Matlab* scripts. Monte Carlo simulations, also computed in Matlab, have been built to verify the results of the tolerance allocation.

3.1.3. Tolerance Allocation

A rigorous tolerance allocation performed on the exactly constrained connector is based upon a four-step algorithm, as described below.

35

^{*} Matlab for Windows is software from The MathWorks, Inc., 24 Prime Park Way, Natick, MA.

- Describe the geometry and dimensional variations in a mathematical form. A parametric model for every component of the connector is established as a function of the nominal dimensions and the corresponding dimensional variations. Since the design of the current connector follows the exact constraint theory, a kinematic analysis of the connections among the different parts supplies a unique solution for the respective location of the components. This solution, accurate and reliable, can be expressed mathematically in a parametric model of the whole assembly.
- Combine dimensional variations in the connector to estimate misalignment of mating fibers. The dimensional variations of the connector are directly related to its assigned tolerances. The dimensional errors within the connector generate a misalignment between the mating fibers. Applying the law of error propagation on the mathematical model of the assembly provides an analytical relation between dimensional variation and fiber misalignment. The unique solution of the mathematical model due to the exact constraint theory makes this approach possible.
- Relate assembly variations to the performance requirements of the connector. The performance of a connector is defined by its capacity to transmit light with as little loss as possible. Connection losses dependent on a mechanical connector are directly related to the misalignments generated by the manufacturing errors of the components. When considering realistic manufacturing variations, lateral misalignment is the most critical parameter. The lateral misalignment between two mating fibers therefore characterizes the performance of a connector. Since the present connector aligns arrays of multiple fibers, its performance will be defined with regard to the maximum misalignment observed in the whole array.
- Relate dimensional tolerances to manufacturing cost. This connector will be mass-produced; hence its manufacturing cost has to be minimized. The magnitude of the acceptable lateral misalignment determines the manufacturing processes that should be used for making the connector. Once the production sequence is selected, it is possible to express the manufacturing cost as a function of the assigned tolerances using cost-tolerance functions.

The algorithm presented in Fig 3-4 includes these four steps. The law of error propagation, applied to the mathematical model of the connector, returns an analytical relation between lateral misalignment and manufacturing tolerances. In parallel, cost-tolerance functions are used to calculate the resulting manufacturing cost. The process is implemented in an optimization loop.

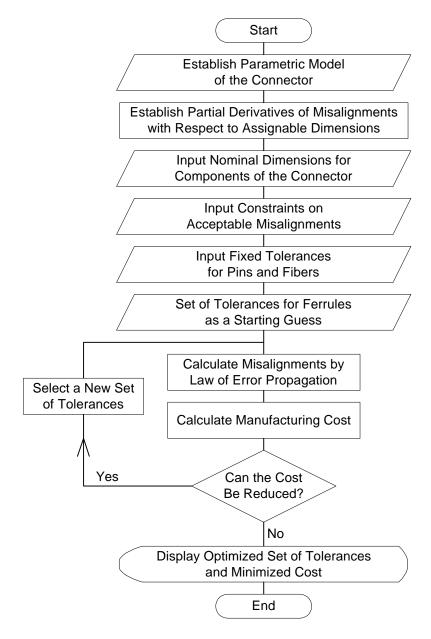


Fig 3-4: Flowchart of the Tolerance Allocation for Optical Fiber Connector

3.2. Mathematical Model

3.2.1. Exact Constraints Within the Connector

The exactly constrained connector follows the rules of kinematic design theory. The main requirement of this feature is two align mechanically two arrays of fibers. Every fiber is located in a vee-groove: there is a cylindrical contact between a fiber and its corresponding ferrule. The two ferrules are aligned by two pins. The male ferrule is connected to the first pin by a vee-groove, and to the second pin by two planes; in both cases, it is a cylindrical contact. The female ferrule has a different design to avoid redundant constraints. In effect, a vee-groove still makes a cylindrical contact between the first pin and the ferrule, but a single plane is touching the second pin for making a linear contact. Finally, the different elements are maintained in position by flexible clips. The corresponding kinematic mapping of the connector is illustrated in Fig 3-5, while its kinematic diagram is represented in Fig 3-6 with four pairs of fibers.

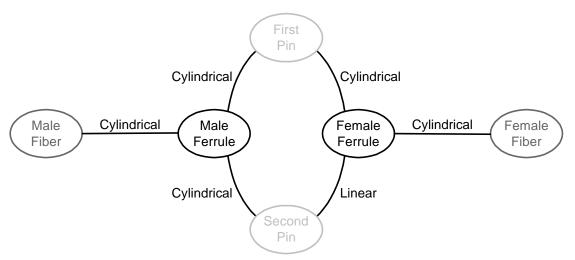


Fig 3-5: Kinematic Analysis of the Exactly Constrained Connector

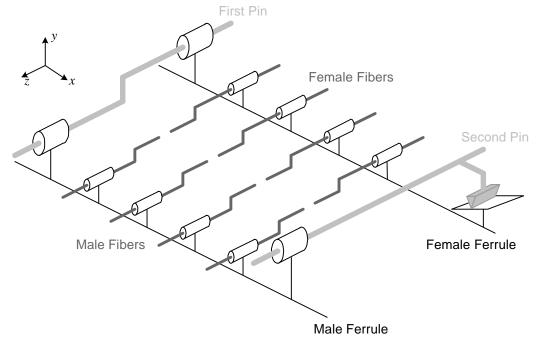


Fig 3-6: 3D Kinematic Diagram of the Exactly Constrained Connector

As discussed previously, lateral misalignment is the major source of transmission loss in mechanical connections. A 2D model of the connector is then a reasonable approximation for representing its geometry. The modeling plane is the *xy*-plane, *z* being the direction along the axes of the fibers. The geometry of the male ferrule is illustrated in the plane perpendicular to the axes of the fibers in Fig 3-7.

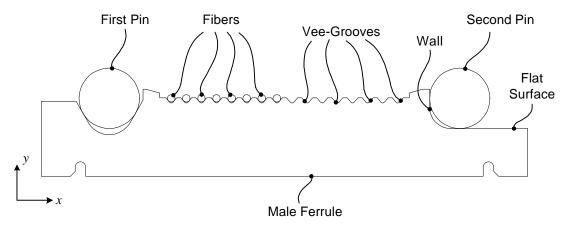


Fig 3-7: Male Ferrule in the xy-Plane

In the 2D configuration, it is possible to establish a direct mathematical relation between the variation of the dimensions in the ferrules and the lateral misalignment between two mating fibers. Since the components are exactly constrained, there is a unique solution for the location of a connection point between two features.

3.2.2. Parametric Model of the Components in the Connector

3.2.2.1. Presentation

The tolerance allocation process is based upon a mathematical model of the assembly that includes the dimensions of the components and their respective variations due to the manufacturing errors. These variations appear at different levels of the assembly. First of all, the fibers have variations that can be represented in 2D as shown in Fig 3-8. If the fiber is perfect, its core and its cladding are concentric and perfectly circular with known diameters. But in a real case, the manufacturing errors affect the dimensions and the shape of a fiber.

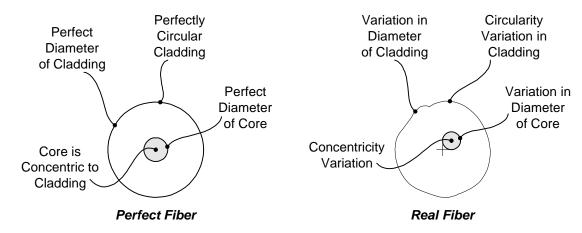


Fig 3-8: 2D Model of a Perfect Fiber and a Real Fiber

The defects previously presented are only for individual fibers. The variations of the ferrules and the alignment pins will also affect the accuracy of the alignment of a whole array of fibers. In theory, this array is a perfectly straight line with a constant pitch between two successive fibers, as illustrated in Fig 3-9. Manufacturing errors in the different components of the connector induce variations in the positioning of the fibers within the array. Fig 3-10 presents some relevant variations that can happen in an array because of the manufacturing errors.

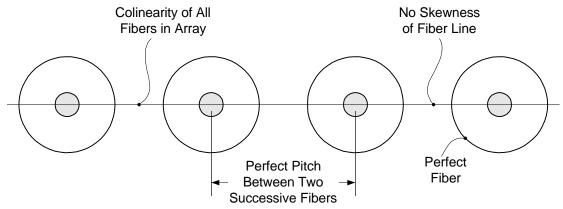


Fig 3-9: 2D Model of a Perfect Array of Fibers

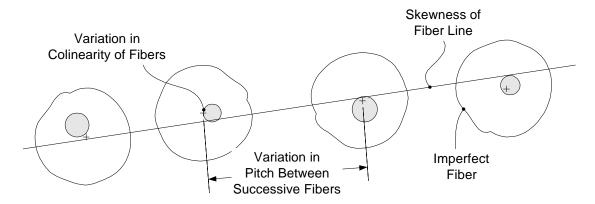


Fig 3-10: 2D Model of an Array of Fibers with Manufacturing Variations

Finally, the function of a connector is to mate two arrays of fibers. Both arrays have their dimensional and geometric variations, as explained before. When mating the arrays, the errors in the fibers, the ferrules, and the alignment pins are combined and produce a lateral misalignment in every pair of mating cores, as shown in Fig 3-11. The parametric model to be established should calculate this lateral misalignment as a function of the manufacturing errors within the different components of the connector, by mathematically expressing this combination of variations.

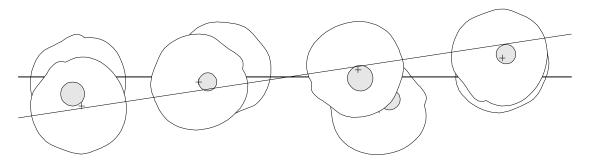


Fig 3-11: 2D Model of Mating Arrays of Fibers with Manufacturing Variations

The manufactured dimensions are interpreted as variables in the mathematical model. This section presents how the different components with their respective errors are parametrically represented. Since a statistical treatment will be performed on the mathematical model, the dimensions subject to manufacturing errors are expressed as randomly distributed variables, with an expected value equal to their nominal dimension and a standard deviation related to their assigned tolerance. Identification of their distribution is important too.

3.2.2.2. Pins and Fiber Claddings

Two pins align the ferrules, and the fibers are located by vee-grooves. These cylindrical features are represented by circles in the 2D model. The diameter is the only dimension that is important for positioning the fibers, since the length of the pins is not taken into consideration in the 2D model. The diameter can vary by its scalar dimension, represented by its magnitude, or by its geometry, defined by its non-circularity, as illustrated in Fig 3-12.

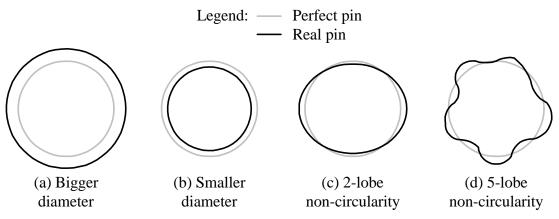


Fig 3-12: Different Possible Errors in a Cylindrical Feature

Knowing the radius of a cylinder is particularly important at the two contact points with the corresponding vee-groove. The parametric model of a random cylinder first defines its average radius as a normally distributed variable: this deals with the strictly dimensional variation of the feature. Then at both contact points, the average radius is multiplied by a random coefficient that stands for the non-circularity of the feature: this is its geometric variation. This coefficient is a normally distributed variable, with an expected value of 1.

3.2.2.3. Cores of Fibers

A fiber is aligned by its cladding in contact with a vee-groove of the ferrule. But light is transmitted through the core of the fiber. Thus the errors of the core position relative to the cladding should be taken into consideration.

In a perfect fiber, the core is exactly concentric to the cladding. In a real one, there may be an eccentricity that can be quantified by the fiber manufacturer. The mathematical model represents this eccentricity with two parameters: its magnitude, which is a normally distributed variable whose expected value equals 0, and its location angle, which is a uniformly distributed variable varying from 0 to 180 degrees. Note that it is not necessary to distribute this angle on a 360-degree range, since the normally distributed magnitude can have a negative value.

Geometry of the core itself can also vary. Its diameter is expressed as a normally distributed variable. Its non-circularity has a negligible effect on the transmission loss,

compared to the other sources of errors. Then a core is assumed to be perfectly circular; this approximation simplifies the mathematical model without affecting its accuracy.

3.2.2.4. Ferrules

The fibers tolerances are determined by industry standards. On the oter hand, it is possible to control the tolerances on the ferrules and the pins to reduce production cost while respecting the functional requirements of the connectors. The geometry of a ferrule is parametrically represented in 2D by a set of lengths and angles, as illustrated in Fig 3-13. All these dimensions are normally distributed variables in the mathematical model.

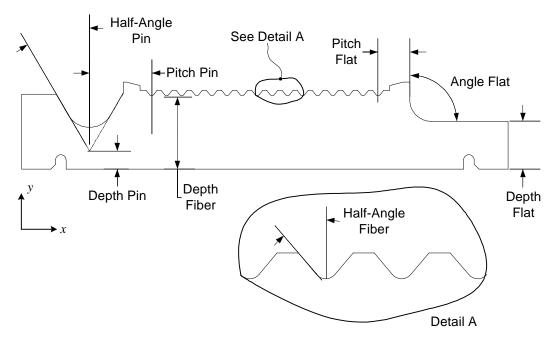


Fig 3-13: 2D Parametric Representation of a Ferrule

Distances in the *x*-direction between vee-grooves are referred to as pitches. A complete parametric model of the ferrule requires three pitches: pitch between the pin vee-groove and the closest fiber vee-groove (identified as "Pitch Pin" in Fig 3-13), pitch between two successive fiber vee-grooves ("Pitch Fiber"), and finally pitch between the wall positioning the second pin and the closest fiber vee-groove ("Pitch Flat").

Since these dimensions only locate the grooves in the *x*-direction, another set of lengths is needed for positioning them in the *y*-direction. These dimensions are called "depth," and they represent the distance between the vertex of a vee-groove and a datum

plane, shown as the bottom of a perfect ferrule in Fig 3-13. The vertex of a groove is actually a virtual point, since it is hidden by the radius of curvature present at the bottom of the groove. Once again, there are three different dimensions for the whole ferrule. The first depth is used by the pin vee-groove ("Depth Pin"). The second one locates the fiber grooves ("Fiber Depth"). The third one is finally the distance between the datum plane and the flat surface positioning the second fiber ("Depth Flat"). This flat surface is modeled in the parametric representation as perfectly parallel to the datum plane; any form variation of the surface, such as flatness error or parallelism error, is included in the variation of the depth. This statement is acceptable because the pin and the ferrule are exactly constrained, so their contact is reduced to one single point in the 2D representation.

The parametric model of the ferrule is completed by the angles of the veegrooves. These features are used to locate the first pin and the fibers. Two angles affect the accuracy of a vee-groove: its aperture angle, and its inclination angle, which is the angle between its bisector and the *y*-axis. Metrology applied to a ferrule cannot directly measure the value of the inclination angle, so it was decided to represent the vee-groove as a combination of two half-angles. The aperture angle is defined as the sum of the two half-angles while the inclination angle is calculated as half their difference. Hence the parametric model uses half-angles for the pin vee-grooves ("Half-Angle Pin") and for the fiber grooves ("Half-Angle Fiber").

The second pin is positioned in the male ferrule by a flat surface and a wall. The mathematical model combines these two surfaces to define them as a single vee-groove. However, since the flat surface is defined as perfectly parallel to the *x*-direction, there is no need to model an inclination angle for this groove. Its aperture angle ("Angle Flat") is sufficient to represent mathematically its geometry and the related variations.

3.2.2.5. List of the Variables

The previous sections present how the variables included in the parametric model of the connector are defined. Table 3-1 summarizes these randomly distributed variables with their respective distributions.

Table 3-1: Variables Used in the 2D Parametric Model of the Connector

	Dimension	Distribution	
Pin	Average diameter	Normal	
	Non-circularity	Normal centered on 1	
Fiber	Average diameter of cladding	Normal	
	Non-circularity of cladding	Normal centered on 1	
	Diameter of core	Normal	
	Magnitude of core eccentricity	Normal centered on 0	
	Angle of core eccentricity	Uniform on a 180-degree range	
Ferrule	Pitch between pin and closest fiber	Normal	
	Pitch between two successive fibers	Normal	
	Pitch between wall and closest fiber	Normal	
	Depth of pin vee-groove	Normal	
	Depth of fiber vee-groove	Normal	
	Depth of flat surface	Normal	
	Half-angle of pin vee-groove	Normal	
	Half-angle of fiber vee-groove	Normal	
	Angle between wall and flat surface	Normal	

3.2.3. Mathematic Description of the Geometric Model

3.2.3.1. Assembly of a Random Cylinder Inside a Random Vee-Groove

Knowing the real location of a cylindrical feature in a vee-groove is of primary interest for modeling the geometry of the connector, since the pins and the fibers are located by vee-grooves. The advantage of such an assembly is that the resting position of the cylindrical feature is defined by only two lines, which is equivalent to an exact constraint for a 2D model. Hence there can only be one resting position for one given cylinder and one vee-groove if the effects of friction and stiffness of the features are neglected. The geometry of a non-round cylinder in a real vee-groove is illustrated in Fig 3-14.

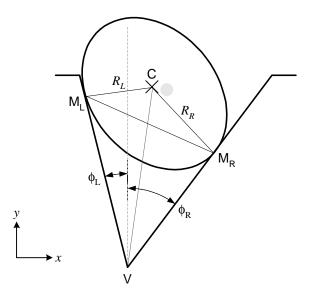


Fig 3-14: Location of a Random Cylinder in a Random Vee-Groove

The geometry of the groove is defined by two angles: \mathbf{f}_L is the angle between the left edge of the vee-groove and the vertical, and \mathbf{f}_R is the one for the right side. The non-round cylinder (pin or fiber) is put inside the vee-groove. C is the center of the non-round cylinder. V is the vertex of the vee-groove. M_L and M_R are respectively the contact points of the cylinder with the left edge of the vee-groove and with the right edge. Consequently, CM_L and CM_R are respectively the radii of the cylinder on the left side and on the right side. The goal is to find the coordinates of vector \overrightarrow{CV} . The known dimensions are the radii CM_L and CM_R , and the angles \mathbf{f}_L and \mathbf{f}_R .

At the contact points M_L and M_R , the non-round cylinder locally acts like a perfect cylinder, so the edges are perpendicular to the respective radii at these contact points, which gives Eqs (3-3)-(3-4):

$$\angle VM_L C = \frac{\mathbf{p}}{2} \tag{3-3}$$

$$\angle CM_R V = \frac{\mathbf{p}}{2} \tag{3-4}$$

From the geometry of triangle (CM_LM_R) , we can get the relation shown in Eq (3-5):

$$M_L M_R = \sqrt{CM_L^2 + CM_R^2 - 2 \cdot CM_L \cdot CM_R \cdot \cos(\angle M_R CM_L)}$$
 (3-5)

On the other hand, the geometry of quadrilatere (CM_LVM_R) provides Eq (3-6):

$$\angle M_L C M_R = 2 \mathbf{p} - \angle M_R V M_L - \angle C M_R V - \angle V M_L C$$
(3-6)

Inserting Eqs (3-3)-(3-4) in Eq (3-6) gives Eq (3-7):

$$\angle M_{I}CM_{R} = \mathbf{p} - \angle M_{R}VM_{I} \tag{3-7}$$

Trigonometric relations applied to Eq (3-7) leads to Eq (3-8):

$$\cos(\angle M_L C M_R) = -\cos(\angle M_R V M_L) \tag{3-8}$$

Eq (3-9) is obtained by expressing Eq (3-8) in terms of the known dimensions:

$$\cos(\angle M_L C M_R) = -\cos(\mathbf{f}_L + \mathbf{f}_R) \tag{3-9}$$

Eq (3-5) can now be modified by inserting Eq (3-9) to become Eq (3-10):

$$M_L M_R = \sqrt{CM_L^2 + CM_R^2 + 2 \cdot CM_L \cdot CM_R \cdot \cos(\mathbf{f}_L + \mathbf{f}_R)}$$
 (3-10)

This equation fully defines the length M_LM_R with respect to known dimensions.

The next step deals with the geometry of triangle (CM_LM_R), which provides Eq (3-11):

$$\cos(\angle M_R M_L C) = \frac{CM_L^2 + M_L M_R^2 - CM_R^2}{2 \cdot CM_L \cdot M_L M_R}$$
(3-11)

Inserting Eq (3-10) in Eq (3-11) gives Eq (3-12), and by simplification Eq (3-13):

$$\angle M_R M_L C = \arccos\left(\frac{2 \cdot C M_L^2 + 2 \cdot C M_L \cdot C M_R \cdot \cos(\mathbf{f}_L + \mathbf{f}_R)}{2 \cdot C M_L \cdot M_L M_R}\right)$$
(3-12)

$$\Rightarrow \angle M_R M_L C = \arccos\left(\frac{CM_L + CM_R \cdot \cos(\mathbf{f}_L + \mathbf{f}_R)}{M_L M_R}\right)$$
 (3-13)

This last equation fully defines the value of angle $\angle CM_LM_R$ with respect to known dimensions.

Then the geometry of rectangle triangles (VM_LC) and (VM_RC) are taken into consideration to establish Eq (3-14)-(3-15):

$$VM_{I}^{2} + CM_{I}^{2} = VC^{2} {3-14}$$

$$VM_R^2 + CM_R^2 = VC^2 (3-15)$$

Combining these two equations results in Eq (3-16):

$$VM_{R}^{2} = VM_{L}^{2} + CM_{L}^{2} - CM_{R}^{2}$$
 (3-16)

At the same time, the geometry of triangle (VM_LM_R) is used to establish Eq (3-17):

$$VM_{R}^{2} = VM_{L}^{2} + M_{L}M_{R}^{2} - 2 \cdot VM_{L} \cdot M_{L}M_{R} \cdot \cos(\angle VM_{L}M_{R})$$
 (3-17)

Equality of Eq (3-16) and Eq (3-17) results in Eq (3-18):

$$M_L M_R^2 - 2 \cdot V M_L \cdot M_L M_R \cdot \cos(\angle V M_L M_R) = R_L^2 - R_R^2$$
 (3-18)

Eq (3-19) is obtained by inserting Eq (3-10) in Eq (3-18):

$$CM_L^2 + CM_R^2 + 2 \cdot VM_L \cdot M_L M_R \cdot \cos(\mathbf{f}_L + \mathbf{f}_R)$$

$$-2 \cdot VM_L \cdot M_L M_R \cdot \cos(\angle VM_L M_R) = CM_L^2 - CM_R^2$$
(3-19)

Trigonometric relations establish Eq (3-20):

$$\cos(\angle VM_L M_R) = \cos\left(\frac{\mathbf{p}}{2} - M_R M_L C\right) = \sin(\angle M_R M_L C) \tag{3-20}$$

This relation is inserted in Eq (3-19) to obtain Eq (3-21):

$$VM_{L} = \frac{CM_{R}^{2} - CM_{L} \cdot CM_{R} \cdot \cos(\mathbf{f}_{L} + \mathbf{f}_{R})}{M_{L}M_{R} \cdot \sin(\angle M_{R}M_{L}C)}$$
(3-21)

Now the geometry of rectangle triangle (VCM_L) is observed to establish Eq (3-22):

$$\tan(\angle CVM_L) = \frac{CM_L}{VM_L} \tag{3-22}$$

Inserting Eq (3-21) in Eq (3-22) results in Eq (3-23):

$$\angle CVM_L = \arctan\left(\frac{CM_L \cdot M_L M_R \cdot \sin(\angle M_R M_L C)}{CM_R^2 + CM_L \cdot CM_R \cdot \cos(\mathbf{f}_L + \mathbf{f}_R)}\right)$$
(3-23)

This equation fully defines angle $\angle CVM_L$ with respect to known dimensions.

The same triangle is used to obtain Eq (3-24):

$$CV = \frac{CM_L}{\sin(\angle CVM_L)} \tag{3-24}$$

The coordinates of vector \overrightarrow{CV} can finally be established with Eqs (3-25)-(3-26):

$$\begin{cases} X_{\overrightarrow{CV}} = CV \cdot \sin(\mathbf{f}_L - \angle CVM_L) \\ Y_{\overrightarrow{CV}} = -CV \cdot \cos(\mathbf{f}_L - \angle CVM_L) \end{cases}$$
(3-25)

By inserting Eq (3-24), these equations can be modified as shown in Eqs (3-27)-(3-28).

$$\begin{cases} X_{\overline{CV}} = \frac{CM_L \cdot \sin(\mathbf{f}_L - \angle CVM_L)}{\sin(\angle CVM_L)} \\ Y_{\overline{CV}} = -\frac{CM_L \cdot \cos(\mathbf{f}_L - \angle CVM_L)}{\sin(\angle CVM_L)} \end{cases}$$
(3-27)

$$Y_{\overline{CV}} = -\frac{CM_L \cdot \cos(\mathbf{f}_L - \angle CVM_L)}{\sin(\angle CVM_L)}$$
(3-28)

These last two equations fully define the coordinates of vector \overrightarrow{CV} with respect to known dimensions, in the local coordinate system of a ferrule.

3.2.3.2. Creating an Array of Fibers

The previous step presents a way to calculate the coordinates of a fiber or a pin in its respective vee-groove. The following step is to define the coordinates of the fibers in the same coordinate system. The general shape of a ferrule is illustrated in Fig 3-15:

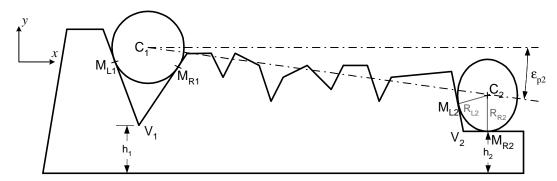


Fig 3-15: Shape of a Random Ferrule in 2D

The temporary coordinate system (indexed A) is such that the bottom of the ferrule is horizontal. The starting point is to define the coordinates of vector $\overrightarrow{C_1C_2}$. This vector can be decomposed like this: $\overrightarrow{C_1C_2} = \overrightarrow{C_1V_1} + \overrightarrow{V_1V_2} + \overrightarrow{V_2C_2}$.

Coordinates of vector $\overrightarrow{C_1V_1}$ can be found with the method presented in Section 3.2.3.1. The *x*-coordinate of vector $\overrightarrow{V_1V_2}$ is a dimension defined by the designer. Its *y*-coordinate can be defined by the dimension scheme presented in Eqs (3-29)-(3-30), related to the bottom of the ferrule:

$${}^{A}Y_{V_{2}} - h_{2} = {}^{A}Y_{V_{1}} - h_{1} {(3-29)}$$

$$\Leftrightarrow^{A} Y_{\overline{V_{1}V_{2}}} = {}^{A} Y_{V_{2}} - {}^{A} Y_{V_{1}} = h_{2} - h_{1}$$
 (3-30)

The second pin is assumed to lie on a horizontal surface, at the contact point M_{R2} . Triangle $(V_2M_{R2}C_2)$ is rectangle in M_{R2} , so the coordinates of vector $\overrightarrow{V_2C_2}$ are given by Eqs (3-31)-(3-32):

$$\begin{cases} {}^{A}X_{\overline{V_{2}C_{2}}} = \frac{C_{2}M_{R2}}{\tan(\angle M_{R2}V_{2}C_{2})} \\ {}^{A}Y_{\overline{V_{2}C_{2}}} = C_{2}M_{R2} \end{cases}$$
(3-31)

Subsequently the coordinates of vector $\overrightarrow{C_1C_2}$ are given by relations presented in Eqs (3-33)-(3-34):

$${}^{A}X_{\overline{C_{1}C_{2}}} = {}^{A}X_{\overline{C_{1}V_{1}}} + {}^{A}X_{\overline{V_{1}V_{2}}} + \frac{C_{2}M_{R2}}{\tan(\angle M_{R2}V_{2}C_{2})}$$
(3-33)

$${}^{A}Y_{C_{1}C_{2}} = {}^{A}Y_{C_{1}V_{1}} + h_{2} - h_{1} + C_{2}M_{R2}$$
(3-34)

The coordinates of every fiber's center are found with a similar dimension scheme.

The next step is to set a new coordinate system, indexed B. Its center is still the center of the reference pin, but the horizontal is now defined as the line going through the centers of the two pins. Hence there is an angle \mathbf{e}_{p2} between coordinate systems A and B. The value of this angle can be defined with the coordinates of the vectors in coordinate system A, as shown in Eq (3-35):

$$\mathbf{e}_{p2} = \arctan\left(\frac{{}^{A}Y_{\overline{C_{1}C_{2}}}}{{}^{A}X_{\overline{C_{1}C_{2}}}}\right)$$
(3-35)

The manufacturing errors in a fiber vee-groove will create a similar offset angle e_f . The coordinates $\binom{B}{A} \binom{B}{f} \binom{B}{f} \binom{B}{f}$ of the center of a fiber in the coordinate system B are then presented in Eqs (3-36)-(3-37):

$${}^{B}X_{f} = \sqrt{{}^{A}X_{f}^{2} + {}^{A}Y_{f}^{2}} \times \cos(\boldsymbol{e}_{f} - \boldsymbol{e}_{p2})$$
 (3-36)

$${}^{B}Y_{f} = \sqrt{{}^{A}X_{f}^{2} + {}^{A}Y_{f}^{2}} \times \sin(\boldsymbol{e}_{f} - \boldsymbol{e}_{p2})$$
 (3-37)

Finally, the coordinates of the core of the fiber are calculated by taking into consideration the eccentricity of the core deviating from the center of the fiber, as shown in Eqs (3-38)-(3-39):

$${}^{B}X_{core} = {}^{B}X_{f} + Ecc_{core} \cdot \cos(\mathbf{f}_{ecc})$$
(3-38)

$${}^{B}Y_{core} = {}^{B}Y_{f} + Ecc_{core} \cdot \sin(\mathbf{f}_{ecc})$$
(3-39)

where Ecc_{core} is the magnitude of the offset of the core and \mathbf{f}_{ecc} is its orientation angle.

3.2.3.3. Mating Two Fibers

The coordinates of the centers of the fibers can be determined independently by the method presented in the previous sections. Since the ferrules are aligned by the two pins, the coordinate system B, whose origin is the center of the first pin and whose *x*-axis is the line that goes through the center of both pins, is common to the two ferrules.

The core of a fiber in the male ferrule is modeled by its coordinates $\binom{B}{X_{coreM}}$, $\binom{B}{Y_{coreM}}$. It has to be aligned with a core of a corresponding fiber in the female ferrule; the coordinates of this second core are $\binom{B}{X_{coreF}}$, $\binom{B}{Y_{coreF}}$. The lateral misalignment d between the two mating cores is then:

$$d = \sqrt{({}^{B}X_{coreM} - {}^{B}X_{coreF})^{2} + ({}^{B}Y_{coreM} - {}^{B}Y_{coreF})^{2}}$$
(3-40)

When dealing with single-mode fibers, applying Marcuse's model [29] on this final result allows calculating the transmission loss in decibels due to the geometric variations of the features assembled in the connector.

Transmission loss depends upon lateral misalignment but also upon the optical properties of the fibers. Contrarily to multi-mode fibers, single-mode fibers work with a specific wavelength I (defined in meters). It is then possible to define a free space propagation constant k (unit: m^{-1}) for a single-mode connection, with Eq (3-41):

$$k = \frac{2\mathbf{p}}{l} \tag{3-41}$$

Marcuse starts by defining a dimensionless V_i parameter for the ith fiber with Eq (3-42):

$$V = k \cdot a_i \cdot \sqrt{n_{core}^2 - n_{cladding}^2}$$
 (3-42)

where a_i is the core radius of the fiber (in m). This V_i parameter is used for defining the width parameter w_i (in m) of the ith fiber by the empirical formula presented in Eq (3-43):

$$w_i = a_i \cdot \left(0.65 + \frac{1.619}{V_i^{\frac{3}{2}}} + \frac{2.879}{V_i^{6}}\right)$$
 (3-43)

Finally, the transmission coefficient T between two mating fibers indexed with the subscripts 1 and 2 assumes the form shown in Eq (3-44):

$$T = \left(\frac{2 \cdot w_1 \cdot w_2}{w_1^2 + w_2^2}\right)^2 \exp\left(-\frac{2 \cdot d^2}{w_1^2 + w_2^2}\right)$$
(3-44)

where d is the lateral misalignment defined in Eq (3-40). The corresponding signal loss in dB can be calculated with Eq (3-2).

Such an analytical model cannot be found for multi-mode fibers. The relation between lateral misalignment and connection loss is then established by using experimental data. The experiment consists in mating two fibers with a controlled misalignment. The transmission ratio is recorded while the offset is modified. The collected data are graphically plotted as a point cloud, as illustrated in Fig 3-16. A polynomial regression run on this point cloud returns an empirical relation between transmission ratio and lateral misalignment for multi-mode fibers.

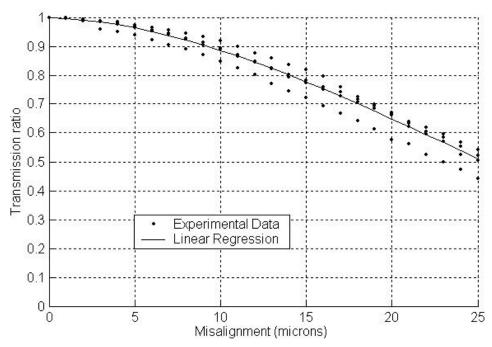


Fig 3-16: Experimental Determination of a Relation Between Loss and Misalignment by Curve Fitting

These equations constitute the parametric model of a connector by establishing a mathematical relation between the transmission loss and the manufacturing dimensions with their respective variations. The model is used in a tolerance allocation procedure to ensure that the maximum acceptable transmission loss is respected while the manufacturing cost is minimized.

3.3. Tolerance Allocation

3.3.1. Overview

This section presents a method for allocating tolerances to dimensions in exactly constrained ferrules used to align optical fibers. The objective is to reduce the manufacturing cost without exceeding a limit on the misalignment between two mating fibers. The allocation procedure is performed on the 2D geometric model of the multifiber connector developed in the previous section. An analytical representation of the connection, based upon statistics, is used for providing a relation between variation in manufactured dimensions and variation in the resulting misalignment of the fibers contained in the array. Optimal tolerances are determined using a non-linear constrained optimization algorithm that minimizes the manufacturing cost while satisfying constraints on the variation of the misalignment of any pair of fibers in the array. The method provides a useful tool when designing mass-produced connectors for multi-fiber cables, for which manufacturing cost and accuracy are critical parameters.

The goal of this study is to select tolerances that are sufficient for aligning optical fibers without excessive loss, but simultaneously minimize manufacturing costs that arise from excessively tight tolerances. Tolerance allocation is generally formulated as an optimization problem with an objective function and a set of constraints. In this case, the objective is to minimize the manufacturing cost which is a function of the tolerances. Tolerance relations for etched silicon parts are not available. However, for other materials like zirconium, a secondary material removal process like grinding may improve the tolerances. In this case, we employ relations developed by Chase [10] to relate manufacturing costs to tolerances. Both cost and signal loss can be defined as

functions of the tolerances allocated by the designer. The optimization constraints are formulated as maximum tolerable signal loss within an entire connector.

In formulating the optimization problem, the greatest challenge is determining a relationship between the tolerances and the performance criteria. For complex assemblies such as an optical fiber connector, Monte Carlo simulations are effective means for relating final tolerance of an assembly to the tolerances of the components [42]. However, it may be difficult to implement Monte Carlo simulations within the optimization algorithm due to computational time. We instead use an alternative approach in which a few Monte Carlo simulations provide a mathematical model relating assembly tolerances to component tolerances. Knowing the geometry and the dimensions of the connector, it is possible to define the signal loss of the fiber connection as a function of the tolerances of the ferrules.

This section presents a process to efficiently allocate the tolerances for veegroove fiber alignment. The first step is to construct a mathematical model of the dimensions and geometry of the connector, which was detailed in the previous section. The second step is to define, through a statistical study, the misalignment of the fiber as a function of the tolerances in the ferrules. The third step is to estimate a relation between the tolerances and the manufacturing costs. Finally, tolerances are allocated with an optimization algorithm that minimizes the manufacturing cost for a given maximum limit on signal loss.

3.3.2. Variation Analysis by the Law of Error Propagation

Tolerance allocation requires a relation between dimensional variations and connection loss. It is established by applying the law of error propagation [25] on the mathematical model of the connectors. This method is computationally efficient when used in a tolerance allocation algorithm.

The geometric model of the ferrules must be expressed in terms of statistics. Every dimension \mathbf{x}_i , presented in Table 3-1, is defined as a randomly distributed variable. Its mean \mathbf{m} equals the value of the nominal dimension, while its standard deviation \mathbf{s}_i is a

third of the tolerance. For a complete representation of the connector, the same procedure is applied for the dimensions of the fibers and the alignment pins.

The lateral misalignment d_j for the j^{th} pair of fibers is modeled as a vector in the xy-plane. It is possible to define its coordinates, (x_{d_j}, y_{d_j}) , as a function of the dimensions of the ferrules, the fibers, and the pins, as shown in Eqs (3-45)-(3-46):

$$x_{d_i} = f_{x_i}(\mathbf{X}_1, \mathbf{X}_2, ..., \mathbf{X}_i, ..., \mathbf{X}_n)$$
(3-45)

$$y_{d_i} = f_{y_i}(\mathbf{x}_1, \mathbf{x}_2, ..., \mathbf{x}_i, ..., \mathbf{x}_n)$$
(3-46)

n being the total number of assigned dimensions within the connector.

According to the law of error propagation, if the dimensions are independent (which is a reasonable assumption for most applications), then the standard deviations $\mathbf{S}_{x_{d_j}}$ and $\mathbf{S}_{y_{d_j}}$ of the lateral misalignment in the x and y directions are given by Eqs (3-47)-(3-48):

$$\mathbf{s}_{x_{d_j}}^2 \approx \sum_{i=1}^n \left(\frac{\partial f_{x_j}}{\partial \mathbf{x}_i}\right)^2 \mathbf{s}_i^2 \tag{3-47}$$

$$\mathbf{s}_{y_{d_j}}^2 \approx \sum_{i=1}^n \left(\frac{\partial f_{y_j}}{\partial \mathbf{x}_i}\right)^2 \mathbf{s}_i^2 \tag{3-48}$$

For perfect dimensions, the misalignment equals zero. Hence for random dimensions, its variation is directly related to its standard deviation and does not depend on its expected value. The law of error propagation then gives a direct analytical expression of the variance in lateral misalignment as function of the variances in the different dimensions of the connector. Since the current study analyzes the sensitivity of the lateral misalignment to the geometry of the ferrules, the standard deviations related to the dimensions of the fibers and the pins are considered as constants. Only the 9 standard deviations defining the ferrules are identified as the variables to optimize.

Eqs (3-47)-(3-48) return the variances of the components in the x and y directions for the lateral misalignment, but Marcuse's model requires the magnitude of the

misalignment, d_j . Its value could be expressed with a joint probability distribution for x_d and y_d , but an unknown correlation coefficient between the two components compromises the accuracy of the calculation. If the correlation coefficient were negligible, an exact definition of the joint probability distribution could be established with the calculations presented in Appendix A; however the value of the coefficient is too high to be neglected. Therefore a Monte Carlo simulation of the connector is used to determine an empirical relation between the connection loss and the standard deviations of x_{d_j} and y_{d_j} by a two-step process.

The first step consists in collecting data from the Monte Carlo simulation. Its inputs are the nominal values and the tolerances of the different dimensions defining the geometry of a connector. A large number of connectors are virtually generated using the mathematical model previously presented. Their dimensions are normally distributed, with a mean equal to their nominal value and a standard deviation equal to one third of their tolerance. The algorithm calculates the misalignment of each randomly generated sample; then it performs a statistical treatment on the collected results. Finally, it returns the standard deviation of the components in x and y of the lateral misalignment, as well as a cumulative distribution function (cdf) of the connection loss (in dB) for every pair of fibers, as shown in Fig 3-17.

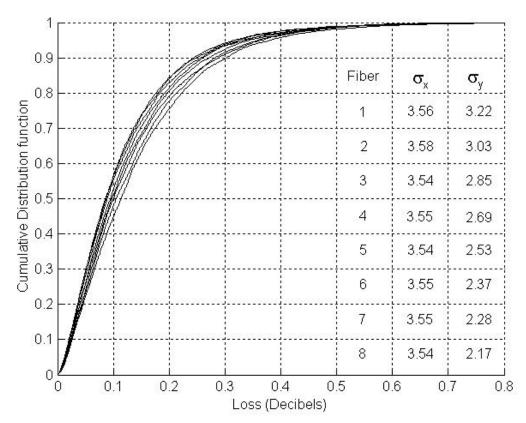


Fig 3-17: Outputs of Monte Carlo Simulation

Every cdf is curve fitted with a two-variable continuous function. Since the tolerance analysis focuses on the highest part of the cdf (beyond 90%), the curve fitting is performed exclusively on this part of the cdf in order to get more reliable approximations. It has been found that for single-mode fibers, the cdf of a Weibull random variable is a good approximation, while a Gamma incomplete function fits well the cdf of the multimode fibers.

The simulation is run many times with different input tolerances. The resulting cdf's are reduced to two parameters defining the fitted curve. Hence the first step of the process returns a set of values for the two fitting parameters as a function of the standard deviations of x_{d_i} and y_{d_i} .

The second step is a new curve fitting procedure. This time, one of the fitting parameters is plotted as a function of the standard deviations of x_{d_j} and y_{d_j} , and it is

curve fitted. The resulting relations are finally compared to new Monte Carlo simulations, and it has appeared that they were extremely reliable. These functions are used as empirical models of the connection loss.

Thereby a variation analysis based upon the law of error propagation, followed by an empirical yet accurate model of the connector performance, provides a relation between the connection loss and the tolerances of the ferrules.

3.3.3. Cost / Tolerance Functions

The cost of a manufactured part depends upon the selected manufacturing process and dimensional tolerances. The cost of achieving a particular tolerance depends upon both the dimension's nominal value and tolerance. The manufacturing cost generally increases if the tolerance is tightened, and it is more expensive to make a given tolerance on a large nominal dimension. Based on this, Chase [10] recommends expressing tolerances as reciprocal power functions for material removal processes. Eq (3-49) expresses the tolerance for the i^{th} dimension, t_i , as a function of cost, C_i , range, R_i , and three constants a_i , b_i , and c_i . The values of the three constants depend upon the range and the manufacturing process. Although a constant term would be necessary for accuracy, it is practically impossible to evaluate and doesn't affect the tolerance allocation.

$$t_i = c_i \times \frac{R_i^{a_i}}{C_i^{b_i}} \tag{3-49}$$

Similar functions are not available for etching processes commonly used with silicon.

Knowing the range and the manufacturing process of every dimension enables the generation of the cost-tolerance functions required to estimate the manufacturing cost of a connector as a function of the tolerances assigned to its different dimensions. The portion of the total manufacturing cost that is attributable to ferrule tolerancing is the sum of the costs for the successive manufacturing processes used for producing a ferrule.

3.3.4. Results of the Tolerance Allocation Algorithm

Optimal tolerances for the dimensions are determined using nonlinear constrained optimization. The problem is formulated as a minimization subject to constraints. The function to minimize is the manufacturing cost of the connector with respect to its tolerances, as defined in the previous section. Constraints are formulated by specifying that the standard deviation of the lateral misalignment, \mathbf{s}_{d_j} , for every pair of fibers within the connector must be positive yet below a critical value. Additional bounds can be specified to prevent the optimization from driving the assigned tolerances to unreasonably high or low values.

Since this optimization only deals with allocating tolerances to the ferrules, it is assumed that the tolerances for the fibers and the alignment pins are already known empirically or predicted by another analysis. The variables of the optimization problem are then the tolerances for the 9 dimensions defining the ferrules.

This method was used to allocate tolerances to an exemplary connector. The objective was to minimize the manufacturing cost of an 8-fiber connector while the connection loss of every pair of single-mode fibers should be less than 0.5 dB. The calculated connection losses along the connectors are displayed in Fig 3-18, and the resulting tolerances allocated by the optimization procedure are listed in Table 3-2.

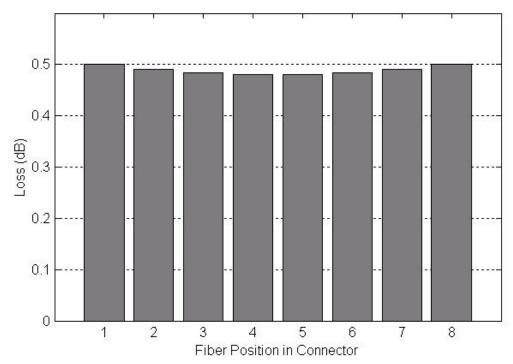


Fig 3-18: Computed Losses for Optimized Exemplary Connector

Table 3-2: Computed Tolerances for Exemplary Connector

Dimension	Nominal Value	Assigned Tolerances
Pitch between pin and closest fiber	1225 μm	0.594 μm
Pitch between two successive fibers	250 μm	0.594 μm
Pitch between wall and closest fiber	1225 μm	20.000 μm
Depth of pin vee-groove	512.11 μm	0.892 μm
Depth of fiber vee-groove	1192.74 μm	0.519 μm
Depth of flat surface	790 μm	1.147 μm
Half-angle of pin vee-groove	1.65806 rad	$1.027 \times 10^{-3} \text{ rad}$
Half-angle of fiber vee-groove	1.65806 rad	$5.760 \times 10^{-3} \text{ rad}$
Angle between wall and flat surface	1.57080 rad	$87.27 \times 10^{-3} \text{ rad}$

The results of the tolerance allocation performed on this case show that special care should be taken when machining the vee-grooves for the pins. The tolerance on their angle is relatively tight, compared to the other dimensions, even if a sub-micron

tolerance is needed for most of the dimensions defining the ferrule. On the other hand, tolerances related to the flat surface of the ferrules are relatively opened. The tolerance allocation demonstrates that the manufacturing cost of the ferrule can be reduced when making this geometric feature, since the flat surface doesn't require the high level of accuracy needed for the rest of the ferrule.

3.3.5. Comparison with Monte Carlo Simulation

Monte Carlo simulation, whose algorithm is presented in Fig 3-19, is used to verify the results of the tolerance allocation. A large number of connectors with random dimensions are virtually generated; then a statistic treatment of the results returns the mean and standard deviation of the signal loss. These simulated data should be comparable to the results obtained with the law of error propagation applied to the parametric model of the connector.

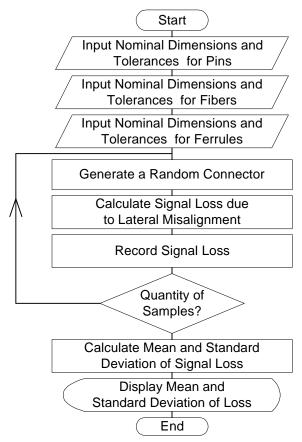


Fig 3-19: Flowchart of Monte Carlo Simulation for Multi-Fiber Connectors

Such Monte Carlo simulation is applied on the exemplary connector, with the nominal dimensions and assigned tolerances presented in Table 3-2. The results are displayed with a cumulative distribution function of the signal loss for every pair of mating fibers, shown in Fig 3-20. As expected, every loss is less than 0.5 dB for 99.5% of the cases with the selected set of tolerances.

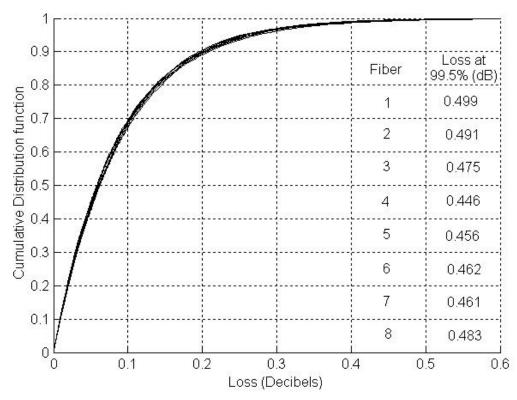


Fig 3-20: Monte Carlo Simulation for Exemplary Connector with Optimized Tolerances

3.4. Manufacturing Process

3.4.1. Introduction

Tolerancing the optical fiber connector leads to the study of their production process. This section presents initial results from investigating the manufacture of high precision micro-scale vee-grooves fabricated in Aluminum 6061-T6. The manufacturing process being tested includes three primary steps. The first step produces the rough shape of the vee-grooves using conventional wire electro discharge machining (wire EDM). The second step coats the grooves with a hard layer using the Sandford process. The final step will produce precise vee-grooves with smooth surfaces by grinding away a

portion of the hard coating. In this chapter, we describe the fabrication process, assess the surfaces of the vee-grooves, and evaluate manufacturing variation in the form of the vee-grooves prior to the grinding step. The recast layer and coating thickness were investigated using metallography.

Micro grooves and channels can be manufactured with material removal processes such as etching [43], mechanical cutting with miniature cutters [44,45], and non-traditional micro machining [46]. Alternatively, they can be formed with processes such as coining [47] and molding.

The objective in this work is to investigate the suitability of a process for producing micro vee-grooves in aluminum 6061-T6 with processes and equipment that are readily available. Etching processes are not readily available to most manufacturers and are not appropriate for aluminum. Mechanical cutting, which is readily available, produces burrs that are significant at this length scale [48] and are difficult to remove. For these reasons, a process based on wire electro discharge machining (wire EDM) and precision grinding is investigated. For testing purposes, the vee-grooves of the first ferrule prototypes were manufactured with nominal width, depth, and aperture angles of approximately 180 µm, 156 µm, and 60 degrees, respectively, after grinding.

3.4.2. Description of the Process

The first step in the manufacturing process is to cut the general shape of the vee-grooves using conventional wire EDM. This process is applicable for any conductive material, and many EDM machines are capable of using wires with diameters as small as 20 im. Wire EDM can therefore produce a wide variety of groove geometries with lengths up to many millimeters. Unfortunately, wire EDM generates a recast layer produced by the re-solidification of molten metal. This undesirable surface is clearly visible with scanning electron microscopy (SEM) as shown in Fig 3-21. The imprecision of the vee-grooves and the rough surface justify grinding after EDM.

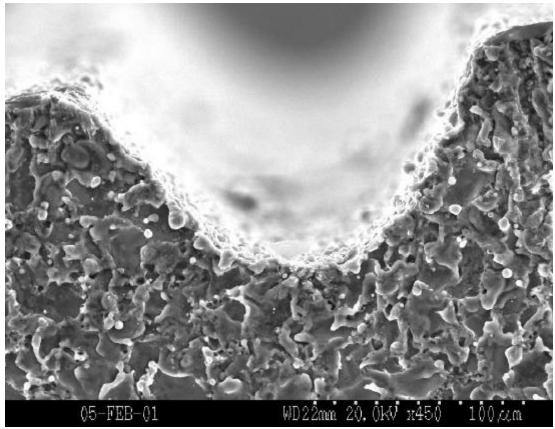


Fig 3-21: SEM Image of Micro Vee-grooves Following Wired EDM Operation

Prior to grinding, a hard coating was applied to the aluminum grooves using the Sandford process [49]. It is an electrochemical process that produces a sapphire-like structure on the surface of aluminum parts by generating an oxide-coating layer. The coating penetrates the base metal and builds up on the surface. The hardness of the coating results in excellent abrasion resistance and is readily ground.

The third and final step in the manufacturing process will be to grind the precise shape of the vee-grooves into the coating to satisfy requirements for surface finish and tolerances. At this time, we have fabricated a set of sample parts that are now ready for the grinding operation.

3.4.3. Metallography Study

A metallography study was conducted to characterize the vee-grooves after wire EDM and after applying the hard coat layer. Hence, the effects of both steps on the final

precision of the vee-grooves can be identified. The metallography study consisted of slicing the manufactured parts, mounting the parts, grinding and polishing the parts' endfaces, and finally observing the faces with an optical microscope.

A part cut with wire EDM but before coating was studied to characterize the recast layer observed in Fig 3-21. The recast layer produced a generally rough profile around the perimeter of the part that varied in thickness from between 4 im and 8 im as shown in Fig 3-22.

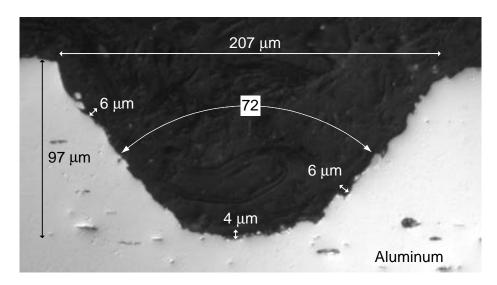


Fig 3-22: Metallography Study of a Vee-Groove Produced with Wire EDM

Fig 3-23 shows an image of a vee-groove after coating with the Sandford process. The thickness of the coating layer was not uniform, and it varied with the geometry of the vee-groove. On the sloped surfaces, the thickness was typically about 32 im thick, but the thickness was only 16 im at the bottom of the grooves. A thicker coating layer is achievable with a longer coating time, and may be necessary if gross errors exist during grinding.

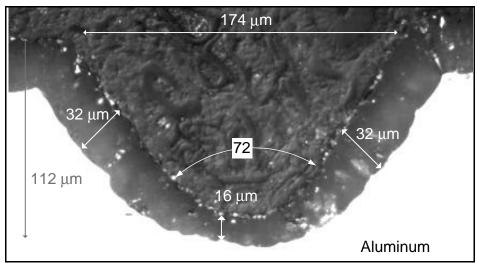


Fig 3-23: Metallographic Study of Coated Vee-Groove

3.4.4. Stylus Profilometry of Grooves

The accuracy and variation of the grooves' 2D shape was assessed prior to coating. Since the width, depth, and length of the grooves were approximately 170 im, 150 im, and 4 mm (before grinding), a 3D approach over the area of the grooves was necessary. Stylus profilometry was selected as the measurement technique since it provided suitable resolution in the z direction (~1 nm) over the necessary scan area (4 mm x 4.6 mm).

The stylus (~0.2 im diameter) traveled along a path in the horizontal plane and recorded the height of the surface. The surface was scanned in a raster fashion by measuring a set of parallel traces. Traces were sequentially measured across the set of parallel grooves (x direction) with an increment in the y direction of 50 im. The scan velocity in the x direction was 200 im/s, and it sampled the height of the surface at 1 im intervals. Thus a 3D point cloud of data points was collected, and it is shown in Fig 3-24 along with the ideal geometry.

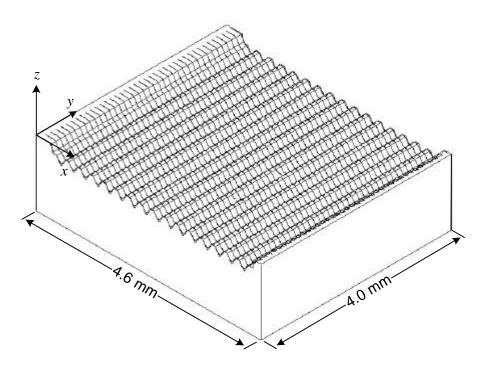


Fig 3-24: Point Cloud from Profilometry Traces

The manufacturing variation in the vee-grooves is observed after projecting the 3D point cloud onto a 2D plane intersecting the parallel vee-grooves. In Fig 3-25, it is evident that the EDM process did not remove the material at the very bottom of the grooves.

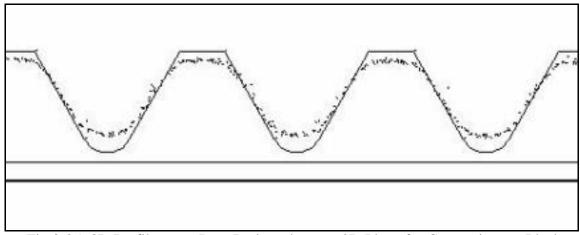


Fig 3-25: 3D Profilometry Data Projected onto a 2D Plane for Comparison to Ideal Model

As shown in Fig 3-26, the geometry of a vee-groove is represented in two dimensions with four parameters and their manufacturing errors:

- angle of aperture, \boldsymbol{a} , and angle error, $\boldsymbol{d}_{\boldsymbol{a}_i}$,
- inclination angle, g, which is the angle between the groove's bisector and a vertical line (ideally gequals zero), and angle error, d_{g_i} ,
- depth to the virtual vertex, h, and error, \boldsymbol{d}_{h_i} , and the
- radius of curvature, r, at the bottom of the groove, and error, d_{r_i} .

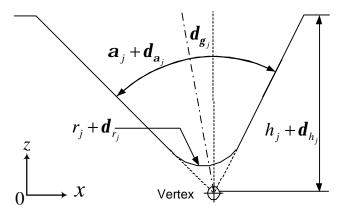


Fig 3-26: Manufacturing Errors in a Vee-Groove

A simple algorithm that calculates the geometric parameters of the grooves from the measured profilometer data was developed [50]. For each vee-groove in a 2D trace, the algorithm fitted a straight line to the inclined edges and determined their slope and intersection. Thus two half-angles for every groove were calculated: the left one, b_L , and the right one, b_R . The angle of aperture was determined as the sum of the half angles. The intersection of the two fitted lines gave the coordinates of the groove's virtual vertex, and so the depth of the groove, h, was determined. The inclination angle was calculated as half the difference between b_L and b_R .

Using this algorithm on 40 traces and 16 grooves per trace yielded the geometric parameters of 640 2D grooves. Statistics characterizing the mean and variation of the parameters are shown in Table 3-3.

Table 3-3: Statistics of 2D Geometric Parameters Describing Vee-Groove Variation

		Estimate of the Mean			Estimate of the Variance		
		(95% Confidence Interval)			(95% Confidence Interval)		
Feature	Target	Lower	Estimated	Upper	Lower	Estimated	Upper
reature	value	Limit	Mean	Limit	Limit	Variance	Limit
Left half angle (degrees)	30.0	34.41	34.63	34.84	7.1	7.9	8.9
Right half angle (degrees)	30.0	35.07	35.30	35.54	8.2	9.2	10.3
Aperture (degrees)	60.0	69.59	69.93	70.27	16.9	18.8	21.1
Inclination (degrees)	0.0	-0.49	-0.34	-0.19	3.5	3.8	4.3
Height (microns)	150	130.9	131.4	131.8	25.7	28.6	32.0

3.4.5. Conclusions

This chapter introduced a manufacturing process to make micro-scale veegrooves in Aluminum 6061T6 and a metrology procedure to measure their dimensional variation. Surface roughness and variation were found to be significant after EDM and coating, and so grinding remains necessary. A metallography study showed that variation in the thickness of the coating layer depended upon groove geometry. The thickness of the coating in the depth of the groove was approximately half the thickness on the flat surfaces.

Despite the dimensional variation after wire EDM and coating, the grooves are acceptable for subsequent grinding operations. The results of the grinding operation will be presented in future work.

Chapter 4: Application to Kinematic Couplings

4.1. Introduction

4.1.1. Presentation

Kinematic couplings, illustrated in Fig 4-1, are widely used for positioning one rigid body with respect to another. Contact between a ball body and a groove body occurs at six points, which is the minimum necessary for static equilibrium. Hence, kinematic couplings exactly constrain [5] all six degrees of freedom without overconstraint and are therefore extremely repeatable techniques for positioning two bodies [51,52]. However, the relative position and orientation of the two bodies are not necessarily accurate. Accuracy must be attained with either mechanical adjustments or tight production tolerances, both of which increase the manufacturing cost of the kinematic coupling.

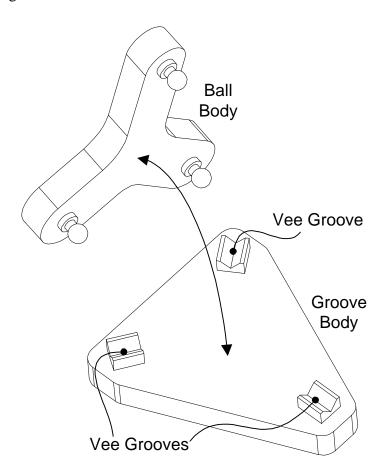


Fig 4-1: Three-Groove Kinematic Coupling

As kinematic couplings increasingly find applications in manufacturing, fixturing, and material handling, it is necessary to consider the effect of inaccurate kinematic couplings. For instance, Vallance and Slocum [4] described the use of kinematic couplings for positioning pallets in flexible assembly systems. In this application, kinematically coupled pallets are routinely exchanged at multiple machine stations, and hence manufacturing errors in each pallet and station contribute to system-wide manufacturing variation.

This chapter presents a method for allocating tolerances to the dimensions of kinematic couplings so that variation in the position and orientation of kinematically coupled bodies is less than a set of design constraints. The geometry of the contacting surfaces is modeled using parametric functions of dimensions that include manufacturing errors. The variation in the kinematic couplings' position and orientation errors are expressed as a function of the tolerances using a multivariate error analysis [26]. The tolerances of the coupled bodies are related to manufacturing costs via cost/tolerance relations for common processes (milling, drilling, grinding, etc.) published by Chase [10]. Finally, a constrained nonlinear optimization problem returns dimensional tolerances for the kinematic coupling that minimize manufacturing costs but satisfy constraints on variation in position and orientation.

4.1.2. Background and Prior Work

Kinematic couplings have been used in precision instruments for many years [53,54], and their utility in precision machines is widely recognized [55]. In traditional applications, often a single ball body and a single groove body are ever coupled together, and so the principal functions of the kinematic coupling are:

- to minimize variation in the position and orientation of the ball body after removing and replacing the ball body, and
- to minimize elastic deformation induced in the ball body due to excessive constraints.

The success of similar anti-distortion mountings and kinematic couplings with regard to these two functions was studied and demonstrated by designers of precision instruments and machines [2,3,56]. As a result, they found increasing application within precision manufacturing equipment and processes [4,57,58]. For some of these applications, multiple ball bodies are coupled with a single or several groove bodies. This introduces system-level variation due to inaccurate production of the mating surfaces within the kinematic coupling, which was described and analyzed by Vallance [26]. To increase the accuracy of each coupling and thereby reduce the system-wide variation, the dimensional variation within the set of ball and groove bodies must be specified and controlled.

Limits on the dimensional variation within the ball and groove bodies can be specified on drawings using standard techniques for dimensional and geometric tolerances [7]. Early tolerancing research resulted in approaches for tolerance analysis that predict the effect of multiple tolerances on the dimensions and geometry of mechanical components [59,60]. The most common approaches use worst-case analyses [61], root-sum-square (RSS) analyses [62], statistical techniques [63], or Monte Carlo simulation [64]. More recent research extended tolerance analysis techniques to assemblies of components [65,66], and some of these techniques are available in tolerance analysis software and may even be integrated with CAD software [67].

Software for tolerance allocation [68], which is the inverse problem of assigning values to the tolerances, is less available. Therefore, tolerance allocation is less common, but it has been demonstrated for particular mechanical systems [69]. Tolerance allocation often uses optimization techniques [70] that minimize cost [71,72] subject to constraints on variation using cost-tolerance relations [73].

This chapter contributes a formulation and solution to tolerance allocation for kinematic couplings, which compliments other analytical tools that assist during design [3,74,75]. The technique for assigning tolerances is statistical, and it uses multivariate error analysis [15] and nonlinear constrained optimization [76] to minimize cost. The technique has been implemented and verified using a set of scripts that execute within Matlab. An additional set of Matlab scripts verifies the results of the allocation using random Monte Carlo simulations.

4.1.3. Tolerance Allocation

Rigorously allocating tolerances to the dimensions of kinematic couplings, requires an algorithm that incorporates the four aspects described below.

- Describe the geometry and dimensional variation in a mathematical form. Both bodies of the kinematic coupling should be represented parametrically, with respect to their nominal dimensions and their dimensional errors. The contact points between the two bodies are of primary interest for defining the assembly variations of the kinematic coupling, so the parametric representation should concentrate on contacting surfaces in terms of the dimension schemes for modeling the ball and groove bodies.
- Combine dimensional variation in the ball body and groove body to estimate variation in the resting position and orientation of the ball body. The limits to dimensional variation in the ball and groove bodies are defined by tolerances. When a ball and groove body with particular dimensional errors are assembled together, the ball body is positioned and oriented with errors in its resting position $(x_r, y_r, z_r, \mathbf{a}_r, \mathbf{b}_r, \mathbf{g}_r)$. A relation between dimensional variation and variation in the resting position and orientation is provided by multivariate error analysis. This approach requires a robust method for determining the resting location of the ball body.
- Relate assembly variation to the performance requirements of the kinematic coupling. The acceptable errors in the resting position and location are defined by the assembly tolerances specified by the designer. If the designer uses error budgeting techniques [77], then the limits on position and orientation errors associated with the kinematic coupling are known. However, these limits are usually specified at operating points, where manufacturing operations are performed, rather than at a reference coordinate system. The performance of the kinematic coupling should therefore be assessed using variation in the position and orientation of operating points.
- Relate dimensional tolerances to manufacturing costs. The objective of the tolerance allocation is to minimize the manufacturing cost of the kinematic coupling, while satisfying tolerances on the assembly errors. It is then necessary to establish cost-tolerance functions relevant to the manufacturing operations used to produce the ball and groove bodies.

These four aspects are incorporated into the algorithm illustrated in Fig 4-2. The multivariate error analysis is an iterative process in which one dimension is perturbed at a time. It returns the variation of the resting location and the manufacturing cost. This process is nested in an optimization loop.

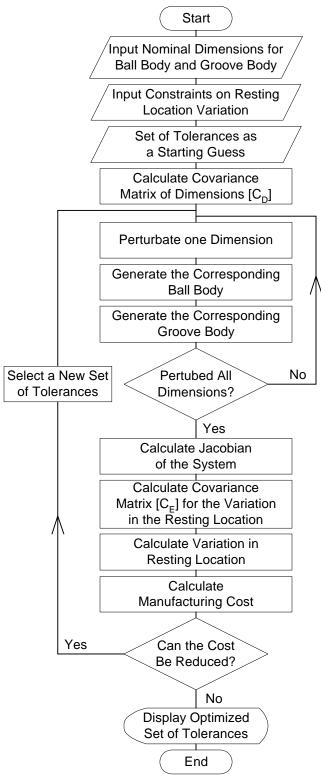


Fig 4-2: Flowchart of the Tolerance Allocation for Kinematic Couplings

4.2. Mathematical Model

4.2.1. Parametric Representation of Contacting Surfaces

We require an analytical representation of the contacting surfaces within a kinematic coupling containing manufacturing errors. A common style of kinematic couplings uses three balls resting in three vee-grooves, as illustrated in Fig 4-1 [74], and so we use the parametric equations for a sphere and flat surface. We distinguish six spherical surfaces since the effective diameter of the ball near the contact point may be slightly different due to out-of-roundness in the ball. The arrangement of the six spherical and flat surfaces is illustrated in Fig 4-3. For computational purposes, coordinate systems are attached to each surface. The 12 surfaces are described in reference coordinate systems located at the coupling centroid of the ball body (*BC*) and groove body (*GC*).

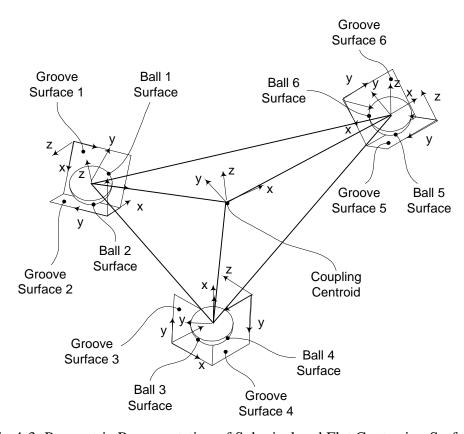


Fig 4-3: Parametric Representation of Spherical and Flat Contacting Surfaces

When load is not critical, the contact between a spherical surface and a flat surface is punctual. Every point contact suppresses a degree of freedom, thus the six contacts fully constraint the two bodies of the kinematic coupling.

Eq (4-1) describes all points $[x_{B_i}, y_{B_i}, z_{B_i}]$ that lie within a spherical surface with diameter, d_{B_i} , and center located by the position vector, ${}^{BC}\vec{P}_{B_i} = \left[{}^{BC}P_{B_i}^x, {}^{BC}P_{B_i}^y, {}^{BC}P_{B_i}^z\right]$. The subscript, B_i , indicates that the points are associated with the i^{th} spherical surface, and the prescript, BC, denotes that the position vector is measured in the coordinate system located at the centroid of a triangle defined by the centers of the three balls. The subsubscript, i, which indicates a particular contact surface, varies between 1 and 6.

$$(x_{B_i}^{-BC}P_{B_i}^x)^2 + (y_{B_i}^{-BC}P_{B_i}^y)^2 + (z_{B_i}^{-BC}P_{B_i}^z)^2 - \frac{1}{4}d_{B_i}^2 = 0 \quad \text{for } i = 1...6$$
 (4-1)

Eq (4-2) describes all points $[X_{F_i}, Y_{F_i}, Z_{F_i}]$ that lie within the flat plane in one of the coupling's vee-grooves. The subscript, F_i , indicates that the variables are associated with the i^{th} flat surface. The plane is defined by a position vector that locates a point in the vee-groove, ${}^{GC}\vec{P}_{F_i} = \left[{}^{GC}P_{F_i}^x, {}^{GC}P_{F_i}^y, {}^{GC}P_{F_i}^z \right]$, and a vector normal to the plane, ${}^{GC}\vec{n}_{F_i} = \left[{}^{GC}n_{F_i}^x, {}^{GC}n_{F_i}^y, {}^{GC}n_{F_i}^z \right]$. The prescript, GC, indicates that the vectors are measured in a coordinate system located at the grooves' coupling centroid.

$${}^{GC}n_{F_i}^x(x_{F_i} - {}^{GC}P_{F_i}^x) + {}^{GC}n_{F_i}^y(y_{F_i} - {}^{GC}P_{F_i}^y) + {}^{GC}n_{F_i}^z(z_{F_i} - {}^{GC}P_{F_i}^z) = 0 \quad \text{for } i = 1...6$$
 (4-2)

The components of the position and normal vectors used in Eqs (4-1)-(4-2) depend upon the manufactured dimensions of the kinematic coupling. Two sets of dimensions, $(d_{B_1}, d_{B_2}, ..., d_{B_m})$ and $(d_{F_1}, d_{F_2}, ..., d_{F_n})$, define the geometry of the ball body and groove body, respectively. The dimensions are measured with respect to two sets of metrology datum frames that define a coordinate system in the ball body denoted with a prescript, BD, and a coordinate system in the groove body denoted with a prescript, GD. The form of these relations depends upon the dimension scheme specified by the designer, but they are expressed generally as shown in Eqs (4-3)-(4-5).

$$^{BD}\vec{P}_{B_i} = f_{B_i} \left(d_{B_1}, d_{B_2}, \dots, d_{B_m} \right)$$
 (4-3)

$$^{GD}\vec{P}_{F_i} = f_{F_i} \left(d_{F_1}, d_{F_2}, \dots, d_{F_n} \right)$$
 (4-4)

$$^{GD}\vec{n}_{F_i} = f_{n_i} (d_{F_1}, d_{F_2}, \dots, d_{F_n})$$
 (4-5)

The position vectors that locate the spherical and flat surfaces are transformed from the coordinate systems determined by the manufacturing datums (BD and GD) to the centroidal coordinate systems (BC and GC) using homogeneous transformation matrices (HTMs), $^{BC}_{BD}T$ and $^{GC}_{GD}T$, as shown in Eqs (4-6)-(4-7).

$${}^{BC}\vec{P}_{B_i} = {}^{BC}_{BD}T \quad {}^{BD}\vec{P}_{B_i} \tag{4-6}$$

$${}^{GC}\vec{P}_{F_i} = {}^{GC}_{GD}T {}^{GD}\vec{P}_{F_i}$$
 (4-7)

The HTMs $^{BC}_{BD}T$ and $^{GC}_{GD}T$ are determined using a triangle defined by the centers of the balls. The origin of the centroidal coordinate system is located at the intersection of the triangle's bisectors [1]. Its *x*-axis points towards the ball that contains contacting surfaces 5 and 6, and the three apices lie in the *xy*-plane. An algorithm for determining $^{BC}_{BD}T$ and $^{GC}_{GD}T$ is presented in Appendix E.

4.2.2. Resting Position and Orientation

When rigid ball and groove bodies are kinematically coupled, the ball body rests in a location that minimizes energy. If friction at the contact points is neglected, the resting location is determined solely from the manufactured geometry of the bodies. The solution described here [26] uses the geometric model presented in the previous section to calculate the relative position and orientation between kinematically coupled bodies that contain manufacturing errors. By avoiding assumptions such as a linear relation between manufacturing errors and resting position, the method remains valid for even large manufacturing errors.

Specification of the resting position and orientation requires that three translations x_r , y_r , and z_r , and three rotations $\mathbf{a}_r = rot(^{BC}Z)$, $\mathbf{b}_r = rot(^{BC}Y)$, and $\mathbf{g}_r = rot(^{BC}X)$ be determined. These degrees of freedom are expressed in a transformation matrix, $_{BC}^{GC}T$, between the centroid coordinate systems in the ball body (BC) and groove body (GC). The objective is to determine the unknowns $(x_r, y_r, z_r, \mathbf{a}_r, \mathbf{b}_r, \mathbf{g}_r)$ and hence $_{BC}^{GC}T$, but this cannot be done without also determining the position vectors that locate the six contact points, $_{BC}^{GC}P_{C_r}$.

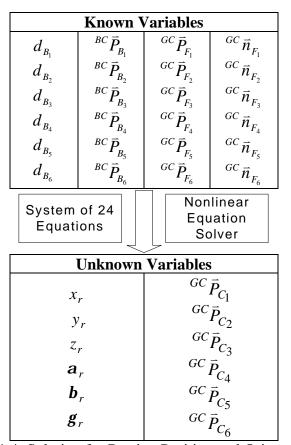


Fig 4-4: Solution for Resting Position and Orientation

As illustrated in Fig 4-4:, the solution employs a system of 24 equations and unknowns that are solved iteratively using a nonlinear numerical technique. The inputs to the solver include the diameters of the spherical contacting surfaces, d_{B_i} , the position vectors that locate the balls in the BC coordinates, ${}^{BC}\bar{P}_{B_i}$, the position vectors that locate the flat surfaces in the GC coordinates, ${}^{GC}\bar{P}_{F_i}$, and the normal vectors at the flat surfaces,

 ${}^{GC}\bar{n}_{F_i}$. The outputs of the algorithm include the translations and rotations of the resting position, x_r , y_r , z_r , a_r , b_r , g_r and the positions vectors that locate the six contact points in the GC coordinate system, ${}^{GC}\bar{P}_C$.

The system of 24 equations is obtained in two distinct sets. The first set of six equations is obtained by requiring that the contact points lie in the plane defined by the flat surfaces. As shown in Eq (4-8), this is accomplished by substituting the coordinates of the contact points into Eq (4-2), which may be done six times for each contact point.

$${}^{GC}n_{F_i}^x(x_{C_i} - {}^{GC}P_{F_i}^x) + {}^{GC}n_{F_i}^y(y_{C_i} - {}^{GC}P_{F_i}^y) + {}^{GC}n_{F_i}^z(z_{C_i} - {}^{GC}P_{F_i}^z) = 0 \text{ for } i = 1...6$$
 (4-8)

The second set of eighteen equations is obtained from six equations that express a closed loop of vectors between the contacting balls and flat surfaces. The vector loop is illustrated in Fig 4-5 for one ball and flat surface. One path in the loop originates at the GC coordinate system and includes the unknown transformation, ${}^{GC}_{BC}T$, and the position of the ball center, ${}^{BC}\bar{P}_{B_i}$. The second path in the loop also originates at the GC coordinate system, but it proceeds to the unknown position of the contact point, ${}^{GC}\bar{P}_{C_i}$, and through a vector normal to the flat surface of magnitude $d_{B_i}/2$. The closed vector loop is expressed mathematically in Eq (4-9), and may be written six times for each contact point.

$${}_{BC}^{GC}T {}^{BC}\vec{P}_{B_i} - {}^{GC}\vec{P}_{C_i} = \frac{d_{B_1}}{2} {}^{GC}\vec{n}_{F_i} \text{ for } i = 1...6$$
 (4-9)

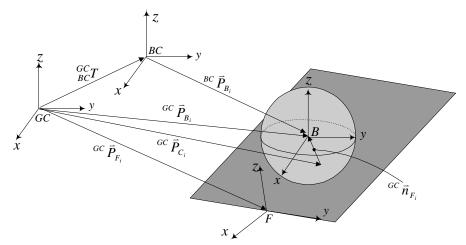


Fig 4-5: Vector Loop Between Ball and Flat Surface

After the iterative solver returns values for the unknown variables, the HTM between the GC and BC coordinate systems is computed as shown in Eq (4-10). If the rotations are small, then the matrix form may be simplified using small angles approximations.

$$\frac{GC}{BC}T = \begin{bmatrix}
\cos(\boldsymbol{a}_r)\cos(\boldsymbol{b}_r) & \cos(\boldsymbol{a}_r)\sin(\boldsymbol{b}_r)\sin(\boldsymbol{g}_r) - \sin(\boldsymbol{a}_r)\cos(\boldsymbol{g}_r) & \cos(\boldsymbol{a}_r)\sin(\boldsymbol{b}_r)\cos(\boldsymbol{g}_r) - \sin(\boldsymbol{a}_r)\sin(\boldsymbol{g}_r) & x_r \\
\sin(\boldsymbol{a}_r)\cos(\boldsymbol{b}_r) & \sin(\boldsymbol{a}_r)\sin(\boldsymbol{b}_r)\sin(\boldsymbol{g}_r) - \cos(\boldsymbol{a}_r)\cos(\boldsymbol{g}_r) & \sin(\boldsymbol{a}_r)\sin(\boldsymbol{b}_r)\cos(\boldsymbol{g}_r) - \cos(\boldsymbol{a}_r)\sin(\boldsymbol{g}_r) & y_r \\
-\sin(\boldsymbol{b}_r) & \cos(\boldsymbol{b}_r)\sin(\boldsymbol{g}_r) & \cos(\boldsymbol{b}_r)\cos(\boldsymbol{g}_r) & z_r \\
0 & 0 & 1
\end{bmatrix}$$
(4-10)

4.2.3. Multivariate Error Analysis of Variation in Resting Location

Tolerance allocation requires a relation between dimensional variation and system-wide variability in the resting position and orientation. This can be accomplished using a Monte Carlo simulation, but multivariate error analysis provides a more computationally efficient approach [26]. After allocating tolerances, a Monte Carlo simulation is an effective means for verifying the results.

Multivariate error analyses use linear approximations derived from Taylor series expansion. For instance, there exists a function, $X(\ _1,d_2,\ _+\)$

As shown in Eq (4-11), an estimate of the deviation in the x-coordinate, d_{x_r} , is expressed using a Taylor series expansion to X that includes only first-order terms consisting of partial derivatives and differential errors in the dimensions, Δd_j .

$$\boldsymbol{d}_{x_r} \approx \Delta d_1 \frac{\partial X}{\partial d_1} + \Delta d_2 \frac{\partial X}{\partial d_2} + \dots + \Delta d_{m+n} \frac{\partial X}{\partial d_{m+n}}$$
(4-11)

Similar expressions are written for the deviations in the remaining degrees of freedom, \boldsymbol{d}_{y_r} , \boldsymbol{d}_{z_r} , \boldsymbol{d}_{b_r} and \boldsymbol{d}_{a_r} . All six approximations are expressed in matrix form by the transformation shown in Eq (4-12). The $6\times(m+n)$ matrix of partial derivatives is referred to as the Jacobian matrix, [J].

$$\begin{bmatrix} \boldsymbol{d}_{x_r} \\ \boldsymbol{d}_{y_r} \\ \boldsymbol{d}_{g_r} \\ \boldsymbol{d}_{b_r} \\ \boldsymbol{d}_{a_r} \end{bmatrix} = \begin{bmatrix} \frac{\partial X}{\partial d_1} & \frac{\partial X}{\partial d_2} & \cdots & \frac{\partial X}{\partial d_{m+n}} \\ \frac{\partial Y}{\partial d_1} & \frac{\partial Y}{\partial d_2} & \cdots & \frac{\partial Y}{\partial d_{m+n}} \\ \frac{\partial Z}{\partial d_1} & \frac{\partial Z}{\partial d_2} & \frac{\partial Z}{\partial d_2} & \cdots & \frac{\partial Z}{\partial d_{m+n}} \\ \frac{\partial \Gamma}{\partial d_1} & \frac{\partial \Gamma}{\partial d_2} & \cdots & \frac{\partial \Gamma}{\partial d_{m+n}} \\ \frac{\partial B}{\partial d_1} & \frac{\partial B}{\partial d_2} & \cdots & \frac{\partial B}{\partial d_{m+n}} \\ \frac{\partial A}{\partial d_1} & \frac{\partial A}{\partial d_2} & \cdots & \frac{\partial A}{\partial d_{m+n}} \end{bmatrix}$$

$$(4-12)$$

Since expressions for the six degrees of freedom are not actually known, the elements of [J] are estimated numerically. This is done by perturbing the value of each dimension from its nominal value, calculating the resting location that gives the six errors, and then evaluating a column in [J].

Assuming the dimensions are continuously distributed random variables and that a tolerance is equivalent to a 3s range, the error analysis can be treated statistically. A covariance matrix organizes variances along its diagonal and covariances in the off-diagonal terms. The diagonal elements are therefore squares of the standard deviations of the corresponding random variables. The covariance matrix, $[C_D]$, of the kinematic coupling's dimensions is given in Eq (4-13). If the dimensions are independent and

therefore uncorrelated, the off-diagonal covariance terms will equal zero. This is a common assumption during tolerance allocation.

$$[C_{D}] = \begin{bmatrix} \mathbf{s}_{d_{1}}^{2} & \cos(d_{1}, d_{2}) & \cdots & \cos(d_{1}, d_{m+n}) \\ \cos(d_{2}, d_{1}) & \mathbf{s}_{d_{2}}^{2} & \cdots & \cos(d_{2}, d_{m+n}) \\ \vdots & \vdots & \ddots & \vdots \\ \cos(d_{m+n}, d_{1}) & \cos(d_{m+n}, d_{2}) & \cdots & \mathbf{s}_{d_{m+n}}^{2} \end{bmatrix}$$
(4-13)

A similar covariance matrix, $[C_E]$, for the variation in the resting location is defined in Eq (4-14).

$$[C_{E}] = \begin{bmatrix} \mathbf{s}_{x_{r}}^{2} & \operatorname{cov}(x_{r}, y_{r}) & \cdots & \operatorname{cov}(x_{r}, \mathbf{a}_{r}) \\ \operatorname{cov}(y_{r}, x_{r}) & \mathbf{s}_{y_{r}}^{2} & \cdots & \operatorname{cov}(y_{r}, \mathbf{a}_{r}) \\ \vdots & \vdots & \ddots & \vdots \\ \operatorname{cov}(\mathbf{a}_{r}, x_{r}) & \operatorname{cov}(\mathbf{a}_{r}, y_{r}) & \cdots & \mathbf{s}_{\mathbf{a}_{r}}^{2} \end{bmatrix}$$
(4-14)

The covariance matrix of the resting location errors, $[C_E]$, is related to the covariance matrix of the dimensions $[C_D]$ by Eq (4-15) [15].

$$[C_E] = [J][C_D][J]^T (4-15)$$

By extracting the diagonal elements of the matrix, $[C_E]$, the multivariate error analysis returns the variation in the resting position and orientation in terms of the tolerances on dimensions.

4.2.4. Variation at Operating Points

The previous section presented a method for estimating the variation in the position and orientation of a coordinate system located at the coupling centroid in the ball body. Although this is useful, the utility of the tolerance allocation is greatly improved if it considers the variation at additional points in the ball body. For instance, in kinematic couplings intended for positioning pallets in flexible assembly operations [4], assembly operations such as insertion and joining are performed to a product held within a fixture attached to the ball body. Hence, the designer's specifications on variation, as determined with an error budget, are preferably specified at *operating points*.

Fig 4-6 illustrates the definition of a single operating point. A coordinate system, denoted with the prescript, OP_k , is defined at the k^{th} operation point. An HTM, $OP_k^{BD}T$, locates the operating point with respect to the manufacturing datum frame in the ball body, BD. A set of p operating points is similarly defined by a set of p HTMs.

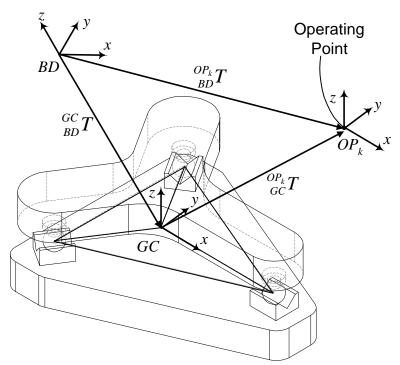


Fig 4-6: Coupled Kinematic Coupling with Operating Point

After determining $^{BC}_{BD}T$ between the ball body's datums and coupling centroid using the algorithm in Appendix E, the position and orientation of the operating points can be calculated in the coordinate system at the groove body's coupling centroid using the transformations shown in Eq (4-16). Since $^{GC}_{BC}T$ contains the resting position errors resulting from coupling the ball and groove bodies, the transformation $^{GC}_{OP_k}T$ reveals the effect of an inaccurate coupling on the position and orientation at the operating point. Larger position errors usually result from amplifying small rotations by the distance separating the operating point from the coupling centroid (Abbe offset).

$${}_{OP_k}^{GC}T = {}_{BC}^{GC}T \quad {}_{BD}^{BC}T \quad {}_{OP_k}^{BD}T \tag{4-16}$$

The multivariate error analysis is expanded to include the operating points. This is accomplished by expanding the vector of errors and the Jacobian matrix as shown in Eq (4-17) so that they incorporate error terms associated with the set of p operating points. If all six degrees of freedom at each operating point are included, then the dimensions of the error vector become $(6+6\times p)\times 1$, and the dimensions of the Jacobian matrix become $(6+6\times p)\times (m+n)$. However, most manufacturing operations have sensitive and insensitive directions, so considering only the sensitive directions simplifies the problem and requires only a subset of the degrees of freedom at each operating point. Evaluation of the new terms in the Jacobian matrix is still determined by perturbing each dimension in the ball and groove body, calculating the resting position and orientation, and subsequently extracting changes in the values within ${}^{GC}_{OP_k}T$.

$$\begin{bmatrix} \mathbf{d}_{x_r} \\ \mathbf{d}_{y_r} \\ \mathbf{d}_{g_r} \\ \mathbf{d}_{b_r} \\ \mathbf{d}_{a_r} \\ \mathbf{d}_{a_r} \\ \mathbf{d}_{x_{OP_1}} \\ \mathbf{d}_{y_{OP_1}} \\ \vdots \\ \mathbf{d}_{a_{OP_p}} \end{bmatrix} = \begin{bmatrix} \frac{\partial X_r}{\partial d_1} & \frac{\partial X_r}{\partial d_2} & \cdots & \frac{\partial X_r}{\partial d_{m+n}} \\ \frac{\partial Y_r}{\partial d_1} & \frac{\partial Y_r}{\partial d_2} & \cdots & \frac{\partial Y_r}{\partial d_{m+n}} \\ \vdots & \vdots & \ddots & \vdots \\ \frac{\partial A_{OP_p}}{\partial d_1} & \frac{\partial A_{OP_p}}{\partial d_2} & \cdots & \frac{\partial A_{OP_p}}{\partial d_{m+n}} \end{bmatrix} \begin{bmatrix} \Delta d_1 \\ \Delta d_2 \\ \vdots \\ \Delta d_{m+n} \end{bmatrix}$$

$$(4-17)$$

With the changes shown in Eq (4-17), the covariance matrix $[C_E]$ calculated with Eq (4-15) takes the alternative form shown in Eq (4-18). This form includes additional terms for the variances and covariances associated with the position and orientation at the operating points.

$$[C_{E}] = \begin{bmatrix} \mathbf{s}_{x_{r}}^{2} & \cos(x_{r}, y_{r}) & \cdots & \cos(x_{r}, x_{OP_{k}}) & \cdots & \cos(x_{r}, \mathbf{a}_{OP_{p}}) \\ \cos(y_{r}, x_{r}) & \mathbf{s}_{y_{r}}^{2} & \cdots & \cos(y_{r}, x_{OP_{k}}) & \cdots & \cos(y_{r}, \mathbf{a}_{OP_{p}}) \\ \vdots & \vdots & \ddots & \vdots & \cdots & \vdots \\ \cos(x_{OP_{k}}, x_{r}) & \cos(x_{OP_{k}}, y_{r}) & \cdots & \mathbf{s}_{x_{OP_{k}}}^{2} & \cdots & \cos(x_{OP_{k}}, \mathbf{a}_{OP_{p}}) \\ \vdots & \vdots & \vdots & \vdots & \ddots & \vdots \\ \cos(\mathbf{a}_{OP_{p}}, x_{r}) & \cos(\mathbf{a}_{OP_{p}}, y_{r}) & \cdots & \cos(\mathbf{a}_{OP_{p}}, x_{OP_{k}}) & \cdots & \mathbf{s}_{\mathbf{a}_{OP_{p}}}^{2} \end{bmatrix}$$

$$(4-18)$$

4.3. Tolerance Allocation

4.3.1. Manufacturing Cost and Tolerances

The cost of manufactured ball and groove bodies depends upon the selected manufacturing process and dimensional tolerances. The cost of achieving a particular tolerance depends upon both the dimension's nominal value and its tolerance. The manufacturing cost generally increases if the tolerance is tightened, and it is more expensive to hold a given tolerance on larger nominal dimensions. Based on this, Chase [10] recommends expressing tolerances as reciprocal power functions. Eq (4-19) expresses the tolerance for the j^{th} dimension, t_j , as a function of cost, C_j , range, R_j , and three constants a_j , b_j , and c_j . The values of the three constants depend upon the range and the manufacturing process. Although a constant term in Eq (4-19) would be necessary for accuracy, it is practically impossible to evaluate and doesn't affect the tolerance allocation.

$$t_j = c_j \times \frac{R_j^{a_j}}{C_i^{b_j}} \tag{4-19}$$

Chase provides a set of cost-tolerance curves for some metal removal processes [10]. By extrapolating these curves, we determine values for the coefficients a_j , b_j and c_j for each dimension in the kinematic coupling. Table 4-1 presents the coefficients calculated for an exemplary kinematic coupling configuration.

Table 4-1: Coefficients for Cost / Tolerance Relations

Dimension	Process	a_j	b_{j}	c_{j}
Thickness of the plate	Milling	0.4431	2.348	0.0355
Length of a leg	Grinding	0.4323	1.385	0.0217
Diameter of a ball	Lapping	0.3862	1.052	0.0130
Location of a hole	Milling	0.4431	2.257	0.0255
Height of a vee-groove	Grinding	0.4323	1.421	0.0228

Using the values in Table 4-1, Eq (4-19) defines the manufacturing cost for every dimension in the exemplary kinematic coupling. Plots of the relations in Fig 4-7 illustrate the effect of tightening tolerances. The portion of the total manufacturing cost that is attributable to tolerancing is then the sum of the costs for all l dimensions in the ball and groove bodies, as shown in Eq (4-20).

$$C_{total} = \sum_{j=1}^{l} \left(\frac{c_j \cdot R_j^{a_j}}{t_j} \right)^{1/b_j}$$

$$(4-20)$$

l being the number of manufacturing processes.

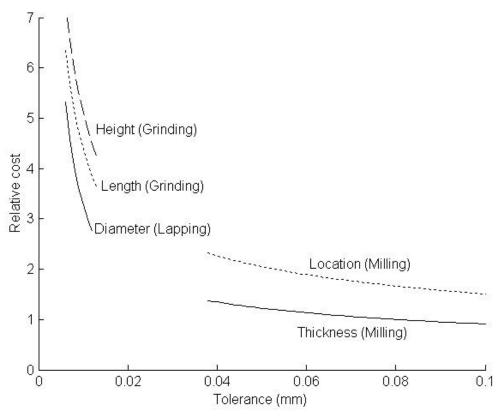


Fig 4-7: Cost / Tolerance Relations for Dimensions

4.3.2. Tolerance Allocation by Optimization

Optimal tolerances for the dimensions are determined using nonlinear constrained optimization. The problem is formulated as shown in Eq (4-21), where the total cost from Eq (4-20) is used as the objective function that is minimized. Constraints are formulated by specifying that the standard deviation of the translation and rotation errors must be positive yet below critical values. Additional bounds can be specified to prevent the optimization from driving the assigned tolerances to unreasonably high or low values.

minimize
$$\left(\sum_{j=1}^{l} \left(\frac{c_{j} \cdot R_{j}^{a_{j}}}{t_{j}}\right)^{1/b_{j}}\right) \text{ such that}$$

$$0 \leq \mathbf{s}_{x_{r}} \leq \mathbf{s}_{x_{r}}^{\max}$$

$$0 \leq \mathbf{s}_{y_{r}} \leq \mathbf{s}_{y_{r}}^{\max}$$

$$0 \leq \mathbf{s}_{z_{r}} \leq \mathbf{s}_{z_{r}}^{\max}$$

$$0 \leq \mathbf{s}_{a_{r}} \leq \mathbf{s}_{a_{r}}^{\max}$$

$$0 \leq \mathbf{s}_{b_{r}} \leq \mathbf{s}_{b_{r}}^{\max}$$

$$0 \leq \mathbf{s}_{g_{r}} \leq \mathbf{s}_{g_{r}}^{\max}$$

$$0 \leq \mathbf{s}_{g_{r}} \leq \mathbf{s}_{g_{r}}^{\max}$$

$$0 \leq \mathbf{s}_{g_{r}} \leq \mathbf{s}_{g_{r}}^{\max}$$

The allocation method was used to allocate tolerances to an exemplary kinematic coupling. The parametric surface representation was based on 25 dimensions in the ball body (m=25) and 18 dimensions (n=18) in the groove body, illustrated in Fig 4-8 and Fig 4-9. Some dimensions may look redundant, but they are actually needed to express the purely geometric tolerances in terms of dimensional tolerances. The cost-tolerance coefficients listed in Table 4-1 and the constraints listed in Table 4-2 were used during the optimization. The resulting tolerances allocated by the optimization procedure are listed in Table 4-3. The different Matlab codes are presented in Appendix D.

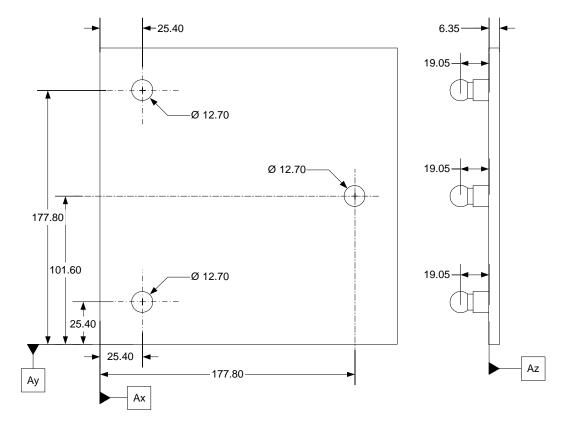


Fig 4-8: Dimension Schemes for the Ball Pallet, in its Datum Frame

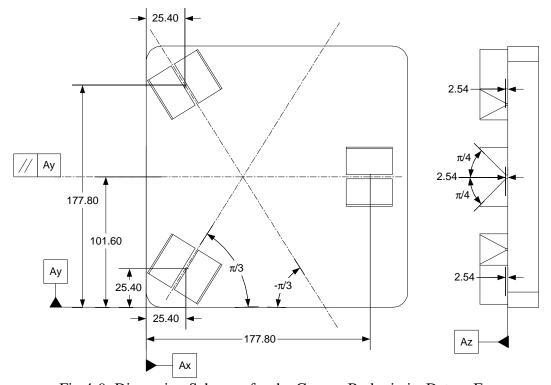


Fig 4-9: Dimension Schemes for the Groove Body, in its Datum Frame

Table 4-2: Constraints Used for Exemplary Tolerance Allocation

Variation	Constraint	Calculated		
$\mathbf{S}_{x_r}^{\mathrm{max}}$	6.67 µm	5.23 μm		
$\mathbf{s}_{y_r}^{\max}$	6.67 µm	6.67 µm		
$\boldsymbol{s}_{z_r}^{\mathrm{max}}$	6.67 µm	4.87 μm		
$oldsymbol{s}_{oldsymbol{g}_r}^{ ext{max}}$	1.164×10 ⁻³ rad	$0.115 \times 10^{-3} \text{ rad}$		
$\boldsymbol{S}_{\boldsymbol{b}_r}^{\max}$	1.164×10 ⁻³ rad	0.068×10 ⁻³ rad		
$\boldsymbol{S}_{\boldsymbol{a}_r}^{\mathrm{max}}$	1.164×10 ⁻³ rad	0.078×10 ⁻³ rad		

Table 4-3: Computed Tolerances

	Dimensions		Nominal Dimension	Assigned Tolerance	
	Thickness of the plate		6.35 mm	1.000 mm	
	Length of a leg (×3	5)	19.05 mm	0.749 mm	
	Ball diameter (×3))	12.70 mm	0.464 mm	
	Roundness of ball at contact	point (×6)	0 mm	0.071 mm	
	X coordinate of a leg-axis at the top of the plate	Leg 1	25.40 mm		
		Leg 2	25.40 mm	0.030 mm	
let		Leg 3	177.80 mm		
Ball Pallet	Y coordinate of a leg-axis at the top of the plate	Leg 1	177.80 mm		
all		Leg 2	25.40 mm	0.030 mm	
B	at the top of the plate	Leg 3	101.6 mm		
	V according to of a log axis at	Leg 1	25.40 mm		
	X coordinate of a leg-axis at the bottom of the plate	Leg 2	25.40 mm	0.030 mm	
		Leg 3	177.80 mm		
	Y coordinate of a leg axis at the bottom of the plate	Leg 1	177.80 mm	0.030 mm	
		Leg 2	25.40 mm		
		Leg 3	101.6 mm		
	Height of the vertices for the groove body (×3)		2.54 mm	0.449 mm	
	Orientation angle of a groove	Groove 1	-π/3 rad		
		Groove 2	$\pi/3$ rad	0.100 rad	
dy		Groove 3	π rad		
Во	Half-angle of aperture of a g	π/4 rad	0.078 rad		
ve	X coordinate of a groove	Groove 1	25.40 mm		
Groove Body		Groove 2	25.40 mm	0.419 mm	
		Groove 3	177.80 mm		
	Y coordinate of a groove	Groove 1	177.80 mm		
		Groove 2	25.40 mm	0.419 mm	
		Groove 3	101.60 mm		

Total number of dimensions: 43

It appears that for the actual kinematic coupling geometry, the position error in the *y*-direction is the critical parameter. The optimization program minimizes the manufacturing cost while reaching this limit.

4.3.3. Verification by Monte Carlo Simulation

The results of the optimization algorithm are verified with a Monte Carlo simulation, illustrated in Fig 4-10. A large number of kinematic couplings are virtually generated using the parametric model. Their dimensions are randomly distributed, with a mean equal to their nominal value and a standard deviation equal to one third of the allocated tolerance.

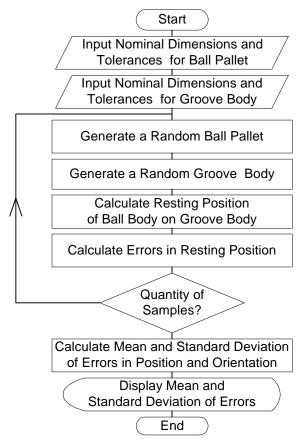


Fig 4-10: Flowchart of Monte Carlo Simulation for Kinematic Couplings

The algorithm calculates the resting position and orientation of each randomly generated sample, then it performs a statistical treatment on the collected results. Finally, it returns the mean and standard deviation of the resting position and orientation.

Table 4-4 compares the results computed by the optimization algorithm with those calculated by the Monte Carlo simulation. The inputs were the nominal dimensions and the assigned tolerances presented in Table 4-3. 10,000 samples were generated for the simulation. For a better comparison, the limits of a 95% confidence interval were computed on the standard deviations of the six errors returned by the simulation.

Table 4-4: Comparison Optimization / Simulation

Standard Deviation	Results of Tolerance Allocation	Simulation: Limits of the 95% confidence interval	
		Lower	Upper
$\boldsymbol{s}_{x_r}(\mu \mathrm{m})$	5.23	5.14	5.28
$\boldsymbol{s}_{y_r}(\mu m)$	6.67	6.66	6.85
$\boldsymbol{s}_{z_r}(\mu\mathrm{m})$	4.87	4.81	4.94
$\mathbf{s}_{\mathbf{g}_r} (\times 10^{-6} \text{ rad})$	115	114	117
$\boldsymbol{s}_{\boldsymbol{b}_r} (\times 10^{-6} \text{ rad})$	67.5	66.1	67.9
$\mathbf{s}_{a_r} (\times 10^{-6} \text{ rad})$	78.4	76.6	78.7

4.4. Conclusion

Kinematic couplings are known as an economical method for precisely locating one body with respect to another, but the relative position and orientation between the coupled bodies depends upon manufacturing errors. In systems that exchange coupled bodies, system-wide variation results from the inaccuracy of dimensions in each body. Therefore, tolerances should be selected so that the system-wide variation is within a specified range.

This chapter presents and demonstrates a method for allocating tolerances to the dimensions of the bodies. A parametric representation of the contacting surfaces is constructed and combined with a procedure that calculates the resting location based on the inaccurate dimensions. An analytical relation between dimensional variation and variation in the resting location is obtained from multivariate error analysis. Optimal tolerances are computed by minimizing the relative manufacturing cost while respecting constraints on variation in the resting position and orientation.

Chapter 5: Conclusions and Future Work

5.1. Conclusions

Exactly constrained systems present interesting characteristics for precision engineering. In effect, they are repeatable, economical to build, and predictable if used advisedly. These properties suggest that it is possible to combine them in order to reduce the manufacturing cost of mass-produced kinematic systems. This thesis verified this hypothesis by developing a rigorous procedure for solving the current problem; then it illustrated the resulting method with two relevant examples.

The cost and the performances of a mechanical assembly are governed by the tolerances assigned to the dimensions and the geometry of the components. That is the reason why the developed procedure was a least cost tolerance allocation. A mathematical model is established for the exactly constrained system by a comprehensive analysis of its kinematic connections. The manufacturing variations are combined by applying principles of statistics similar to the ones used in the SPC method; the developed procedure could then be easily incorporated in a quality policy. A basic study of the functional requirements of the system enables the establishment of a direct relation between its performances and its manufacturing variations. Finally, empirical functions established from experimental observations relate variation and cost in manufacturing. These different analyses are nested in an optimization algorithm in order to perform a least cost tolerance allocation.

In conclusion, this thesis presents an analytical tool for the precision design engineer. It helps him or her to select the tolerances to assign to a kinematic system in order to reduce its manufacturing cost while respecting its functionality. The developed method enables the use of the efficiency of precision engineering for solving a current industrial problem.

5.2. Future Work

The presented method is ready to be used, which is proven by the two performed examples. However, it can be improved. First of all, other methods for analyzing the

variations can be explored in addition to the ones presented in Section 2.2.3. They may be more suitable for other kinematic configurations. Some promising methods are described in literature dealing with optimization problems in general [12]; they can be adapted for least cost tolerance allocation procedures.

Furthermore, new cost / tolerance relations can be experimentally established for manufacturing processes different from the traditional metal removal processes. In effect, the existing relations only deal with these kinds of processes. Other processes like etching, EDM, or LIGA technique can be used to produce exactly constrained components, especially in a precision engineering field. Hence it would be interesting to establish their cost / tolerance relations in order to extend the possibility of the current method.

On the other hand, the presented method reduces the manufacturing cost only by assigning the tolerances. A broader analysis could also optimize the nominal values of the dimensions. This improved method would not only be a least cost tolerance allocation, but a more global design optimization procedure that would be more efficient for reducing the manufacturing cost of the mass-produced components.

Finally, the robustness of the current method can be improved by taking into consideration the effects of mechanical loads, vibrations, and similar constraints. In effect, the presented procedure assumed that these external mechanical disturbances were negligible. Incorporating them into the least cost optimization method would then widen the scope of the analysis. These disturbances would be expressed as additional constraints in the optimization algorithm, since they characterize the performance of the system.

Appendix A:

Probability Density Function of Sum of Squares

Problem statement:

X: Gaussian random variable $X \sim N(0, s_X)$

Y: Gaussian random variable $Y \sim N(0, s_Y)$

X and Y are independent.

What is the probability density function of $R = \sqrt{X^2 + Y^2}$?

Joint density function of *X* and *Y*:

$$f_{XY}(x, y) = \frac{1}{2\boldsymbol{p} \cdot \boldsymbol{s}_{X} \cdot \boldsymbol{s}_{Y}} \times \exp\left[-\frac{1}{2}\left(\frac{x^{2}}{\boldsymbol{s}_{X}^{2}} + \frac{y^{2}}{\boldsymbol{s}_{Y}^{2}}\right)\right]$$
(A1)

Let $X = R \cos q$ and $Y = R \sin q$

Jacobian of the transformation:

$$J = \begin{vmatrix} \frac{\partial X}{\partial R} & \frac{\partial Y}{\partial R} \\ \frac{\partial X}{\partial q} & \frac{\partial Y}{\partial q} \end{vmatrix} = \begin{vmatrix} \cos q & \sin q \\ -R\sin q & R\cos q \end{vmatrix} = R(\cos^2 q + \sin^2 q) = R$$
 (A2)

$$f_{Rq}(R,q) = f_{XY}(x,y) \times |J| \tag{A3}$$

$$\Leftrightarrow f_{Rq}(R, \mathbf{q}) = \frac{R}{2\mathbf{p} \cdot \mathbf{s}_{X} \cdot \mathbf{s}_{Y}} \times \exp \left[-\frac{R^{2}}{2} \left(\frac{\cos^{2} \mathbf{q}}{\mathbf{s}_{X}^{2}} + \frac{\sin^{2} \mathbf{q}}{\mathbf{s}_{Y}^{2}} \right) \right]$$
(A4)

$$\Leftrightarrow f_{Rq}(R, \mathbf{q}) = \frac{R}{2\mathbf{p} \cdot \mathbf{s}_{X} \cdot \mathbf{s}_{Y}} \times \exp \left[-\frac{R^{2}}{2} \left(\frac{1}{\mathbf{s}_{Y}^{2}} + \frac{\mathbf{s}_{Y}^{2} - \mathbf{s}_{X}^{2}}{\mathbf{s}_{X}^{2} \cdot \mathbf{s}_{Y}^{2}} \cos^{2} \mathbf{q} \right) \right]$$
(A5)

$$\Leftrightarrow f_{Rq}(R, \mathbf{q}) = \frac{R \times \exp\left(-\frac{R^2}{2\mathbf{s}_{Y}^2}\right)}{2\mathbf{p} \cdot \mathbf{s}_{X} \cdot \mathbf{s}_{Y}} \times \exp\left(-\frac{R^2}{2} \cdot \frac{\mathbf{s}_{Y}^2 - \mathbf{s}_{X}^2}{\mathbf{s}_{X}^2 \cdot \mathbf{s}_{Y}^2} \cdot \cos^2 \mathbf{q}\right)$$
(A6)

Probability density function of R:

$$f_R(R) = \int_{0}^{2\mathbf{p}} f_{R\mathbf{q}}(R, \mathbf{q}) \cdot d\mathbf{q}$$
 (A7)

 $\left.f_{R\boldsymbol{q}}\left(R,\boldsymbol{q}\right)\right|_{R=cons \, \mathrm{tan} \, t}$ is a π -periodical even function, so:

$$f_R(R) = 4 \int_0^{\mathbf{p}/2} f_{R\mathbf{q}}(R, \mathbf{q}) \cdot d\mathbf{q}$$
 (A8)

$$\Leftrightarrow f_{R}(R) = \frac{2R \times \exp\left(-\frac{R^{2}}{2\mathbf{s}_{Y}^{2}}\right)}{\mathbf{p} \cdot \mathbf{s}_{X} \cdot \mathbf{s}_{Y}} \times \int_{0}^{\mathbf{p}/2} \exp\left(-\frac{R^{2}}{2} \cdot \frac{\mathbf{s}_{Y}^{2} - \mathbf{s}_{X}^{2}}{\mathbf{s}_{X}^{2} \cdot \mathbf{s}_{Y}^{2}} \cdot \cos^{2}\mathbf{q}\right) \cdot d\mathbf{q}$$
(A9)

Change of variables: let $z = \cos q \iff q = \arccos z$

Derivation:
$$d\mathbf{q} = -\frac{dz}{\sqrt{1-z^2}}$$

Limits: if
$$q = 0$$
 then $z = 1$

if
$$q = \frac{p}{2}$$
 then $z = 0$

$$\Leftrightarrow f_R(R) = \frac{2R \times \exp\left(-\frac{R^2}{2\mathbf{s}_Y^2}\right)}{\mathbf{p} \cdot \mathbf{s}_X \cdot \mathbf{s}_Y} \times \int_0^1 \frac{1}{\sqrt{1-z^2}} \cdot \exp\left(-\frac{R^2}{2} \cdot \frac{\mathbf{s}_Y^2 - \mathbf{s}_X^2}{\mathbf{s}_X^2 \cdot \mathbf{s}_Y^2} \cdot z^2\right) \cdot dz$$
(A10)

Note:
$$\int_{0}^{1} \frac{\exp(-A \cdot x^{2})}{\sqrt{1 - x^{2}}} dx = \frac{\mathbf{p}}{2} \exp\left(-\frac{A}{2}\right) \times Bessell\left(0, \frac{A}{2}\right), \quad A \text{ being a constant and}$$

BesselI(v, x) being a function that satisfies the modified Bessel equation: $x^2 \cdot y'' + x \cdot y' - (x^2 + v^2) \cdot y = 0$

Then:

$$f_{R}(R) = \frac{R \times \exp\left(-\frac{R^{2}}{2\boldsymbol{s}_{Y}^{2}}\right)}{\boldsymbol{s}_{X} \cdot \boldsymbol{s}_{Y}} \times \exp\left(-\frac{R^{2}}{4} \cdot \frac{\boldsymbol{s}_{Y}^{2} - \boldsymbol{s}_{X}^{2}}{\boldsymbol{s}_{X}^{2} \cdot \boldsymbol{s}_{Y}^{2}}\right) \times Bessell\left(0, \frac{R^{2}}{4} \cdot \frac{\boldsymbol{s}_{Y}^{2} - \boldsymbol{s}_{X}^{2}}{\boldsymbol{s}_{X}^{2} \cdot \boldsymbol{s}_{Y}^{2}}\right)$$
(A11)

$$\Leftrightarrow f_{R}(R) = \frac{R}{\mathbf{s}_{X} \cdot \mathbf{s}_{Y}} \times \exp\left(-\frac{R^{2} \cdot (\mathbf{s}_{X}^{2} + \mathbf{s}_{Y}^{2})}{4 \cdot \mathbf{s}_{X}^{2} \cdot \mathbf{s}_{Y}^{2}}\right) \times Bessell\left(0, \frac{R^{2}}{4} \cdot \frac{\mathbf{s}_{Y}^{2} - \mathbf{s}_{X}^{2}}{\mathbf{s}_{X}^{2} \cdot \mathbf{s}_{Y}^{2}}\right)$$
(A12)

Appendix B:

Matlab Codes for Kinematic Couplings

B1. Optimization: Objective Function

```
function f = kct_obj(x)
% COEFFICIENTS
% Coefficients CA
CA_{lap} = 0.3862;
CA\_grind = 0.4323;
CA_ream = 0.2880;
CA mill = 0.4431;
CA_turn = 0.3515;
% It will be CA-1 for the angles
% Ranges R
R_{\text{Thick}} = 6.35;
R_Length = 19.05;
R_{Diam} = 12.70;
R_Circ = R_Diam;
R_PosB = 177.8; % X and Y should have the same tolerance
R Height = 31.75; % Hypothenuse
R Orient = 38.1;
R_Halfa = R_Height;
R_PosG = 177.8; % X and Y should have the same tolerance
% Coefficients CB
CB\_Thick = 2.3480;
CB Length = 1.3847;
CB_Diam = 1.0516;
CB Circ = CB Diam;
CB_{pos} = 2.2568;
CB_Height = 1.4207;
CB_Orient = 1.3490;
CB_Halfa = CB_Height;
CB_{posG} = 2.2568;
% Coefficients Bm
Bm Thick = 0.3420;
Bm\_Length = 0.1578;
Bm_Diam = 0.0410;
Bm_Circ = Bm_Diam;
Bm_PosB = 0.5440;
```

```
Bm_Height = 0.1999;
Bm_Orient = 0.2714;
Bm_Halfa = Bm_Height;
Bm PosG = 0.5440;
% Coefficients CG
CG_Thick = Bm_Thick^CB_Thick / R_Thick^CA_mill;
CG_Length = Bm_Length^CB_Length / R_Length^CA_grind;
CG_Diam = Bm_Diam^CB_Diam / R_Diam^CA_lap;
CG_Circ = Bm_Circ^CB_Circ / R_Circ^CA_lap;
CG_PosB = Bm_PosB^CB_PosB / R_PosB^CA_mill;
CG_Height = Bm_Height^CB_Height / R_Height^CA_grind;
CG_Orient = Bm_Orient^CB_Orient / R_Orient^CA_grind;
CG Halfa = Bm Halfa^CB Halfa / R Halfa^CA grind;
CG_PosG = Bm_PosG^CB_PosG / R_PosG^CA_mill;
% COST FUNCTION
f = (CG\_Thick * R\_Thick^CA\_mill / x(1))^(1/CB\_Thick) +
(CG_Length * R_Length^CA_grind / x(2))^(1/CB_Length) +
(CG Diam * R Diam^CA lap / x(3))^(1/CB Diam) + (CG Circ *
R Circ^CA lap / x(4))^(1/CB Circ) + (CG PosB *
R_PosB^CA_mill / x(5))^(1/CB_PosB) + (CG_Height *
R_Height^CA_grind / x(6))^(1/CB_Height) + (CG_Orient *
R_Orient^(CA_grind-1) / x(7))^(1/CB_Orient) + (CG_Halfa *
R_Halfa^(CA_grind-1) / x(8))^(1/CB_Halfa) + (CG_PosG *
R_PosG^CA_mill / x(9))^(1/CB_PosG);
f= real(f);
```

B2. Optimization: Constraint Functions

```
function [c, ceq] = kct_const(x)
% NOMINAL DIMENSIONS
% For the ball pallet
Xb nomB = [1 1 7] * 25.4;
Yb_nomB = [7 1 4] * 25.4;
t = 6.35;
L = [0.75 \ 0.75 \ 0.75] * 25.4;
D = [0.5 \ 0.5 \ 0.5] * 25.4;
% For the groove body
Xp nomG = [1.0 1.0 7.0] * 25.4;
Yp\_nomG = [7.0 1.0 4.0] * 25.4;
Hvertex = [0.1 \ 0.1 \ 0.1] * 25.4;
Or = [-60 \ 60 \ 180] * pi/180;
Halfa = [45 45 45
                     45 45 45] * pi/180;
Dpft = 12.7;
% TOLERANCES
% x(1) = Thick_tol  % x(2) = Length_tol
% x(3) = Diam_tol
                       % x(4) = Circ_tol
% x(5) = PosB tol
                       % x(6) = Heightv tol
                     % x(8) = Halfa_tol
% x(7) = Orient_tol
% x(9) = PosG tol
% MAXIMUM TOLERANCES DEFINED BY THE DESIGNER
Xmax = 0.02;
Ymax = 0.02;
Zmax = 0.02i
Amax = 0.002;
Bmax = 0.002;
Gmax = 0.002;
% CONSTRAINT FUNCTION
[Xcalc, Ycalc, Zcalc, Acalc, Bcalc, Gcalc] =
kct_errors(Xb_nomB, Yb_nomB, t, L, D, Xp_nomG, Yp_nomG,
Hvertex, Or, Halfa, Dpft, x(1), x(2), x(3), x(4), x(5),
x(6), x(7), x(8), x(9));
calc = [Xcalc Ycalc Zcalc];
c = [real(Xcalc)-Xmax, real(Ycalc)-Ymax, real(Zcalc)-Zmax];
ceq = [];
```

B3. Optimization: Invoking File

```
close all; clear all;
% Invoke constrained optimization routine
Lower_bounds = [0.001 0.001 0.001 0.001 0.001 0.001 0.002
0.0002 0.001];
Upper_bounds = [1 1 1 1 1 1 0.1 0.1 1];
Starting = 0.1*Lower_bounds;

options =
optimset('LargeScale','off','Diagnostics','on','Display','i
ter','MaxFunEvals',4000,'TolFun',0.01);
[x, fval, exitflag, output] = fmincon(@kct_obj, Starting,
[], [], [], Lower_bounds, Upper_bounds, @kct_const,
options);
Cost = fval
```

B4. Monte Carlo Simulation

```
% Kinematic Coupling Tolerances, Monte Carlo Simulation
% Dimensions in mm and radians
clear all; close all;
% PARAMETERS FOR THE SIMULATION
N \text{ samples} = 10000;
% NOMINAL DIMENSIONS
% For the ball pallet
Xb_{nomB} = [1 \ 1 \ 7] * 25.4; % Fixed
Yb_nomB = [7 1 4] * 25.4; % Fixed
t = 6.35;
L = [0.75 \ 0.75 \ 0.75] * 25.4;
D = [0.5 \ 0.5 \ 0.5] * 25.4;
% For the groove body
Xp_nomG = [1.0 1.0 7.0] * 25.4; % Fixed
Yp\_nomG = [7.0 1.0 4.0] * 25.4; % Fixed
Hvertex = [0.1 0.1 0.1] * 25.4;
Or = [-60 \ 60 \ 180] * pi/180;
Halfa_nom = [45 45 45 45 45] * pi/180;
Dpft = 12.7; % Fixed
% TOLERANCES
Thick tol = 1.00;
Length_tol = 0.9927;
Diam_tol = 0.0312;
Circ_tol = 0.0122;
XB tol = 0.0078;
YB tol = 0.0078;
Heightv tol = 0.0320;
Orient_tol = 0.1;
Halfa tol = 0.0039;
XG_{tol} = 0.0277;
YG_{tol} = 0.0277;
for is = 1:N samples
% GENERATING RANDOM VARIABLES
% For the ball pallet
    for one plate
    for i = 1:3
       Length(i) = normrnd(L(i), Length_tol/3);
       Diam(i) = normrnd(D(i), Diam_tol/3);
```

```
Circ(2*i-1) = normrnd(0, Circ tol/3);
        Circ(2*i) = normrnd(0, Circ_tol/3);
        dXtop_B(i) = normrnd(0, XB_tol/3);
        dYtop_B(i) = normrnd(0, YB_tol/3);
        dXbot B(i) = normrnd(0, XB tol/3);
        dYbot_B(i) = normrnd(0, YB_tol/3);
% For the groove body
        Heightv(i) = normrnd(Hvertex(i), Heightv tol/3);
        Orient(i) = normrnd(Or(i), Orient_tol/3);
        Halfa(2*i-1) = normrnd(Halfa_nom(i), Halfa_tol/3);
        Halfa(2*i) = normrnd(Halfa_nom(i), Halfa_tol/3);
        dXpin G(i) = normrnd(0, XG tol/3);
        dYpin_G(i) = normrnd(0, YG_tol/3);
    end
% CALCULATING RESTING POSITION
    [X_B_BC, Y_B_BC, Z_B_BC, Db_row] =
kct_ballgeom(Xb_nomB, Yb_nomB, Thick, Length, Diam, Circ,
dXtop B, dYtop B, dXbot B, dYbot B);
    PB1=[X B BC(1); Y B BC(1); Z B BC(1); 1];
    PB2=[X_B_BC(2); Y_B_BC(2); Z_B_BC(2); 1];
    PB3=[X_B_BC(3); Y_B_BC(3); Z_B_BC(3); 1];
    PB4=PB3;
    dB=Db_row';
    [TG11 G, TG12 G, TG21 G, TG22 G, TG31 G, TG32 G] =
kct_groovegeom(Xp_nomG, Yp_nomG, Hvertex, Or, Halfa, Dpft,
dXpin G, dYpin G);
[alpha, beta, gamma, xr, yr, zr, Pc1, Pc2, Pc3, Pc4, Pc5, Pc6]=kct_res
t(PB1,PB2,PB3,PB4,dB,TG11_G,TG12_G,TG21_G,TG22_G,TG31_G,TG3
2_G);
    Amcs(is) = alpha; Bmcs(is) = beta; Gmcs(is) = gamma;
    Xmcs(is) = xr; Ymcs(is) = yr;
                                        Zmcs(is) = zr;
end
% STATISTICS
mu_A = mean(Amcs);
                               sigma_A = std(Amcs);
mu_B = mean(Bmcs);
                               sigma_B = std(Bmcs);
                              sigma_G = std(Gmcs);
mu G = mean(Gmcs);
mu_X = mean(Xmcs);
                              sigma_X = std(Xmcs);
mu Y = mean(Ymcs);
                              sigma Y = std(Ymcs);
mu_Z = mean(Zmcs);
                              sigma_Z = std(Zmcs);
```

B5. Sub-Function: kct_ballgeom

function [X_B_BC, Y_B_BC, Z_B_BC, Db] =

```
kct_ballgeom(X_B_nomB, Y_B_nomB, Thick, Lft, Diam, Circ,
DeltaX_Top_datB, DeltaY_Top_datB, DeltaX_Bottom_datB,
DeltaY_Bottom_datB)
% X_B_nomB: X coord of the 3 balls 3*1
% Y_B_nomB: Y coord of the 3 balls 3*1
% Thick: Thickness of the plate is a scalar
% Lft: Length of a foot (until center of the ball) is a 3*1
% Diam: Diameter of a ball is a 3*1
% Circ: Circularity of a radius is a 6*1
% DeltaX_Top_datB: X Offset at the top of the plate, is a
3 * 1
% DeltaY_Top_datB: Y Offset at the top of the plate, is a
3*1
% DeltaX_Bottom_datB: X Offset at the bottom of the plate,
is a 3*1
% DeltaY_Bottom_datB: X Offset at the bottom of the plate,
is a 3*1
for ib = 1:3
    X_Top_datB(ib) = X_B_nomB(ib) + DeltaX_Top_datB(ib);
    Y_Top_datB(ib) = Y_B_nomB(ib) + DeltaY_Top_datB(ib);
    X_Bottom_datB(ib) = X_B_nomB(ib) +
DeltaX_Bottom_datB(ib);
    Y_Bottom_datB(ib) = Y_B_nomB(ib) +
DeltaY Bottom datB(ib);
    Z_Bottom_datB(ib) = -Thick; % Same thickness for
one plate
% CALCULATIONS
%% Coordinates of the balls, in the datum CSYS (starting
point + magnitude * unit direction vector)
    Magn_Vect_Axis(ib) = sqrt((X_Top_datB(ib)-
X_Bottom_datB(ib))^2 + (Y_Top_datB(ib)-Y_Bottom_datB(ib))^2
+ Z Bottom datB(ib)^2);
    X_B_datB(ib) = X_Bottom_datB(ib) + (X_Bottom_datB(ib) -
X_Top_datB(ib)) * Lft(ib) / Magn_Vect_Axis(ib);
    Y_B_datB(ib) = Y_Bottom_datB(ib) + (Y_Bottom_datB(ib) -
Y_Top_datB(ib)) * Lft(ib) / Magn_Vect_Axis(ib);
    Z_B_datB(ib) = Z_Bottom_datB(ib) + Z_Bottom_datB(ib) *
Lft(ib) / Magn Vect Axis(ib);
end
```

```
%% Geometry of the coupling triangle
%%% Length of the sides
Side_TriB(1) = sqrt((X_B_datB(2)-X_B_datB(3))^2 +
(Y_B_datB(2)-Y_B_datB(3))^2 + (Z_B_datB(2)-Z_B_datB(3))^2
);
Side_TriB(2) = sqrt((X_B_datB(3)-X_B_datB(1))^2 +
(Y_B_datB(3)-Y_B_datB(1))^2 + (Z_B_datB(3)-Z_B_datB(1))^2
Side_TriB(3) = sqrt((X_B_datB(1)-X_B_datB(2))^2 +
(Y_B_datB(1)-Y_B_datB(2))^2 + (Z_B_datB(1)-Z_B_datB(2))^2
);
%%% Apex angles
Apex TriB(1) = acos((Side TriB(2)^2 + Side TriB(3)^2 -
Side_TriB(1)^2) / (2*Side_TriB(2)*Side_TriB(3)) );
Apex_TriB(2) = acos((Side_TriB(3)^2 + Side_TriB(1)^2 -
Side_TriB(2)^2) / (2*Side_TriB(3)*Side_TriB(1)) );
Apex_TriB(3) = acos((Side_TriB(1)^2 + Side_TriB(2)^2 -
Side TriB(3)^2 / (2*Side TriB(1)*Side TriB(2)) );
%%% Coordinates of the centers of the balls in the BC CSYS
X_B_BC(3) = Side_TriB(2) * sin(Apex_TriB(1)/2) /
cos(Apex TriB(2)/2);
Y_B_BC(3) = 0; % By definition, Ball 3 is on the X-
axis
X_B_BC(1) = X_B_BC(3) - Side_TriB(2) * cos(Apex_TriB(3)/2);
Y_B_B(1) = Y_B_B(3) + Side_TriB(2) * sin(Apex_TriB(3)/2);
X_B_BC(2) = X_B_BC(3) - Side_TriB(1) * cos(Apex_TriB(3)/2);
Y_B_BC(2) = Y_B_BC(3) - Side_TriB(1) * sin(Apex_TriB(3)/2);
for ib = 1:3
    Z_B_B(ib) = 0; % In BC CSYS, the Z-plane goes
through the 3 balls
   Rb(2*ib-1) = Diam(ib)/2; % Fix the average radius on
one side of the ball
   Rb(2*ib) = Diam(ib)/2; % Fix the average radius on
the other side
end
for i = 1:6
   Db(i) = 2*(Rb(i) + Circ(i)); % Add out of roundness
end
```

B6. Sub-Function: kct_centroid

```
function [T] = kct centroid(X, Y, Z)
% Calculates the coordinates of the apices of a coupling
triangle in its centroid coordinates system
% Length of the sides
Side(1) = sqrt((X(2)-X(3))^2 + (Y(2)-Y(3))^2 + (Z(2)-Y(3))^3 + (Z(2)-Y(2))^3 + (Z(2)-Y(2))^2 + (Z(2)-Y(2))^3 + (Z(2)-Y(2))^3 + (Z(2)-Y(2))^3 + (Z(2)-Y(2))^2 + (Z(2)-Y(2))^2 + (Z(2)-Y(2))^2 + (Z(2)-Y(2))^2 + (Z(2)-Y(2))^2
Z(3))^2);
Side(2) = sqrt((X(3)-X(1))^2 + (Y(3)-Y(1))^2 + (Z(3)-Y(1))^3 + (Z(3)-Y(1))^4 + (Z(3)-Y(1))^4
Z(1))^2;
Side(3) = sqrt((X(1)-X(2))^2 + (Y(1)-Y(2))^2 + (Z(1)-Y(2))^3
Z(2))^2;
% Apex angles
Apex(1) = acos( (Side(2)^2 + Side(3)^2 - Side(1)^2) /
(2*Side(2)*Side(3)));
Apex(2) = acos( (Side(3)^2 + Side(1)^2 - Side(2)^2) /
(2*Side(3)*Side(1)));
Apex(3) = acos((Side(1)^2 + Side(2)^2 - Side(3)^2) /
(2*Side(1)*Side(2)) );
% Coordinates of the centers of the balls in the centroid
CSYS
    X CC(3) = Side(2) * sin(Apex(1)/2) / cos(Apex(2)/2);
    Y CC(3) = 0; % By definition, Ball 3 is on the X-axis
    X_{CC}(1) = X_{CC}(3) - Side(2) * cos(Apex(3)/2);
    Y_{CC}(1) = Y_{CC}(3) + Side(2) * sin(Apex(3)/2);
    X_{CC(2)} = X_{CC(3)} - Side(1) * cos(Apex(3)/2);
    Y_{CC}(2) = Y_{CC}(3) - Side(1) * sin(Apex(3)/2);
    for i = 1:3
                    Z CC(i) = 0; % In centroid CSYS, the Z-plane goes
through the 3 balls
    end
% Unit vectors
U_31 = [X(1)-X(3); Y(1)-Y(3); Z(1)-Z(3)] / Side(2);
U 32 = [X(2)-X(3); Y(2)-Y(3); Z(2)-Z(3)] / Side(1);
U_3C = [U_31(1)+U_32(1); U_31(2)+U_32(2); U_31(3)+U_32(3)]
/ sqrt((U_31(1)+U_32(1))^2 + (U_31(2)+U_32(2))^2 +
(U_31(3)+U_32(3))^2;
% Coordinates of centroid
Dist_3C = Side(2) * sin(Apex(1)/2) / cos(Apex(2)/2);
Xc = X(3) + Dist_3C * U_3C(1);
```

```
Yc = Y(3) + Dist_3C * U_3C(2);
Zc = Z(3) + Dist_3C * U_3C(3);
Bc = asin((Zc-Z(3)) / X_CC(3));
% Rotation about the Y axis
Ac = acos((X(3)-Xc) / (X_CC(3)*cos(Bc)));
% Rotation about the Z axis
Gc = asin((Z(2) - Zc + X_CC(2)*sin(Bc)) /
% Set the elements within the homogenous transformation
matrix
T(1:4,1) = [\cos(Ac) * \cos(Bc);
sin(Ac)*cos(Bc);
                                        -sin(Bc);
01;
T(1:4,2) = [\cos(Ac) * \sin(Bc) * \sin(Gc) - \sin(Ac) * \cos(Gc);
sin(Ac)*sin(Bc)*sin(Gc)+cos(Ac)*cos(Gc); cos(Bc)*sin(Gc);
0];
T(1:4,3) = [\cos(Ac) * \sin(Bc) * \cos(Gc) + \sin(Ac) * \sin(Gc);
sin(Ac)*sin(Bc)*cos(Gc)-cos(Ac)*sin(Gc); cos(Bc)*cos(Gc);
T(1:4,4) = [Xc; Yc; Zc; 1];
```

B7. Sub-function: kct errors

```
function [X_tol, Y_tol, Z_tol, A_tol, B_tol, G_tol] =
kct_errors(Xb_nomB, Yb_nomB, t, L, D, Xp_nomG, Yp_nomG,
Hvertex, Or, Halfa, Dpft, thick_tol, Length_tol, Diam_tol,
circ_tol, PosB_tol, Heightv_tol, Orient_tol, Halfa_tol,
PosG tol)
% Xb nomB: X coord of the 3 balls 3*1
% Yb_nomB: Y coord of the 3 balls 3*1
% t: Thickness of the plate is a scalar
% L: Length of a foot (until center of the ball) is a 3*1
% D: Diameter of a ball is a 3*1
% Xp_nomG: nominal X coord of a vee-groove, is a 3*1
% Yp_nomG: nominal Y coord of a vee-groove, is a 3*1
% Hvertex: Distance between the top of the plate and the
vertex of a vee-groove, is a 3*1
% Or: Orientation angle of the grooves, is a 3*1
% Halfa: Half-Angle of aperture of the vee-grooves is a 6*1
% Dpft: Diameter of a perfect virtual ball, is a scalar
% GENERATING DIMENSIONS
                        % Thickness of the ball plate
Dim(1) = t;
for i = 1:3
   Dim(1+i) = L(i); % Foot length for the ball plate
   Dim(4+i) = D(i);
                        % Ball diameter for the ball plate
   Dim(6+2*i) = 0;
                        % Circularity on one side for the
ball plate
   Dim(7+2*i) = 0;
                        % Circularity on the other side
for the ball plate
   Dim(13+i) = 0; % X offset at the top for the ball
plate
    Dim(16+i) = 0;
                        % Y offset at the top for the ball
plate
    Dim(19+i) = 0; % X offset at the bottom of the
ball plate
    Dim(22+i) = 0; % Y offset at the bottom of the
ball plate
    Dim(25+i) = Hvertex(i);
                                   % Height of the
vertices for the groove body
   Dim(28+i) = Or(i);
                                   % Orientation angle of
the grooves for the groove body
    Dim(30+2*i) = Halfa(2*i-1);
                                  % Half-angle on one
side of the groove, for the groove body
    Dim(31+2*i) = Halfa(2*i);
                                   % Half-angle on the
```

other side of the groove, for the groove body

```
Dim(37+i) = 0; % X offset of a pin, for the
groove body
   Dim(40+i) = 0; % Y offset of a pin, for the
groove body
end
N_dims = size(Dim, 2);
for i = 1:3
   ball plate
  ball plate
  side for the ball plate
  Varia(7+2*i) = circ_tol;
                          % Circularity on the
other side for the ball plate
  Varia(13+i) = PosB_tol;
                          % X offset at the top
for the ball plate
  Varia(16+i) = PosB tol;
                         % Y offset at the top
for the ball plate
  for the ball plate
  Varia(22+i) = PosB_tol;
                         % Y offset at the bottom
for the ball plate
  Varia(25+i) = Heightv_tol; % Height of the vertices
for the groove body
  Varia(28+i) = Orient_tol;
                          % Orientation angle of
the grooves for the groove body
  Varia(30+2*i) = Halfa_tol;
                          % Half-angle on one side
of the groove, for the groove body
   Varia(31+2*i) = Halfa_tol;
                          % Half-angle on the
other side of the groove, for the groove body
  Varia(37+i) = PosG_tol;
                         % X offset of a pin, for
the groove body
  the groove body
end
% CALCULATING THE JACOBIAN
for i1 = 1:N_dims % the dimension we are looking at
   for i2 = 1: N_dims % loop to create the perturbed
array
      if i1 == i2
         Perturb(i2) = Dim(i2) + Varia(i2);
      else
```

```
Perturb(i2) = Dim(i2);
        end
    end
    t_p = Perturb(1);
    for i = 1:3
        L_p(i) = Perturb(1+i);
        D_p(i) = Perturb(4+i);
        ci_B_p(2*i-1) = Perturb(6+2*i);
        ci_B_p(2*i) = Perturb(7+2*i);
        dXtop_B_p(i) = Perturb(13+i);
        dYtop_B_p(i) = Perturb(16+i);
        dXbot B p(i) = Perturb(19+i);
        dYbot_B_p(i) = Perturb(22+i);
        Hvertex p(i) = Perturb(25+i);
        Or_p(i) = Perturb(28+i);
        Halfa_p(2*i-1) = Perturb(30+2*i);
        Halfa_p(2*i) = Perturb(31+2*i);
        dXpin_G_p(i) = Perturb(37+i);
        dYpin_G_p(i) = Perturb(40+i);
    end
    % For the ball pallet
    [X_B_BC, Y_B_BC, Z_B_BC, Db] = kct_ballgeom(Xb_nomB,
Yb_nomB, t_p, L_p, D_p, ci_B_p, dXtop_B_p, dYtop_B_p,
dXbot_B_p, dYbot_B_p);
    PB1=[X_B_BC(1); Y_B_BC(1); Z_B_BC(1); 1];
    PB2=[X_B_BC(2); Y_B_BC(2); Z_B_BC(2); 1];
    PB3=[X_B_BC(3); Y_B_BC(3); Z_B_BC(3); 1];
    PB4=PB3;
    dB=Db';
    % For the groove body
    [TG11_G, TG12_G, TG21_G, TG22_G, TG31_G, TG32_G] =
kct_groovegeom(Xp_nomG, Yp_nomG, Hvertex_p, Or_p, Halfa_p,
Dpft, dXpin G p, dYpin G p);
    % CALCULATING RESTING POSITION
[alpha,beta,gamma,xr,yr,zr,Pc1,Pc2,Pc3,Pc4,Pc5,Pc6]=kct res
t(PB1,PB2,PB3,PB4,dB,TG11_G,TG12_G,TG21_G,TG22_G,TG31_G,TG3
2_G);
    dXdDim(i1) = xr / Varia(i1);
    dYdDim(i1) = yr / Varia(i1);
    dZdDim(i1) = zr / Varia(i1);
    dAdDim(i1) = alpha / Varia(i1);
    dBdDim(i1) = beta / Varia(i1);
    dGdDim(i1) = gamma / Varia(i1);
```

end

B8. Sub-Function: kct_groovegeom

```
function [T_V11_GC, T_V12_GC, T_V21_GC, T_V22_GC, T_V31_GC,
T_V32_GC] = kct_groovegeom(X_V_nomG, Y_V_nomG,
Height_V_mfgG, Orient_mfgG, Halfangle, Diam, DeltaX_mfgG,
DeltaY_mfgG)
% X_V_nomG: nominal X coord of a vee-groove, is a 3*1
% Y V nomG: nominal Y coord of a vee-groove, is a 3*1
% Height_V_mfgG: Distance between the top of the plate and
the vertex of a vee-groove, is a 3*1
% Orient_mfqG: Orientation angle of the grooves, is a 3*1
% Halfangle: Half-Angle of aperture of the vee-grooves is a
6*1
% Diam: Diameter of a perfect virtual ball, is a scalar
% DeltaX mfqG: X Offset of the pin, is a 3*1
% DeltaY_mfgG: Y Offset of the pin, is a 3*1
% FLAT SURFACES IN MFG COORDINATES SYSTEM
% Translation of the vertex
for iq = 1:3
    X_V_mfgG(ig) = X_V_nomG(ig) + DeltaX_mfgG(ig);
    Y_V_mfgG(ig) = Y_V_nomG(ig) + DeltaY_mfgG(ig);
end
T V Tr 1 = [1 \ 0 \ 0 \ X V mfqG(1); \ 0 \ 1
                                         0 \quad Y \quad V \quad mfqG(1);
0 1 Height_V_mfgG(1); 0 0 0 1];
T_V_Tr_2 = [1 \ 0 \ 0 \ X_V_mfgG(2); \ 0 \ 1]
                                        0 \quad Y_V_mfgG(2);
0 1 Height_V_mfgG(2); 0 0 0 1];
T_V_Tr_3 = [1 \ 0 \ 0 \ X_V_mfgG(3); \ 0 \ 1]
                                        0 \quad Y_V_mfgG(3); \quad 0
0 1 Height_V_mfgG(3); 0 0 0 1];
% Rotation about the Z axis of the vertex
T_V_{RinZ_11} = [cos(Orient_mfgG(1)-pi/2)]
sin(Orient_mfgG(1)-pi/2) 0 0; sin(Orient_mfgG(1)-pi/2)
cos(Orient_mfgG(1)-pi/2) 0
                             0;
                                 0 0 1 0; 0 0 0 1];
T_V_{RinZ_12} = [cos(Orient_mfgG(1)+pi/2)]
sin(Orient_mfgG(1)+pi/2) = 0   0; sin(Orient_mfgG(1)+pi/2)
cos(Orient_mfgG(1)+pi/2) 0 0; 0 0 1 0; 0 0 0 1];
T V RinZ 21 = [\cos(Orient mfgG(2)-pi/2)]
sin(Orient mfqG(2)-pi/2) = 0 = 0; sin(Orient mfqG(2)-pi/2)
cos(Orient_mfgG(2)-pi/2) 0 0; 0 0 1 0; 0 0
T_V_{RinZ_22} = [cos(Orient_mfgG(2)+pi/2)]
sin(Orient_mfgG(2)+pi/2) = 0   0; sin(Orient_mfgG(2)+pi/2)
cos(Orient_mfgG(2)+pi/2) 0 0; 0 0 1 0; 0 0 0 1];
```

```
T_V_{RinZ_31} = [cos(Orient_mfgG(3)-pi/2) -
sin(Orient_mfgG(3)-pi/2) = 0 + sin(Orient_mfgG(3)-pi/2)
cos(Orient_mfgG(3)-pi/2) 0 0; 0 0 1 0; 0 0 0 1];
T_V_{RinZ_32} = [cos(Orient_mfgG(3)+pi/2) -
sin(Orient mfqG(3)+pi/2) = 0   0; sin(Orient mfqG(3)+pi/2)
cos(Orient_mfgG(3)+pi/2) 0 0; 0 0 1 0; 0 0 0 1];
% Rotation about the Y axis of the vertex
T_V_RinY_11 = [cos(pi/2-Halfangle(1)) 0 sin(pi/2-Halfangle(1))]
Halfangle(1)) 0; 0 1 0 0; -sin(pi/2-Halfangle(1))
cos(pi/2-Halfangle(1)) 0; 0 0 1];
T V RinY 12 = [\cos(pi/2-Halfangle(2))] 0 \sin(pi/2-Halfangle(2))
Halfangle(2)) 0; 0 1 0 0; -sin(pi/2-Halfangle(2))
                                                         0
cos(pi/2-Halfangle(2)) 0; 0 0 1];
T_V_RinY_21 = [cos(pi/2-Halfangle(3)) 0 sin(pi/2-Halfangle(3))]
Halfangle(3)) 0; 0 1 0 0; -sin(pi/2-Halfangle(3))
cos(pi/2-Halfangle(3)) 0; 0 0 1];
T_V_RinY_22 = [cos(pi/2-Halfangle(4)) 0 sin(pi/2-Halfangle(4))]
Halfangle(4)) 0; 0 1 0 0; -sin(pi/2-Halfangle(4))
                                                         0
cos(pi/2-Halfangle(4)) 0; 0 0 1];
T V RinY 31 = [\cos(pi/2 - Halfangle(5))] = 0 \sin(pi/2 - Halfangle(5))
Halfangle(5)) 0; 0 1 0 0; -sin(pi/2-Halfangle(5))
cos(pi/2-Halfangle(5)) 0; 0 0 1];
T_V_RinY_32 = [cos(pi/2-Halfangle(6)) 0 sin(pi/2-Halfangle(6))]
Halfangle(6)) 0; 0 1 0 0; -sin(pi/2-Halfangle(6))
cos(pi/2-Halfangle(6)) 0; 0 0 1];
% Combination of the transformations
% You give coord in local CSYS, this matrix will return the
coord in the mfg CSYS
T_V11_mfgG = T_V_Tr_1 * T_V_RinZ_11 * T_V_RinY_11;
T_V12_mfgG = T_V_Tr_1 * T_V_RinZ_12 * T_V_RinY_12;
T_V21_mfgG = T_V_Tr_2 * T_V_RinZ_21 * T_V_RinY_21;
T_V22_mfgG = T_V_Tr_2 * T_V_RinZ_22 * T_V_RinY_22;
T V31 mfgG = T V Tr 3 * T V RinZ 31 * T V RinY 31;
T_V32_mfgG = T_V_Tr_3 * T_V_RinZ_32 * T_V_RinY_32;
% GROOVE CENTROID IN MFG COORDINATES SYSTEM
for ig = 1:3
    Dist_CV(ig) = (Diam/2) / sin((Halfangle(2*ig-1) +
Halfangle(2*ig)) / 2); % Distance between vertex and
center of the ball
    X_G_mfgG(ig) = X_V_mfgG(ig) - Dist_CV(ig) *
sin((Halfangle(2*ig-1) - Halfangle(2*ig)) /2) *
sin(Orient_mfgG(ig));
```

```
Y_G_mfgG(ig) = Y_V_mfgG(ig) + Dist_CV(ig) *
sin((Halfangle(2*ig-1) - Halfangle(2*ig)) /2) *
cos(Orient_mfgG(ig));
    Z_G_mfgG(ig) = Height_V_mfgG(ig) + Dist_CV(ig) *
cos((Halfangle(2*ig-1) - Halfangle(2*ig)) /2);
end
T_GC_mfgG = kct_centroid(X_G_mfgG, Y_G_mfgG, Z_G_mfgG);
% You give coord in centroid CSYS, this matrix will return
the coord in the mfg CSYS
% FLAT SURFACES IN GROOVE CENTROID COORDINATES SYSTEM
T_V11_GC = inv(T_GC_mfgG) * T_V11_mfgG;
T_V12_GC = inv(T_GC_mfgG) * T_V12_mfgG;
T_V21_GC = inv(T_GC_mfgG) * T_V21_mfgG;
T_V22_GC = inv(T_GC_mfgG) * T_V22_mfgG;
T_V31_GC = inv(T_GC_mfgG) * T_V31_mfgG;
T_V32_GC = inv(T_GC_mfgG) * T_V32_mfgG;
```

B9. Sub-Function: kct_perturb

```
close all; clear all;
% Perturbations
% INPUT
% For the ball pallet
Xb nomB = [1 1 7] * 25.4; % Fixed
Yb_nomB = [7 1 4] * 25.4; % Fixed
t = 6.35;
L = [0.75 \quad 0.75 \quad 0.75] * 25.4;
D = [0.5 \ 0.5 \ 0.5] * 25.4;
% For the groove body
Xp\_nomG = [1.0 1.0 7.0] * 25.4; % Fixed
Yp_nomG = [7.0 \ 1.0 \ 4.0] * 25.4; % Fixed
Hvertex = [0.1 \ 0.1 \ 0.1] * 25.4;
Or = [-60 \ 60 \ 180] * pi/180;
Halfa = [45 45 45 45 45] * pi/180;
Dpft = 12.7; % Fixed
% TOLERANCES
thick tol = 0.02;
Length tol = 0.05;
Diam_tol = 0.03;
circ_tol = 0.01;
XB_{tol} = 0.05;
YB\_tol = 0.05;
Heightv tol = 0.05;
Orient_tol = 0.002;
Halfa tol = 0.003;
XG_{tol} = 0.05;
YG tol = 0.05;
% GENERATING DIMENSIONS
Dim(1) = t;
                          % Thickness of the ball plate
for i = 1:3
    Dim(1+i) = L(i);
                         % Foot length for the ball plate
    Dim(4+i) = D(i);

Dim(6+2*i) = 0;
                        % Ball diameter for the ball plate
                         % Circularity on one side for the
ball plate
    Dim(7+2*i) = 0; % Circularity on the other side
for the ball plate
```

```
Dim(13+i) = 0; % X offset at the top for the ball
plate
                    % Y offset at the top for the ball
   Dim(16+i) = 0;
plate
   Dim(19+i) = 0; % X offset at the bottom of the
ball plate
   Dim(22+i) = 0; % Y offset at the bottom of the
ball plate
   Dim(25+i) = Hvertex(i);
                              % Height of the
vertices for the groove body
   Dim(28+i) = Or(i);
                               % Orientation angle of
the grooves for the groove body
   Dim(30+2*i) = Halfa(2*i-1); % Half-angle on one
side of the groove, for the groove body
   Dim(31+2*i) = Halfa(2*i);
                               % Half-angle on the
other side of the groove, for the groove body
   Dim(37+i) = 0; % X offset of a pin, for the
groove body
   Dim(40+i) = 0; % Y offset of a pin, for the
groove body
end
N dims = size(Dim, 2);
for i = 1:3
   ball plate
   Varia(4+i) = Diam_tol;
                              % Ball diameter for the
ball plate
   side for the ball plate
   Varia(7+2*i) = circ_tol;
                          % Circularity on the
other side for the ball plate
   Varia(13+i) = XB_tol;
                              % X offset at the top
for the ball plate
   Varia(16+i) = YB_tol;
                              % Y offset at the top
for the ball plate
   Varia(19+i) = XB_tol;
                              % X offset at the
bottom for the ball plate
   Varia(22+i) = YB_tol;
                              % Y offset at the
bottom for the ball plate
   Varia(25+i) = Heightv_tol; % Height of the
vertices for the groove body
   Varia(28+i) = Orient_tol;
                              % Orientation angle of
the grooves for the groove body
   Varia(30+2*i) = Halfa_tol;
                              % Half-angle on one
side of the groove, for the groove body
```

```
other side of the groove, for the groove body
   Varia(37+i) = XG_tol;
                                 % X offset of a pin,
for the groove body
   Varia(40+i) = YG tol; % X offset of a pin,
for the groove body
end
% CALCULATING THE JACOBIAN
for i1 = 1:N_dims % the dimension we are looking at
   for i2 = 1: N_dims % loop to create the perturbed
array
       if i1 == i2
           Perturb(i2) = Dim(i2) + Varia(i2);
           Perturb(i2) = Dim(i2);
       end
   end
   t p = Perturb(1);
   for i = 1:3
       L p(i) = Perturb(1+i);
       D_p(i) = Perturb(4+i);
       ci_B_p(2*i-1) = Perturb(6+2*i);
       ci_B_p(2*i) = Perturb(7+2*i);
       dXtop_B_p(i) = Perturb(13+i);
       dYtop_B_p(i) = Perturb(16+i);
       dXbot_B_p(i) = Perturb(19+i);
       dYbot_B_p(i) = Perturb(22+i);
       Hvertex_p(i) = Perturb(25+i);
       Or_p(i) = Perturb(28+i);
       Halfa_p(2*i-1) = Perturb(30+2*i);
       Halfa_p(2*i) = Perturb(31+2*i);
       dXpin_G_p(i) = Perturb(37+i);
       dYpin G p(i) = Perturb(40+i);
   end
   % For the ball pallet
    [X_B_BC, Y_B_BC, Z_B_BC, Db] = kct_ballgeom(Xb_nomB,
Yb_nomB, t_p, L_p, D_p, ci_B_p, dXtop_B_p, dYtop_B_p,
dXbot_B_p, dYbot_B_p);
   PB1=[X_B_BC(1); Y_B_BC(1); Z_B_BC(1); 1];
   PB2=[X_B_BC(2); Y_B_BC(2); Z_B_BC(2); 1];
   PB3=[X_B_BC(3); Y_B_BC(3); Z_B_BC(3); 1];
   PB4=PB3;
   dB=Db';
```

```
% For the groove body
    [TG11_G, TG12_G, TG21_G, TG22_G, TG31_G, TG32_G] =
kct_groovegeom(Xp_nomG, Yp_nomG, Hvertex_p, Or_p, Halfa_p,
Dpft, dXpin_G_p, dYpin_G_p);
    % CALCULATING RESTING POSITION
[alpha,beta,gamma,xr,yr,zr,Pc1,Pc2,Pc3,Pc4,Pc5,Pc6]=kct res
t(PB1,PB2,PB3,PB4,dB,TG11_G,TG12_G,TG21_G,TG22_G,TG31_G,TG3
2_G);
    dXdDim(i1) = xr / Varia(i1);
    dYdDim(i1) = yr / Varia(i1);
    dZdDim(i1) = zr / Varia(i1);
    dAdDim(i1) = alpha / Varia(i1);
    dBdDim(i1) = beta / Varia(i1);
    dGdDim(i1) = gamma / Varia(i1);
end
Jacob = [dXdDim; dYdDim; dZdDim; dAdDim; dBdDim; dGdDim]
% COVARIANCE MATRICES
CoMtx Dim = zeros(N dims, N dims);
for i = 1:N_dims
    CoMtx_Dim(i,i) = Varia(i)^2 / 9;
end
CoMtx_Err = Jacob * CoMtx_Dim * Jacob'
X_{tol} = 3 * sqrt(CoMtx_Err(1,1))
Y_{tol} = 3 * sqrt(CoMtx_Err(2,2))
Z_{tol} = 3 * sqrt(CoMtx_Err(3,3))
A_{tol} = 3 * sqrt(CoMtx_Err(4,4))
B_{tol} = 3 * sqrt(CoMtx_Err(5,5))
G_{tol} = 3 * sqrt(CoMtx_Err(6,6))
```

B10. Sub-Function: kct_rest

```
[alpha,beta,gamma,xr,yr,zr,Pc1,Pc2,Pc3,Pc4,Pc5,Pc6]=kct_res
t(PB1,PB2,PB3,PB4,dB,TG11_G,TG12_G,TG21_G,TG22_G,TG31_G,TG3
2_G)
% This function calls the fsolve routine to solve the 24
nonlinear equations that provide the resting position of
the ball body of a kinematic coupling in a groove body.
Vectors PB1, PB2, PB3, and PB4 locate the centers of the
balls in coordinate sytem located at the coupling centroid.
TG11_G,TG12_G,TG21_G,TG22_G,TG31_G, and TG32_G are the
transformations from groove surfaces to groove coordinate
system (ideally equal to ball coupling centroid).
beta, and gamma, are rotations about x,y, and z,
respectively. xr, yr, and zr are displacements, and
Pc1,Pc2,Pc3,Pc4,Pc5, and Pc6 are position vectors to the
contact points.
% Setup initial guesses for unknowns
for i=1:6
   vars(i)=0; % Initial guess for the error components are
all set to zero
end
vars(7:9)=PB1(1:3); % Initial guess for the coordinates of
contact point #1 are set to the center of ball #1
vars(10:12)=PB1(1:3); % Initial guess for the coordinates
of contact point #2 are set to the center of ball #2
vars(13:15)=PB2(1:3); % Initial guess for the coordinates
of contact point #3 are set to the center of ball #3
vars(16:18)=PB2(1:3); % Initial guess for the coordinates
of contact point #4 are set to the center of ball #4
vars(19:21)=PB3(1:3); % Initial guess for the coordinates
of contact point #5 are set to the center of ball #5
vars(22:24)=PB3(1:3); % Initial guess for the coordinates
of contact point #6 are set to the center of ball #6
vars=vars';
% Setup params vector to pass variables to fsolve routine
params(1:3)=PB1(1:3);
params(4:6)=PB2(1:3);
params(7:9) = PB3(1:3);
params(10:12)=PB4(1:3);
params(13:15) = TG11_G(1:3,1);
params(16:18)=TG11_G(1:3,2);
params(19:21)=TG11 G(1:3,3);
params(22:24)=TG11_G(1:3,4);
```

```
params(25:27)=TG12_G(1:3,1);
params(28:30)=TG12_G(1:3,2);
params(31:33) = TG12_G(1:3,3);
params(34:36)=TG12_G(1:3,4);
params(37:39)=TG21 G(1:3,1);
params(40:42)=TG21_G(1:3,2);
params(43:45)=TG21_G(1:3,3);
params(46:48)=TG21_G(1:3,4);
params(49:51)=TG22_G(1:3,1);
params(52:54)=TG22\_G(1:3,2);
params(55:57)=TG22_G(1:3,3);
params(58:60)=TG22 G(1:3,4);
params(61:63)=TG31_G(1:3,1);
params(64:66)=TG31_G(1:3,2);
params(67:69) = TG31_G(1:3,3);
params(70:72)=TG31_G(1:3,4);
params(73:75)=TG32\_G(1:3,1);
params(76:78) = TG32_G(1:3,2);
params(79:81)=TG32_G(1:3,3);
params(82:84)=TG32 G(1:3,4);
params(85) = dB(1);
params(86)=dB(2);
params(87)=dB(3);
params(88) = dB(4);
params(89)=dB(5);
params(90)=dB(6);
params=params';
% Solve the nonlinear system of equations
retvars=fsolve(@kct_seat,vars,optimset('Display','off'),par
ams);
alpha=retvars(1);
beta=retvars(2);
qamma=retvars(3);
xr=retvars(4);
yr=retvars(5);
zr=retvars(6);
Pc1=[retvars(7:9);1];
Pc2=[retvars(10:12);1];
Pc3=[retvars(13:15);1];
Pc4=[retvars(16:18);1];
Pc5=[retvars(19:21);1];
Pc6=[retvars(22:24);1];
TB_G(1:4,1) = [\cos(alpha)*\cos(beta); \sin(alpha)*\cos(beta); -
sin(beta);0];
```

```
%TB_G(1:4,2)=[cos(alpha)*sin(beta)*sin(gamma)-
sin(alpha)*cos(gamma);sin(alpha)*sin(beta)*sin(gamma)+cos(a
lpha)*cos(gamma);cos(beta)*sin(gamma);0];
%TB_G(1:4,3)=[cos(alpha)*sin(beta)*cos(gamma)+sin(alpha)*sin(gamma);sin(alpha)*sin(beta)*cos(gamma)-
cos(alpha)*sin(gamma);cos(beta)*cos(gamma);0];
%TB_G(1:4,4)=[xr;yr;zr;1];
```

B11. Sub-Function: kct_seat

alpha=vars(1);

function retvars=kct_seat(vars, params)

% This function evaluates the 24 functions that are the system of non-linear equations that can be solved for the seating position (transformation) of the ball body in the groove body. When used with fsolve.m the system can be solved for the x,y,z,alpha,beta, and gamma pose coordinates as well as the coordinates of the 6 contact points. This function must be sent the positions of the balls in a coordinate system located at the coupling centroid, the contact normal vectors, and the ball diameter in the components of the vector params.

% Rotation angle about z-axis

```
beta=vars(2);
                   % Rotation angle about y-axis
qamma=vars(3);
                   % Rotation angle about x-axis
xr=vars(4);
                   % Position in x-axis
yr=vars(5);
                   % Position in y-axis
zr=vars(6);
                    % Position in z-axis
Pc1(1:4)=[vars(7:9);1]; Pc1=Pc1';
                                        % Contact point 1's
coordinates
Pc2(1:4)=[vars(10:12);1]; Pc2=Pc2';
                                      % Contact point 2's
coordinates
Pc3(1:4)=[vars(13:15);1]; Pc3=Pc3';
                                       % Contact point 3's
coordinates
Pc4(1:4)=[vars(16:18);1]; Pc4=Pc4';
                                       % Contact point 4's
coordinates
Pc5(1:4)=[vars(19:21);1]; Pc5=Pc5';
                                       % Contact point 5's
coordinates
Pc6(1:4)=[vars(22:24);1]; Pc6=Pc6'; % Contact point 6's
coordinates
% Extract values in params vector into meaningful notation
Pb1=[params(1:3)];Pb1(4)=1;
                                   % Position of ball 1 in
coordinate system at coupling centroid in ball body
Pb2=[params(4:6)]; Pb2(4)=1;
                                  % Position of ball 2 in
coordinate system at coupling centroid in ball body
Pb3=[params(7:9)];Pb3(4)=1;
                                   % Position of ball 3 in
coordinate system at coupling centroid in ball body
Pb4=[params(10:12)];Pb4(4)=1;
                                % Position of ball 4 in
coordinate system at coupling centroid in ball body
TG11_G=[params(13:15),params(16:18),params(19:21),params(22
:24)]; % Transformation from surface 1_1 to Groove coord
TG11_G(4,1:4) = [0,0,0,1];
```

```
TG12_G=[params(25:27),params(28:30),params(31:33),params(34
:36)]; % Transformation from surface 1_2 to Groove coord
system
TG12_G(4,1:4) = [0,0,0,1];
TG21_G = [params(37:39), params(40:42), params(43:45), params(46)]
:48)]; % Transformation from surface 2_1 to Groove coord
system
TG21_G(4,1:4) = [0,0,0,1];
TG22_G=[params(49:51),params(52:54),params(55:57),params(58
:60)]; % Transformation from surface 2_2 to Groove coord
system
TG22\_G(4,1:4) = [0,0,0,1];
TG31_G=[params(61:63),params(64:66),params(67:69),params(70
:72)]; % Transformation from surface 3 1 to Groove coord
system
TG31_G(4,1:4) = [0,0,0,1];
TG32_G=[params(73:75),params(76:78),params(79:81),params(82
:84)]; % Transformation from surface 3_2 to Groove coord
system
TG32 G(4,1:4) = [0,0,0,1];
rB(1)=params(85)/2; % Radius of Balls
rB(2) = params(86)/2;
rB(3) = params(87)/2;
rB(4) = params(88)/2;
rB(5) = params(89)/2;
rB(6) = params(90)/2;
%Extract normal vectors at contact points from the
transformation matrices
n1=[TG11\_G(1:3,3);1];
                         % Unit vector in direction of
contact force 1 at contact point 1
n2=[TG12\_G(1:3,3);1];
                          % Unit vector in direction of
contact force 2 at contact point 2
n3=[TG21\_G(1:3,3);1];
                          % Unit vector in direction of
contact force 3 at contact point 3
n4=[TG22\_G(1:3,3);1];
                          % Unit vector in direction of
contact force 4 at contact point 4
                          % Unit vector in direction of
n5 = [TG31_G(1:3,3);1];
contact force 5 at contact point 5
n6 = [TG32_G(1:3,3);1];
                          % Unit vector in direction of
contact force 6 at contact point 6
% Calculate elements within the homogenous transformation
matrix representing resting position
```

 $T(1:4,1)=[\cos(alpha)*\cos(beta);\sin(alpha)*\cos(beta);-$

sin(beta);0];

```
T(1:4,2) = [\cos(alpha) * \sin(beta) * \sin(gamma) -
 sin(alpha)*cos(gamma);sin(alpha)*sin(beta)*sin(gamma)+cos(a
 lpha)*cos(gamma);cos(beta)*sin(gamma);0];
T(1:4,3) = [\cos(alpha)*\sin(beta)*\cos(qamma)+\sin(alpha)*\sin(qa)
mma); sin(alpha)*sin(beta)*cos(gamma)-
cos(alpha)*sin(gamma);cos(beta)*cos(gamma);0];
T(1:4,4) = [xr;yr;zr;1];
retvars(1:24)=zeros(24,1);
retvars(1:4) =T*Pb1-Pc1-rB(1)*n1;
retvars(4:7) = T*Pb1-Pc2-rB(2)*n2;
retvars(7:10) =T*Pb2-Pc3-rB(3)*n3;
retvars(10:13)=T*Pb2-Pc4-rB(4)*n4;
retvars(13:16)=T*Pb3-Pc5-rB(5)*n5;
retvars(16:19)=T*Pb4-Pc6-rB(6)*n6;
retvars(19) = TG11_G(3,4) + 1/TG11_G(3,3) * (TG11_G(1,3) * (TG11
 1,4)-Pc1(1))+TG11_G(2,3)*(TG11_G(2,4)-Pc1(2)))-Pc1(3);
retvars(20) = TG12_G(3,4) + 1/TG12_G(3,3) * (TG12_G(1,3) * (TG12
 1,4)-Pc2(1))+TG12_G(2,3)*(TG12_G(2,4)-Pc2(2)))-Pc2(3);
retvars(21) = TG21 G(3,4) + 1/TG21 G(3,3) * (TG21 G(1,3) * (TG21
 1,4)-Pc3(1)+TG21 G(2,3)*(TG21 G(2,4)-Pc3(2))-Pc3(3);
retvars(22) = TG22\_G(3,4) + 1/TG22\_G(3,3) * (TG22\_G(1,3) * (TG22\_G(1,3) * (TG22\_G(3,4) + 1/TG22\_G(3,3) * (TG22\_G(1,3) * (TG22_G(1,3) * (TG2
 1,4)-Pc4(1))+TG22_G(2,3)*(TG22_G(2,4)-Pc4(2)))-Pc4(3);
retvars(23) = TG31_G(3,4) + 1/TG31_G(3,3) * (TG31_G(1,3) * (TG31
 1,4)-Pc5(1)+TG31_G(2,3)*(TG31_G(2,4)-Pc5(2)))-Pc5(3);
retvars(24) = TG32_G(3,4) + 1/TG32_G(3,3) * (TG32_G(1,3) * (TG32
 1,4)-Pc6(1)+TG32 G(2,3)*(TG32 G(2,4)-Pc6(2))-Pc6(3);
retvars=retvars';
```

Appendix C:

Determining the HTM from a Metrology Datum Frame to a Centroidal Coordinate System

The coordinates of the triangles' three apices B_1 ($^Dx_{B_1}$, $^Dy_{B_1}$, $^Dz_{B_1}$), B_2 ($^Dx_{B_2}$, $^Dy_{B_2}$, $^Dz_{B_2}$) and B_3 ($^Dx_{B_3}$, $^Dy_{B_3}$, $^Dz_{B_3}$) are measured in a metrology datum frame, denoted with the prescript D, as shown in Fig C1.

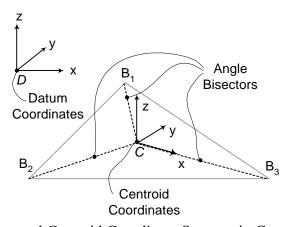


Fig C1: Datum and Centroid Coordinate Systems in Coupling Triangle

The centroidal coordinate system, denoted with the prescript C, is defined by three criteria:

- ① Its origin is located at the intersection of the triangle's bisectors, which is the centroid C.
- ② Its x-axis points towards B_3 .

Criterion \Im implies that the z-coordinates of the apices are equal to zero, as shown in Eq (C1):

$${}^{C}z_{B_{1}} = {}^{C}z_{B_{2}} = {}^{C}z_{B_{3}} = 0$$
 (C1)

The complete geometry of triangle $(B_1B_2B_3)$ is determined by calculating the edge lengths using Eq (C2)-(C4) and the internal angles using Eq (C5)-(C7).

$$B_1 B_2 = \sqrt{\left({}^D x_{B_2} - {}^D x_{B_1}\right)^2 + \left({}^D y_{B_2} - {}^D y_{B_1}\right)^2 + \left({}^D z_{B_2} - {}^D z_{B_1}\right)^2}$$
(C2)

$$B_2 B_3 = \sqrt{\left({}^D x_{B_3} - {}^D x_{B_2}\right)^2 + \left({}^D y_{B_3} - {}^D y_{B_2}\right)^2 + \left({}^D z_{B_3} - {}^D z_{B_2}\right)^2}$$
 (C3)

$$B_3 B_1 = \sqrt{\left({}^D x_{B_1} - {}^D x_{B_3}\right)^2 + \left({}^D y_{B_1} - {}^D y_{B_3}\right)^2 + \left({}^D z_{B_1} - {}^D z_{B_3}\right)^2}$$
(C4)

$$\angle B_1 = \arccos\left(\frac{B_3 B_1^2 + B_1 B_2^2 - B_2 B_3^2}{2 \times B_3 B_1 \times B_1 B_2}\right)$$
 (C5)

$$\angle B_2 = \arccos\left(\frac{B_1 B_2^2 + B_2 B_3^2 - B_3 B_1^2}{2 \times B_1 B_2 \times B_2 B_3}\right)$$
 (C6)

$$\angle B_3 = \arccos\left(\frac{B_2 B_3^2 + B_3 B_1^2 - B_1 B_2^2}{2 \times B_2 B_3 \times B_3 B_1}\right) \tag{C7}$$

Applying the law of sine's in triangle (B_1CB_3) gives Eq (C8):

$$\frac{CB_3}{\sin\left(\frac{\angle B_1}{2}\right)} = \frac{B_3B_1}{\sin(\angle B_1CB_3)} \tag{C8}$$

Since the three angles of a triangle are supplementary, triangle (B_1CB_3) provides Eq (C9).

$$\angle B_1 C B_3 = \boldsymbol{p} - \angle C B_1 B_3 - \angle C B_3 B_1 \tag{C9}$$

Applying the same rule on triangle $(B_1B_2B_3)$ gives Eq (C10):

$$\angle B_2 = \mathbf{p} - \angle B_1 - \angle B_3 \tag{C10}$$

By definition, the bisectors divide the triangle's internal angles into two equal angles. This rule gives Eq (C11) and Eq (C12).

$$\angle CB_1B_3 = \frac{\angle B_1}{2} \tag{C11}$$

$$\angle CB_3B_1 = \frac{\angle B_3}{2} \tag{C12}$$

Inserting Eq (C10)-(C12) into Eq (C9) provides Eq (C13):

$$\angle B_1 C B_3 = \frac{\mathbf{p}}{2} + \frac{\angle B_2}{2} \tag{C13}$$

Eq (C14) results from a trigonometry relation applied on Eq (C13):

$$\sin\left(\angle B_1 C B_3\right) = \cos\left(\frac{\angle B_2}{2}\right) \tag{C14}$$

Eq (C15) is obtained by inserting Eq (C14) into Eq (C8):

$$\Rightarrow CB_3 = B_3 B_1 \times \frac{\sin\left(\frac{\angle B_1}{2}\right)}{\cos\left(\frac{\angle B_2}{2}\right)}$$
 (C15)

Criteria ① and ② imply that the *x*-coordinate of apex B_3 is equal to the length CB_3 . This condition gives Eq (C16) and Eq (C17):

$$\begin{cases} {}^{C}x_{B_{3}} = B_{3}B_{1} \times \frac{\sin\left(\frac{\angle B_{1}}{2}\right)}{\cos\left(\frac{\angle B_{2}}{2}\right)} \\ {}^{C}y_{B_{3}} = 0 \end{cases}$$
(C16)

The relative position of apex B_1 with respect to apex B_3 is known, so its coordinates in the centroidal coordinate system can be found as shown in Eq (C18) and (C19):

$$\begin{cases} {}^{C}x_{B_1} = {}^{C}x_{B_3} - B_3B_1 \times \cos\left(\frac{\angle B_3}{2}\right) \\ {}^{C}y_{B_1} = B_3B_1 \times \sin\left(\frac{\angle B_3}{2}\right) \end{cases}$$
(C18)

Coordinates of apex B_2 are similarly defined in Eq (C20) and (C21):

$$\begin{cases} {}^{C}x_{B_2} = {}^{C}x_{B_3} - B_1B_2 \times \cos\left(\frac{\angle B_3}{2}\right) \\ {}^{C}y_{B_1} = B_1B_2 \times \sin\left(\frac{\angle B_3}{2}\right) \end{cases}$$
(C20)

$${}^{C}y_{B_{1}} = B_{1}B_{2} \times \sin\left(\frac{\angle B_{3}}{2}\right) \tag{C21}$$

Finding the rotation angles about the three axes of the centroidal coordinate system requires the definition of three distinct unit vectors that start from apex B₃ and point respectively towards B₁, B₂ and C. The coordinates of these unit vectors in the metrology datum frame are presented in Eq (C22)-(C24):

$${}^{D}\vec{u}_{B_{3}B_{1}} = \frac{1}{B_{3}B_{1}} \times \begin{bmatrix} {}^{D}x_{B_{1}} - {}^{D}x_{B_{3}} \\ {}^{D}y_{B_{1}} - {}^{D}y_{B_{3}} \\ {}^{D}z_{B_{1}} - {}^{D}z_{B_{3}} \end{bmatrix}$$
(C22)

$${}^{D}\vec{u}_{B_{3}B_{2}} = \frac{1}{B_{2}B_{3}} \times \begin{bmatrix} {}^{D}x_{B_{2}} - {}^{D}x_{B_{3}} \\ {}^{D}y_{B_{2}} - {}^{D}y_{B_{3}} \\ {}^{D}z_{B_{2}} - {}^{D}z_{B_{3}} \end{bmatrix}$$
(C23)

$${}^{D}\vec{u}_{B_{3}C} = \frac{1}{\sqrt{\left({}^{D}u_{B_{3}B_{1}}^{x} + {}^{D}u_{B_{3}B_{2}}^{x}\right)^{2} + \left({}^{D}u_{B_{3}B_{1}}^{y} + {}^{D}u_{B_{3}B_{2}}^{y}\right)^{2} + \left({}^{D}u_{B_{3}B_{1}}^{z} + {}^{D}u_{B_{3}B_{2}}^{z}\right)^{2}}} \times \begin{bmatrix} {}^{D}u_{B_{3}B_{1}}^{x} + {}^{D}u_{B_{3}B_{2}}^{x}} \\ {}^{D}u_{B_{3}B_{1}}^{y} + {}^{D}u_{B_{3}B_{2}}^{y}} \\ {}^{D}u_{B_{3}B_{1}}^{z} + {}^{D}u_{B_{3}B_{2}}^{z}} \end{bmatrix}$$
(C24)

Then the coordinates of the centroid C in the metrology datum frame are defined by Eq (C25)-(C27):

$$\int_{0}^{D} x_{C} = {}^{D} x_{B_{2}} + CB_{3} \times {}^{D} u_{B,C}^{x}$$
 (C25)

$$\begin{cases} {}^{D}x_{C} = {}^{D}x_{B_{3}} + CB_{3} \times {}^{D}u_{B_{3}C}^{x} \\ {}^{D}y_{C} = {}^{D}y_{B_{3}} + CB_{3} \times {}^{D}u_{B_{3}C}^{y} \\ {}^{D}z = {}^{D}z_{3} + CB_{3} \times {}^{D}u_{B_{3}C}^{z} \end{cases}$$
(C25)

Hence the rotation $_{D}^{C}\mathbf{b}$ about the y-axis, between the two coordinate systems, is obtained by Eq (C28):

$${}_{D}^{C}\boldsymbol{b} = \arcsin\left(\frac{{}^{D}z_{C} - {}^{D}z_{B_{3}}}{{}^{C}x_{B_{3}}}\right)$$
 (C28)

The following step is the definition of the rotation ${}^{C}_{D}\boldsymbol{a}$ about the z-axis, between the two coordinate systems, whose definition is presented in Eq (C29):

$${}_{D}^{C}\boldsymbol{a} = \arccos\left(\frac{{}^{D}\boldsymbol{x}_{B_{3}} - {}^{D}\boldsymbol{x}_{C}}{{}^{C}\boldsymbol{x}_{B_{3}} \times \cos\left({}^{C}_{D}\boldsymbol{b}\right)}\right)$$
(C29)

Finally, the rotation ${}^{C}_{D}\mathbf{g}$ about the *x*-axis, between the two coordinate systems, is defined by Eq (C30):

$${}_{D}^{C}\boldsymbol{g} = \arcsin\left(\frac{{}^{D}z_{B_{2}} - {}^{D}z_{C} + {}^{C}x_{B_{2}} \times \sin\left({}^{C}_{D}\boldsymbol{b}\right)}{{}^{C}y_{B_{2}} \times \cos\left({}^{C}_{D}\boldsymbol{b}\right)}\right)$$
(C30)

To conclude, the Homogeneous Transformation matrix ${}^{C}_{D}T$ between the two coordinate systems is defined by equation (C31).

$${}^{C}_{D}T = \begin{bmatrix} \cos\binom{c}{D}\boldsymbol{a}\cos\binom{c}{D}\boldsymbol{b} & \cos\binom{c}{D}\boldsymbol{a}\sin\binom{c}{D}\boldsymbol{b}\sin\binom{c}{D}\boldsymbol{g} - \sin\binom{c}{D}\boldsymbol{a}\cos\binom{c}{D}\boldsymbol{g} & \cos\binom{c}{D}\boldsymbol{a}\sin\binom{c}{D}\boldsymbol{b}\cos\binom{c}{D}\boldsymbol{g} - \sin\binom{c}{D}\boldsymbol{a}\sin\binom{c}{D}\boldsymbol{b}\sin\binom{c}{D}\boldsymbol{g} \\ \sin\binom{c}{D}\boldsymbol{a}\cos\binom{c}{D}\boldsymbol{b} & \sin\binom{c}{D}\boldsymbol{a}\sin\binom{c}{D}\boldsymbol{b}\sin\binom{c}{D}\boldsymbol{g} - \cos\binom{c}{D}\boldsymbol{a}\cos\binom{c}{D}\boldsymbol{g} & \sin\binom{c}{D}\boldsymbol{a}\sin\binom{c}{D}\boldsymbol{b}\cos\binom{c}{D}\boldsymbol{g} - \cos\binom{c}{D}\boldsymbol{a}\sin\binom{c}{D}\boldsymbol{g} \\ -\sin\binom{c}{D}\boldsymbol{b} & \cos\binom{c}{D}\boldsymbol{b}\sin\binom{c}{D}\boldsymbol{g} & \cos\binom{c}{D}\boldsymbol{a}\sin\binom{c}{D}\boldsymbol{g} & \cos\binom{c}{D}\boldsymbol{b}\cos\binom{c}{D}\boldsymbol{g} \\ 0 & 0 & 0 & 1 \end{bmatrix}$$

$$(C31)$$

References

[1] Slocum AH. Precision Machine Design, SME Press. Dearborn, Michigan. 1992.

- [2] Slocum AH. "Kinematic Couplings for Precision Fixturing Part I: Formulation of Design Parameters". *Precision Engineering*. Vol. 10, No. 2. 1988. P. 85-91.
- [3] Schmiechen P. & Slocum AH. "Analysis of Kinematic Systems: a Generalized Approach". *Precision Engineering*. Vol. 19, no.1. 1996. P. 11-18.
- [4] Vallance RR. & Slocum AH. "Kinematic Couplings for Pallets in Flexible Assembly Systems". *Proceedings of the 15th Annual Meeting of the ASPE*. Scottsdale, AZ. October 22-27, 2000.
- [5] Blanding DL. Exact Constraint: Machine Design Using Kinematic Principles. SME Press. New York. 1999.
- [6] International Organization for Standardization, *ISO 3952-1: Kinematic Diagram Graphical Symbols*. Geneva, Switzerland. 1981.
- [7] American National Standards Institute, *ASME/ANSI Y14.5M: Dimensioning and Tolerancing*. New York. 1994.
- [8] International Organization for Standardization, ISO 129: Technical Drawings Dimensioning General Principles, Definitions, Methods of Execution and Special Indications. Geneva, Switzerland. 1985
- [9] Groover MP. Automation, Production Systems, and Computer-Integrated Manufacturing. Prentice-Hall. Upper Saddle River, New Jersey. 2001.
- [10] Chase KW. "Tolerance Allocation Methods for Designers", ADCATS Report No. 99-6. Brigham Young University, Utah. 1999.
- [11] Hansen BL. *Quality Control: Theory and Applications*. Prentice-Hall. Upper Saddle River, New Jersey. 1963.
- [12] Venkataraman P. *Applied Optimization with MATLAB® Programming*. John Wiley & sons, New York. 2002.

- [13] Déplanche Y. Mémo Formulaire. Editions Casteilla. Paris, France. 1991.
- [14] Craig JJ. *Introduction to Robotics*. Addison-Wesley Publishing Company. Palo Alto, California. 1989.
- [15] Clifford AA. Multivariate Error Analysis. John Wiley & Sons. New York. 1973.
- [16] Serrano SE. *Engineering Uncertainty and Risk Analysis*. HydroScience Inc. Lexington, Kentucky. 2001.
- [17] Rubinstein RY. Simulation and the Monte Carlo Method. John Wiley & Sons. New York. 1981.
- [18] Hii KF. *Kinematically Constrained Spindles*. MSME Thesis. University of Kentucky, Lexington, KY. 2002.
- [19] Chase KW & Greenwood WH. "Design Issues in Mechanical Tolerance Analysis". *Manufacturing Review*. Vol.1, No 1. March 1988. pp 50-59.
- [20] Doty LA. Statistical Process Control. Indutrial Press Inc. New York, 1996.
- [21] Samson C, Hart P & Rubin C. *Fundamentals of Statistical Quality Control*. Addison-Wesley Publishing Company. Reading, MA, 1970.
- [22] Barlier C & Poulet B. *Mémotech Génie Mécanique*. Editions Casteilla. Paris, France, 1993.
- [23] Conversation with KW Chase at the ASPE Summer Topical Meeting on Tolerance Modeling and Analysis. Charlotte, NC. July 15-16, 2002.
- [24] Chase KC, Gao J, Magleby SP & Sorensen CD. "Including Geometric Feature Variations in Tolerance Analysis of Mechanical Assemblies". *IIE Transactions*. Vol. 28, 1996. pp 795-807.
- [25] Arenberg JW. "On the Origins of the Law of Error Propagation and its Uses". *Proceedings of the ASPE 2002 Summer Topical Meeting*, Charlotte, NC, pp 80-84.
- [26] Vallance RR. Precision Connector Assembly Automation. PhD Thesis.
 Massachusetts Institute of Technology. Cambridge, MA, USA. 1999.

- [27] Ray WH & Szekely J. *Process Optimization with Applications in Metallurgy and Chemical Engineering*. John Wiley & Sons, Inc. New York, 1973.
- [28] Zanger H & Zanger C. Fiber Optics, Communication and Other Applications. Macmillan Publishing Company, New York, 1991.
- [29] Marcuse D. "Loss Analysis of Single-Mode Fiber Splices". *The Bell System Technical Journal*. May-June 1977. pp. 703-718.
- [30] Gangopadhyay S & Sarkar SN. "Misalignment Considerations in Laser Diode to Single-Mode Fiber Excitation via Hemispherical Lens on the Fiber Tip". *Journal of Optical Communications*. Vol. 19, No 6. Dec 1998.
- [31] Jebens R, Trimmer W & Walker J. "Microactuators for aligning optical fibers". *Sensors and Actuators*. Vol. 20, No 1-2. Nov 1989. pp 65-73.
- [32] Haibara T, Nakashima T, Matsumoto M & Hanafusa H. "Connection loss reduction by thermally-diffused expanded core fiber". *IEEE Photonics Technology Letters*. Vol. 3, No 4. Apr 1991. pp 348-350.
- [33] Cook S. "Composite Ferrules Pass Optical-Fiber Connector Performance Tests". *Lightwave*. Vol. 16, No 5. Apr 1999. pp 85-86.
- [34] Iizuka Y et al. "Injection Molded Multifiber Optical Connector Using Thermoplastic Resin". *Fujikura Technical Review*. 2001. pp 17-23.
- [35] Dunkel K et al. "Injection-moulded fibre ribbon connectors for parallel optical links fabricated by the LIGA technique". *Journal of Micromechanics and Microengineering*. Vol. 8. 1998. pp 301-306.
- [36] Poteat TL. "Submicron Accuracies in Anisotropic Etched Silicon Piece Parts A Case Study". *Studies in Electrical and Electronic Engineering Micromachining and Micropackaging of Transducers*. Vol. 20. 1985.
- [37] Ohta T, Sigematsu T, Kihara Y & Kawazoe H. "Low loss single-mode multi-fiber plastic connector". *Proceedings of International Wire and Cable Symposium Proceedings of 38th International Wire and Cable Symposium (IWCS)*. Nov 14-16 1989. Atlanta, GA.

- [38] Concejo T & Takeuchi H. "A New Glass-Ceramic Ferrule Technology for Optical Connectors". *Lightwave*. Vol. 16, No. 12. 1999. pp 86-87.
- [39] Broadwater K & Mead PF. "Experimental and Numerical Studies in the Evaluation of Epoxy-Cured Fiber Optic Connectors". *Proceedings of the 2000 Electronic Components and Technology Conference*. 2000. pp 981-988.
- [40] Breedis JB. "Monte Carlo Tolerance Analysis of a Passively Aligned Silicon Waferboard Package". *Proceedings of the 2001 Electronic Component and Technology Conference*. 2001.
- [41] Uhing J, Thomas S & Christodoulou C. "A Statistical Approach for Estimating the Loss Contribution of Concatenated Connectors in Fiber-Optic Links". *Proceedings of the 1990 Electronic Component and Technology Conference*. 1990. pp 239-245.
- [42] Rachakonda P, Barraja M, Vallance RR, Kiani S & Lehman J. "2D Error Models and Monte Carlo Simulations for Budgeting Variation in Optical-Fiber Array Connectors". *Proceedings of the ASPE 2001 Annual Meeting*. pp 509-512.
- [43] Madou M. Fundamentals of Microfabrication. CRC Press. New York. 1997.
- [44] Vasile MJ, Friedrich CR, Kikkeri B & McElhannon R. "Micrometer-Scale Machining: Tool Fabrication and Initial Results". *Precision Engineering*. Vol. 19. 1996. p. 180-186.
- [45] Schaller Th, Bohn L, Mayer J & Schubert K. "Microstructure Grooves with a Width of Less than 50 µm cut with Ground Hard Metal Micro End Mills". *Precision Engineering*. Vol. 23, No. 4. October 1999. p. 229-235.
- [46] Masuzawa T & Tönshoff HK. "Three-Dimensional Micromachining by Machine Tools". Keynote Paper. *Annals of the CIRP*. Vol. 46, No. 2. 1997. p. 621-628.
- [47] Hirt G & Rattay B. "Coining of Thin Plates to Produce Micro Channel Structures". *Initiatives of Precision Engineering at the Beginning of a Millennium*. Proceedings of the 10th Int. Conf. on Precision Engineering. JSPE. Yokohama, Japan. July 18-20, 2001. Kluwer Academic Publishers, Boston, MA. p. 32-36.

- [48] Lee K, Stirn B & Dornfeld DA. "Burr Formation in Micro-Machining Aluminum, 6061-T6". *Initiatives of Precision Engineering at the Beginning of a Millennium*. Proceedings of the 10th Int. Conf. on Precision Engineering. JSPE. Yokohama, Japan. July 18-20, 2001. Kluwer Academic Publishers, Boston, MA. p. 47-51.
- [49] Sanford Process. http://www.sanfordprocess.com
- [50] Rachakonda K et al. "Stylus Profilometry to Qualify Vee-Grooves for Optical Fiber Alignment", *Proceedings of the 17th annual meeting of the ASPE*, St. Louis, MO. October 20-25, 2002.
- [51] Slocum AH & Donmez A. "Kinematic Couplings for Precision Fixturing Part II: Experimental Determination of Repeatability and Stiffness", *Precision Engineering* 1988; 10; 115-121.
- [52] Schouten CH, Rosielle PCJN & Schellekens PHJ. Design of a Kinematic Coupling for Precision Applications. Precision Engineering 1997; 20; 46-52.
- [53] Whipple RS. The Design and Construction of Scientific Instruments. Transactions of the Optical Society 1920-1921; 22; 3-52.
- [54] Evans C. Precision Engineering: an Evolutionary View. Bedford, UK: Cranfield Press, 1989.
- [55] Schellekens PHJ et al. Design for Precision: Current Status and Trends. Annals of CIRP 1998; 47.
- [56] Jones RV. Anti-Distortion Mountings for Instruments and Apparatus. Journal of Scientific Instruments 1961; 38; 408-409.
- [57] Culpepper ML & Slocum AH. Quasi-Kinematic Couplings: A Low-Cost Method for Precision Coupling of Product Components and the Like in Manufacturing Processes. Proceedings of the 14th Annual Meeting of the American Society for Precision Engineering, Monteray, CA. 1999.

- [58] Van Doren MJ. Precision Machine Design for the Semiconductor Equipment Manufacturing Industry. PhD Thesis. Massachusetts Institute of Technology. Cambridge, MA, USA. 1995.
- [59] Fortini ET. Dimensioning for Interchangeable Manufacturing. Industrial Press, 1967. P. 48.
- [60] Bjørke Ø. Computer Aided Tolerancing. New York: ASME Press, 1989.
- [61] Balling RJ, Free JC & Parkinson AR. Consideration of Worst-Case Manufacturing Tolerances in Design Optimization. ASME Journal of Mechanisms, Transmissions, and Automation in Design 1986; 108; 438-441.
- [62] Wolff ER. Safe Tolerancing for Cumulative Dimensions. Product Engineering, January 1961; 40-43.
- [63] Bender A. Statistical Tolerancing as it Relates to Quality Control and the Designer, Society of Automotive Engineers, May 1968; SAE paper No. 680490.
- [64] Corlew GT & Oakland F. Monte Carlo Simulation for Setting Dimensional Tolerances. Machine Design; 50, 9; 60-63.
- [65] Chase KW et al. Including Geometric Feature Variation in Tolerance Analysis of Mechanical Assemblies. IIE Transactions 1996; 28; 795-807.
- [66] Whitney DE, Gilbert OL & Jastrzebski M. Representation of Geometric Variations Using Matrix Transforms for Statistical Tolerance Analysis in Assemblies. Research in Engineering Design 1994; 6; 191-210.
- [67] Turner JU & Gangoiti AB. Tolerance Analysis Approaches in Commercial Software. Concurrent Engineering Issues, Technology, and Practice 1991; 1; 11-23.
- [68] Spotts MF. Allocation of Tolerances to Minimize Cost of Assembly. ASME Journal of Engineering for Industry 1973; 762-764.

- [69] Edel DH & Auer TB. Determine the Least Cost Combination for Tolerance Accumulations in a Drive Shaft Seal Assembly. General Motors Engineering Journal, Fourth Quarter 1964, 37-38; First Quarter 1965, 36-38.
- [70] Parkinson DB. Assessment and Optimization of Dimensional Tolerances. Computer Aided Design 1985; 17; 191-199.
- [71] Speckhart FH. Calculation of Tolerances Based on a Minimum Cost Approach. ASME Journal of Engineering for Industry 1972; 94; 447-453.
- [72] Michael W & Siddal JN. The Optimal Tolerance Assignment with Less Than Full Acceptance. ASME Journal of Mechanical Design 1982; 104; 855-860.
- [73] Dong Z, Hu W & Xue D. New Production Cost-Tolerance Models for Tolerance Synthesis. ASME Journal of Engineering for Industry 1994; 116; 116-206.
- [74] Slocum AH. Design of Three-Groove Kinematic Couplings. Precision Engineering 1992; 14; 67-76.
- [75] Hale LC & Slocum AH. Optimal Design Techniques for Kinematic Couplings. Precision Engineering 2001; 25; 114-127.
- [76] Powell MJD. The Convergence of Variable Metric Methods For Nonlinearly Constrained Optimization Calculations. Nonlinear Programming 3. O.L. Mangasarian, R.R. Meyer, and S.M. Robinson eds. Academic Press, 1978.
- [77] Donaldson RR. Error Budgets. Technology of Machine Tools, Vol. 5. Machine Tool Task Force, Hocken RJ, chairman. 1980.

VITA

Personal Data

Date of Birth: August 31, 1978. Place of Birth: Bourges, France.

Education

Master's Degree, ISAT Nevers, France, June 2001.

Work Experience

- Research Assistant at PSL, University of Kentucky, August 2000 September 2002.
- Assistant Engineer at Ciatesa, Spain, March 2000 June 2000.
- Technician at AIA-CP, France, April 1998 June 1998.
- Operator at Mécaplast, Monaco, February 1997 March 1997.

Publications

- Barraja M, Rachakonda P & Vallance RR. "Errors in Aluminum Micro-Scale Grooves Produced with Wire EDM for Subsequent Grinding". *Proceedings of the 16th annual meeting of the ASPE*, Arlington, VA. November 10-15, 2001.
- Barraja M & Vallance RR. "Tolerance Allocation for Kinematic Couplings". *Proceedings of the ASPE Topical Meeting on Tolerance Modeling and Analysis*, Charlotte, NC. July 15-16, 2002.
- Barraja M, Vallance RR, Kiani S, Lehman J & Hunsaker B. "Allocating Tolerances for Vee-Groove Fiber Alignment". *Proceedings of the 17th annual meeting of the ASPE*, St. Louis, MO. October 20-25, 2002.